# Expression and Function of $Ca^{2+}$ Channels in the Autonomic Major Pelvic Ganglion Neuron Innervating the Urogenital System

**Yu-Jin Won**

**The Graduate School**
**Yonsei University**
**Department of Medicine**

# Expression and Function of $Ca^{2+}$ Channels in the Autonomic Major Pelvic Ganglion Neuron Innervating the Urogenital System

A Dissertation
Submitted to the Department of Medicine
and the Graduate School of Yonsei University
in partial fulfillment of the
requirements for the degree of
Doctor of Philosophy

Yu-Jin Won

August 2006

The certifies that the dissertation
of Yu-Jin Won is approved.

---

**Thesis Supervisor : Seong-Woo Jeong**

---

**Committee Member : Joong-Woo Lee**

---

**Committee Member : In Deok Kong**

---

**Committee Member : Jung-Ha Lee**

---

**Committee Member : Byoung Young Choi**

The Graduate School

Yonsei University

August 2006

# ACKNOWLEDGEMENTS

I would like to thank my advisor, Dr. Seong-woo Jeong who gave me a great opportunity, the challenge of a Ph.D. During the past four years, he has advised me with his invaluable insight, heartful encouragement and endless support. I would like to extend my sincere gratitude to my dissertation committee, Drs. Joong-Woo Lee, In Deok Kong, Jung-Ha Lee and Byoung Young Choi, for their valuable comments and suggestions on the dissertation and for their readiness to help me. I also would like to express heartful gratitude to Dr. Woo-Hyeon, Byeon and for his concerns and encouragement during my graduate training. I especially thank to the members of department physiology laboratory for their discussion, support, and encouragement.

I would like to thank my best friends, Y.J., Min, and H.Y., Kim. Very special thanks are expressed to Jeong-Keun Park for his endless support and encouragement.

Finally, I would like to express my sincerest appreciation and thanks to my loving family, mother, father and sister, for their love, support and encouragement. Without my family, I would not be able to finish my graduate work.

# CONTENTS

# LIST OF TABLES

# LIST OF FIGURES

## ABSTRACT

# Expression and Function of $Ca^{2+}$ Channels in the Autonomic Major Pelvic Ganglion Neuron Innervating the Urogenital System

**Won, Yu-Jin**

**Dept. of Medicine**

**The Graduate School**

**Yonsei University**

Among the autonomic ganglia, the major pelvic ganglia (MPG) innervating the urogenital system are very unique since both sympathetic and parasympathetic neurons are colocalized within one ganglion capsule. Sympathetic MPG neurons are discriminated from parasympathetic ones by expression of low voltage-activated $Ca^{2+}$ channels that primarily arise from the T-type α1H isoform and contribute to generation of low-threshold spikes. MPG neurons expressed transcripts encoding all of the HVA $Ca^{2+}$ channel isoforms (α1B, α1C, α1D and α1E) with the exception of the α1A. Unexpectedly, the expression profile of HVA $Ca^{2+}$ channel isoforms was identical in the two populations of the MPG neurons. Interestingly, the R-type $Ca^{2+}$ currents were sensitive to $NiCl_2$, but not to SNX-482 which was able to potently block the recombinant $\alpha 1E/\delta_2\alpha/\beta_2$ $Ca^{2+}$ currents expressed in HEK 293 cells. RT-PCR

amplification revealed that the MPG neurons expressed the alternative splicing variant of the α1E which has a shorter II-III loop and a longer N-and C-terminus when compared with the originally cloned rat version (L15453), which is reminiscent of the SNX-482-resistant celebellum type (called as Rc, G3, or α1Ee).

Sympathetic and parasympathetic MPG neurons show tonic and phasic firing patterns in response to prolonged current injection, respectively. The firing patterns of the sympathetic and parasympathetic MPG neurons are regulated by $Ca^{2+}$-dependent channels activities. RT-PCR analysis revealed that the MPG neurons expressed transcripts encoding the small conductance $Ca^{2+}$-activated $K^+$ channels, SK2 and SK3 isoforms and the large conductance $Ca^{2+}$-activated $K^+$ channels, BK a and $\beta_4$ subunits. The SK channels were found to be responsible for generation of medium AHP (mAHP), while the BK channels were for repolarization of action potential and generation of fast AHP in the MPG neurons. Application of ω-conotoxin GVIA, an N-type $Ca^{2+}$ channel blocker enhanced firing of action potentials in both sympathetic and parasympathetic neurons by reducing apamin-sensitive $I_{AHP}$ and mAHP. Conversely, nimodipine, an L-type $Ca^{2+}$ channel blocker greatly reduced the firing frequency by enhancing $Cl^-$ channel blocker-sensitive $I_{AHP}$ and AHP in the sympathetic neurons with little affecting that in the parasympathetic ones. $CdCl_2$, a non-specific $Ca^{2+}$ channel blocker, exerted negligible effects on firing of the sympathetic neurons, which might be resulted from the opposite effects of ω-conotoxin GVIA and nimodipine. Taken together, these results suggest that in the sympathetic and parasympathetic MPG neurons, $Ca^{2+}$ influx through L- and N-type $Ca^{2+}$ channels contributes to regulation of excitability through differential coupling to $Ca^{2+}$-activated $K^+$ and $Cl^-$ channels, respectively.

In conclusion, MPG neurons functionally expressed L-, N- and R-type HVA $Ca^{2+}$ channel isoforms that contribute to regulation of neuronal excitability in different ways

**Key Words** : Major Pelvic Ganglion, Calcium, Voltage activated $Ca^{2+}$ channel, $Ca^{2+}$ activated $K^{+}$ channel, Afterhyperpolarization (AHP), neuronal excitability

# I. INTRODUCTION

## 1.1. Characteristics of the major pelvic ganglion

The pelvic plexus provide autonomic innervation to the urogenital system including the descending colon, the urinary bladder, and the external genitalia (Dail et al. 1983; Langworthy 1965). The pelvic plexus consists of autonomic ganglia as well as axonal pathways that convey afferent and efferent signals between the CNS and the peripheral target organs. Therefore, the pelvic plexus mediates autonomic visceral reflexes such as urination, evacuation, ejaculation, and erection (Dail et al., 1983). Accordingly, it is important to understand the precise neuronal circuit and neural regulation of the pelvic plexus for treatment of dysfunctions of pelvic organs such as urinary incontinence, constipation, and impotence. Pelvic ganglia in most animal species are widely dispersed among the pelvic viscera. Exceptionally, pelvic ganglion neurons in male rat are located in a pair of one large ganglion called the "major pelvic ganglion (MPG)" (Fig 1) and "paracervical ganglion" in the female. The MPG are located on the lateral surfaces of the prostate gland and contain significantly larger number of ganglion cell (about 30,000) than paracervical ganglion (about 10,000) (Greenwood et al., 1985). Because the MPG are morphologically simple, it has been widely used in a variety of anatomical, pharmacological and physiological studies. Many previous studies have reported that anatomical and functional plasticity of the MPG are observed in pathophysiologically complex processes such as dysfunction of micturation and impotence (Groat and Booth, 1992). For examples, obstruction of bladder outlet produces marked hypertrophy of the MPG neurons innervating the bladder (Groat et al., 1992). Decreased testosterone levels by castration reduced erectile response of the MPG neurons, and resulted erectile dysfunction (Mills et al., 1992; Giuliano et al.,

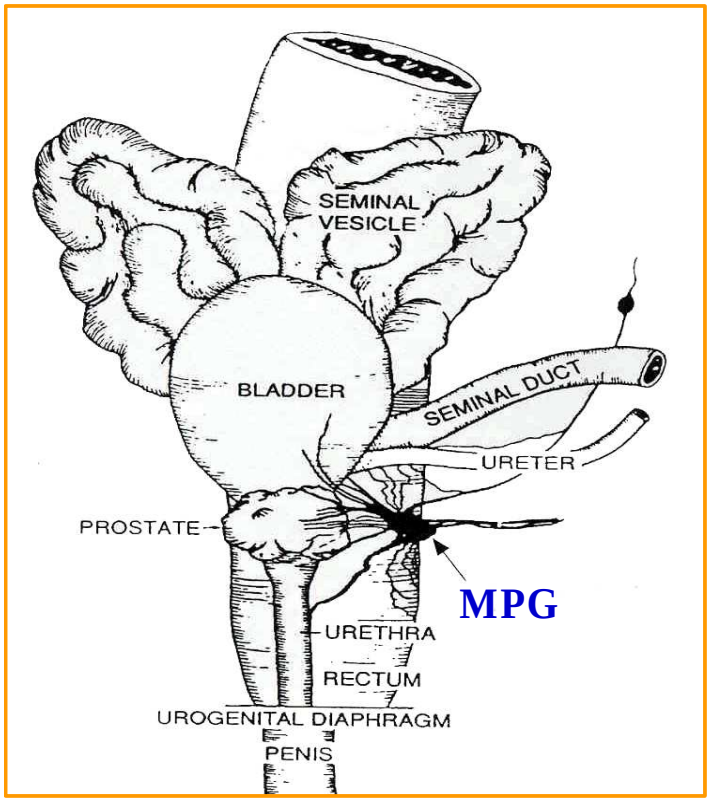


**Fig. 1. Location of the major pelvic ganglia in rat (Maggi, 1993, Nervous Control of the Urogenital System)**

1993). Therefore, the MPG neurons provides a useful model system for studying the autonomic control of pelvic organs during normal and pathological conditions.

The most prominent feature of the pelvic ganglia is that both sympathetic and parasympathetic neurons reside in one ganglion capsule (Keast, 1995). According to earlier studies, the MPG neurons can be distinguished the cell types of based on properties such as cell size, tyrosine hydroxylase immunoreactivity, and expression of T-type $Ca^{2+}$ channels (Zhu et al., 1995).

It was established that $Ca^{2+}$ influx through voltage-activated $Ca^{2+}$ channels plays important roles in control of neurotransmitter release and excitability in autonomic ganglia neurons (Hirning et al., 1988; Toth et al., 1993). Therefore, studies on $Ca^{2+}$ channels and their modulation in the MPG is necessary for understanding the physiology and pathophysiology of the urogenital system. Smith and Cunnane (1996) have shown that multiple high voltage-activated (HVA) $Ca^{2+}$ channels control neurotransmitter release from postganglionic sympathetic neurons in guinea-pig (Smith and Cunnane, 1996). Recent studies have shown that T-type $Ca^{2+}$ channels mainly arise from the $Ni^{2+}$ and $Zn^{2+}$- sensitive $\alpha$1H isoform in the MPG neurons. This study has shown that $\alpha$1H T-type $Ca^{2+}$ currents contribute to generation of low-threshold spikes in the sympathetic MPG neurons (Lee et al., 2002). However, to date, it still remains unknown which isoforms of HVA $Ca^{2+}$ channels are functionally expressed in the MPG neurons. More importantly, functional roles of HVA $Ca^{2+}$ channels in regulation of on excitability still remains unanswered.

## 1.2. Classification and characteristics of voltage-activated $Ca^{2+}$ channels

In neuronal cells, the $Ca^{2+}$ ion is an important second messenger for intracellular signal transduction (Somlyo et al., 1994). Rises in intracellular $Ca^{2+}$ trigger a wide variety of processes including neuronal excitability, neurotransmitter release, secretion of hormone, regulation of synaptic plasticity, muscle contraction, gene expression, cell growth, development, survival and apoptosis. Although there are many channels involved in controlling intracellular $Ca^{2+}$ levels, $Ca^{2+}$ influx across the plasma membrane primarily occurs through voltage activated $Ca^{2+}$ channels (VACCs). Based on their activation threshold, VACCs can be divided into two main groups, low voltage-activated (LVA) and high voltage-activated (HVA) $Ca^{2+}$ channels.

In general, VACCs are be composed of the pore forming $\alpha 1$ subunit and different auxiliary subunits- $\beta$, $\alpha_2\delta$ and $\gamma$ (Fig. 2). The $\alpha 1$ pore forming subunit is a transmembrane protein organized into four domains (I-IV), each containing six transmembrane segments (1–6). The $\beta$ subunit is entirely cytoplasmic and has a molecular weight of 52~78 kDa. The diversity of $Ca^{2+}$ channel structure and function is substantially enhanced by multiple $\beta$ subunits. Four $\beta$ subunit genes have been identified. The different $\beta$ subunit isoforms cause increment of current amplitude, and shifts in the kinetics and voltage dependence of gating, which can substantially alter the physiological function of an $\alpha 1$ subunit (Pichler et al., 1997). The $\alpha_2\delta$ subunit has a molecular weight of 140~170 kDa and consists of two disulphide-linked peptides, encoded by same gene (Jongh, et al., 1990), and is membrane-anchored with a heavily glycosylated extracellular domain. Genes encoding four $\alpha_2\delta$ subunits ($\alpha_2\delta$1-4) have been identified (Klugbauer et al 1999), functional coexpression of the $\alpha_2\delta$ subunit with various combinations of $\alpha 1$ and $\beta$ subunits results in an increase in the current densities or dihydropyridine (DHP)-binding sites (Singer et al.,1991; Welling et al.,

1993), acceleration of current activation and inactivation, and a shift of the voltage-dependence for gating in a hyperpolarizing direction (Singer et al., 1991; Felix et al., 1997). Finally, fourth subunit, γ has been recently described in skeletal muscle (Glossmann et al., 1987) and neuronal cell (Letts et al., 1998), These are composed of four transmembrane segments and cytoplasmic N-and C-termini. Until now, eight γ subunits (32 kDa) have been reported. Although the functional roles have not yet been completely elucidated, γ subunits downregulate $Ca^{2+}$ channel activity by causing a hyperpolarizing shift in the inactivation curve (Black, 2003).

VACCs have been classified into five essential groups, termed T, L, N, P/Q and R according to their elecrophysiological and pharmacological properties (Ellinor et al., 1993; Fox, et al., 1987; Usowicz et al., 1992; Miller et al., 1992). Until now, molecular cloning studies have revealed ten distinct genes encoding different α1 subunits which are now classified into three subfamilies (Table 1) : $Ca_v1$ (α1C, α1D, α1F, α1S), $Ca_v2$ (α1A, α1B, α1E), and $Ca_v3$ (α1G, α1H, α1I), (Catterall et al. 2003). The $Ca_v1$ subfamily encodes HVA L-type channels. Of the $Ca_v2$ subfamily, α1A, α1B, and α1E genes correspond to HVA P/Q-, N-, and R-type channels, respectively. The members of the $Ca_v3$ subfamily correspond to LVA T-type $Ca^{2+}$ channels. Generally, each neural tissue displays its own expression profile of VACCs compounding different isoforms. Since HVA $Ca^{2+}$ channels, i.e. L-, N-, P-, Q-, and R-types, show overlapping biophysical properties, use of specific pharmacological tools is crucial in probing each type of HVA $Ca^{2+}$ channel.

The biophysical properties of L-type currents were first reported for chick dorsal root ganglion neurons in 1985 (Nowycky et.al. 1985) and L-type VDCCs were shown to be widely distributed in all types of cells except for platelets. In sensory neurons, L-type $Ca^{2+}$ currents showed a slight inactivation during application of 200-msec depolarization pulses, the decay time constant being higher than 500 msec (Long-lasting), (Fox et al., 1987). The current begins to inactivate at holding potentials

more positive than -60 mV and, when elicited from a holding potential of -60 mV, it reaches its maximum amplitude around +10 mV. L-type channels are ubiquitous, particularly in skeletal and cardiac muscle, where they play an essential role in excitation-contraction coupling (Flockerzi et al., 1982). Pharmacologically, L-type $Ca^{2+}$ channels can be identified by use of dihydropyridines such as nifedipine and nicardipine (Bean 1984).

N-type $Ca^{2+}$ channels are widely distributed in “N”eurons (“N”either L nor T). In dorsal root ganglion neurons (Fox et al., 1987), the N-type channel is distinguished by having a conductance of 13 pS, a range of inactivation between -120 and -30 mV, and a decay time constant between 50 and 80 msec. In dorsal root ganglion neurons, the N-type $Ca^{2+}$ current was isolated from other $Ca^{2+}$ currents and recorded simply by adjusting the holding potentials and the test potentials (Ferroni etal., 1989). Although N-type $Ca^{2+}$ currents with various biophysical characteristics have been described, the greatest variety in inactivation rates were reported with range from 100 msec in sympathetic neurons when measured in equivalent divalent ion concentrations. The N-type VDCC plays a role in some forms of neurotransmitter release (Miller, 1987). Direct measurement of $Ca^{2+}$ currents from the presynaptic terminal region of the chicken ciliary ganglion calyx synapse showed that the predominant $Ca^{2+}$ channel has pharmacological characteristics similar to those of N-type channels (Stanley and Atrakchi, 1990). N-type channels are highly sensitive to ω-conotoxin GVIA isolated from the fish-hunting sea snail (Olivera et al. 1994).

P/Q-type $Ca^{2+}$ channels termed "P" because it was first described in "P"urkinje cells in 1989 (Llinás et al., 1989). P-type $Ca^{2+}$ currents activate above -50 mV, peak at around +10 mV, and display very little if any inactivation over a period of one second. In contrast to the N-type channel, the P-type channel has a unique monovalent

ion selectivity in the absence of divalent cations. The sequence from the most permeable to the least is: $Rb^+ > Na^+ > K^+ > Li^+ > Cs^+$. In 1995, Randall and Tsien reported subsequent designations of the Q-type $Ca^{2+}$ channel as a separate category. Because Q-type current is rapidly inactivated, it requires prior elimination of P- and N-type $Ca^{2+}$ current components before it can be studied in isolation (Randall and Tsien, 1995). Immunohistological studies have shown that the P/Q-type channel is widely expressed in the mammalian central nervous system and that the channel appears to serve both as a generator of intrinsic activity and as a modulator of neuronal integration and transmitter release (Liu et al., 1996) P- and Q-type channels are identified by application of a spider toxin, ω-agatoxin IVA at low and high concentrations, respectively (Bourinet et al. 1999).

The existence of an LVA $Ca^{2+}$ current was first discovered in 1981 in neurons of the guinea pig inferior olivary nucleus using intracellular sharp electrodes (Llinás et al., 1981). T-type channels start to open with weak depolarizations reaching voltages much more negative than those required to activate other VDCCs, and the currents elicited are "T"ransient. Whole-cell recording from chick and rat dorsal root ganglion neurons has shown that the T-type current is activated at approximately -50 mV and reaches its maximum value between -40 and -10 mV. Channel inactivation is prevented at very negative potentials, while channel opening is inhibited at a holding potential more positive than -60 mV. These low voltage-activated (LVA) and might be important for cardiac pacemaker activity and the oscillatory activity of several thalamic neurons. $Ni^{2+}$ sensitivity is not reliable parameter by which to identify T-type currents because there is a high variability of sensitivity of different expressed subunits to $Ni^{2+}$ and L-type channels can also be blocked by $Ni^{2+}$ (Ertel, 1997). New drugs such as mibefradil, are being proposed as relatively specific T-and R-type $Ca^{2+}$ channel

blockers (Clozel et al., 1999), although further experimentation also required to confirm the selectivity.

R-type (termed as the following letter of "R"emaining channel) currents are defined as the residual HVA $Ca^{2+}$ current observed after the application of toxins that selectively block N-, L-, P-, and Q-type currents (Pearson et al., 1995; Zhang et al., 1993). Due to their insensitivity to pharmacological blockers, R channels remain less well characterized. The biophysical properties of this current are difficult to distinguish from N- and Q-type currents in the whole-cell mode. There are even some parameters that are reminiscent of T-type currents (decay time constant of inactivation: 22 msec at 0 mV). R-type current are found to be relatively more sensitive to nickel than other HVA $Ca^{2+}$ channels. Recently, another spider toxin called SNX-482 is available for selectively blocking R-type calcium channels (Newcomb et al., 1998). However, splicing variants of R-type $Ca^{2+}$ channels resistant to SNX-482 also have been described in some central nervous system neurons, such as retinal ganglion neurons, hippocampal CA1 neurons, and cerebellar granule neurons (Newcomb et al., 1998; Tottene et al., 2000; Sochivko et al., 2002).

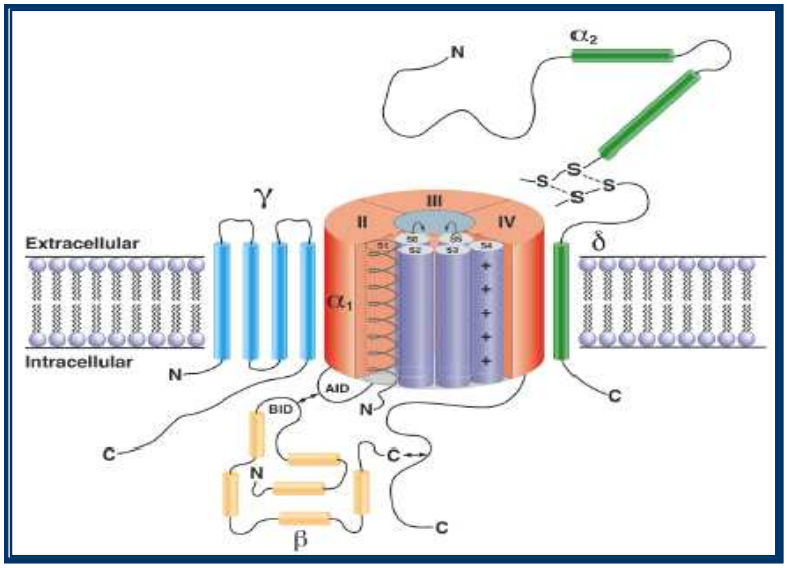


**Fig 2. Structure of the voltage-dependent $Ca^{2+}$ channel.**

The prototypical HVA voltage-dependent $Ca^{2+}$ channel consists of at least three subunits. The α1 pore forming subunit is a transmembrane protein organized into four domains (I-IV), each containing six transmembrane segments (1 – 6). The cytoplasmic β subunits bind to the I – II loop. Associated with the α1 subunit are the entirely intracellular β subunit, the four times membrane traversing γ subunit, and the $\alpha_2\delta$ (proteolytically cleaved into $\alpha_2$ and δ). $\alpha_2\delta$ subunit pairing consists of the single transmembrane crossing δ subunit disulfide linked (S-S) to the entirely extracellular $\alpha_2$ subunit. (Randall and Benham, 1999, Mol.Cell. Neurosci., 14:255-272).

**Table 1. Nomenclature and pharmacology of voltage-activated $Ca^{2+}$ channels.**

| | Numerial Classificaion | Calcium current type | Name of α1 genes | Distribution | Specific blocker |
|---|---|---|---|---|---|
| HVA | $Ca_v1.1$ | L | α1S | skelectal muscle | DHPs |
| | $Ca_v1.2$ | | α1C | heart/smooth muscle | |
| | $Ca_v1.3$ | | α1D | neurons/endocrine | |
| | $Ca_v1.4$ | | α1F | retina | |
| | $Ca_v2.1$ | P/Q | α1A | neurons | w-agatoxin IVA |
| | $Ca_v2.2$ | N | α1B | | w-conotoxin GVIA |
| | $Ca_v2.3$ | R | α1E | | SNX-482 |
| LVA | $Ca_v3.1$ | T | α1G | neurons | no specific blocker |
| | $Ca_v3.2$ | | α1H | neurons/heart | |
| | $Ca_v3.3$ | | α1I | neurons | |

## 1.3. Voltage activated $Ca^{2+}$ channels and neuronal excitability

$Ca^{2+}$ signals act as intracellular second messengers that are capable of mediating a range of cytoplasmic responses, including release of neurotransmitter, $Ca^{2+}$ dependent gene transcription and to regulate neuronal excitability. Especially, $Ca^{2+}$ activated ion channel were known to generate the afterpotentials following a single spike action potential or a spike train. Afterpotential can mediate the negative or positive regulation of excitability (Sah P, 1996; Storm., 1990; Azouz et al., 1996; Caeser et al., 1993). Activation of $Ca^{2+}$ activated $K^+$ channels are particularly important for negative regulation of excitability. $K^+$ channels generate outward currents that outlast the action potentials and tend to hyperpolarize the cell, thus generating afterhyperpolarizations (AHPs). These AHP generating $Ca^{2+}$ activated $K^+$ currents are essential determinants of refractoriness, inter-spike interval durations and trajectories and spike timing, discharge patterns and discharge frequencies. Conversely, opening of $Ca^{2+}$ activated $Cl^-$ channels are important to positive regulation of excitability. Inward currents evoked by $Ca^{2+}$ activated $Cl^-$ channels can generate afterdepolarizations (ADPs) that facilitate extra spikes and bursts. Therefore, ADPs inducing by $Ca^{2+}$ activated $Cl^-$ channel increased neuronal excitability.

## 1.4. Characteristics of $Ca^{2+}$-activated $K^+$ channels

Three subclasses of $Ca^{2+}$-activated $K^+$ channels called BK, SK, and IK channels have been identified based on biophysical and pharmacological properties (Sah, 1996). BK channels with large conductances called "MaxiK" have been first described and found to be abundant in smooth muscles (Marty, 1981). Similar to other type of ion channels, BK channels consist of two distinct subunits: $\alpha$ and $\beta$, which are arranged in a 1:1 stoichiometry (Knaus et al., 1994). The $\alpha$-subunit is the pore-forming unit

whereas the β-subunit is the regulatory unit. Whereas only one α-subunit has been identified until now, four putative β-subunit types have been cloned (β1–β4). BK channels are highly $K^+$-selective and have single channel conductances of 200-400 pS and require both $Ca^{2+}$ and membrane depolarization for activation (Marty, 1981). These $Ca^{2+}$ and membrane potential-dependent properties are critical for feedback regulation of excitability by activation of BK channels. Several pharmacological blockers of BK channels are known: tetraethylammonium (TEA) at millimolar range concentration (Blatz and Magleby, 1987), and the two scorpion-derived peptides, charybdotoxin and iberiotoxins (Galvez et al., 1990). Recently, the mycotoxin paxilline and penitrem A have also been described to block the BK channels (Strobaek et al., 2000). Of these ones, iberiotoxin and paxilline are selective for the BK channels (Giangiacomo et al., 1992), while the other ones non-specifically block a number of other $K^+$ channels.

The second type of small $Ca^{2+}$-activated $K^+$ channel called SK channels, has a single channel conductance of 2 – 20 pS (Blatz and Magleby, 1987; Lang and Ritchie, 1987). SK channels are activated by rises in cytosolic $Ca^{2+}$ with half maximal activation in the 400 – 800 nM range of $Ca^{2+}$ (Blatz and Magleby, 1987). Unlike the BK channels, the SK channels are voltage-independent and insensitive to TEA at low concentrations, charybdotoxin, and iberiotoxin. However, the SK channels are potently blocked by apamin, a bee venom (Blatz and Magleby, 1987; Romey et al., 1984), tubocurarine, and quaternary salts of bicuculline (Johnson and Seutin, 1997). Furthermore, 1-ethyl-2-benzimidazolinone (1-EBIO) has been found to activate the SK channels by altering their $Ca^{2+}$ sensitivity and open probability (Olesen et al., 1994). Since SK channels were first described in skeletal muscle (Romey and Lazdunski, 1984) they have been found in many other tissues from neurons to smooth muscle (Kohler et al., 1996).

The third type of $Ca^{2+}$-activated potassium channel has an intermediate single channel conductance (20 – 100 pS) (Ishii et al., 1997; Joiner et al., 1997). These channels was called IK (intermediate conductance) channels and have only been

identified in a few non-neuronal cell types, in particular epithelial and red blood cells (Ishii et al., 1997). IK channels have been poorly studied due to their sparse distribution. IK channels are also voltage-independent and activated by cytosilic $Ca^{2+}$. Their pharmacological profile has shown sensitivity to charybdotoxin, clotrimazole and 1-EBIO, but not to apamin and iberiotoxin (Ishii et al., 1997).

## 1.5. Characteristics of AHPs induced by $Ca^{2+}$-activated $K^+$ channels

Three classes of AHPs - i.e. fast afterhyperpolarization (fAHP), the medium AHP (mAHP), and the slow AHP (sAHP) could be distinguished based on their time course and pharmacological properties. The fAHP is activated immediately during the action potential and lasts several tens of milliseconds. The mAHP is also activated rapidly (<5 ms) but decays with a time course of several hundred milliseconds. The sAHP rises to a peak over several hundred milliseconds and can last up to 5 s following an action potential. The sAHP is more commonly seen following a train (4-10) of spikes (Faber et al., 2001), although it has been described following a single action potential in some neurons (Sah and McLachlan, 2003).

All three types of AHP are known to be produced by activities of $Ca^{2+}$-activated $K^+$ channels. The current underlying the fAHP has been named Ic. This current is voltage-dependent (Adams et al., 1982) and blocked by TEA at low concentrations, iberiotoxin, and paxilline suggesting that the underlying channels are BK-type channels (Adams et al., 1982; Lancaster and nicoll, 1987). In many neuronal cells, BK channel inducing fAHP contribute to repolarization of the membrane which limits further $Ca^{2+}$ entry. Two types of BK channel have been reported according to biophysical properties. Cerebellar purkinje cells have type I BK channels with fast deactivation gating after action potential repolarization (Swensen and Bean, 2003), whereas hippocampal CA1 pyramidal cells and lateral amygdalar neurons have type II BK

channels with slow deactivation gating after action potential repolarization (Shao et al., 1999; Faber and Sah, 2003). Especially, the type II BK channel is resistant to iberiotoxin and charybdotoxin. Heterogenous coexpression of the accessory BK-β4 subunit with BK-α subunits confers pharmacological and biophysiological properties similar to those of type II BK channels (Meera et al., 2000; Behrens et al., 2000).

In contrast, the mAHP is blocked by apamin but not BK channel blockers indicating involvement of SK channels (Sah and McLachlan, 2001). The medium $I_{AHP}$ underlying the mAHP (Adams et al., 1982) peaks rapidly following $Ca^{2+}$ influx (<5 ms) and decays with a time constant of 50 to several hundred milliseconds (Sah, 1996). Activation of SK channels produce mAHP which is responsible for generating the phenomenon of spike frequency adaptation (Lancaster and Nicoll 1987; Sah, 1996; Storm, 1987, 1990). Until now, three types of SK subunits (SK1-3) isoforms have been identified. These subunits are assembled as either homomultimer or heteromultimer, that have similar properties of $mI_{AHP}$. Moreover, the distribution of SK channel subunits closely mirrors the distribution of $mI_{AHP}$ type currents (Stocker et.al., 1999; Stocker and Pdarzani, 2000). Even though the exact subunit composition of $mI_{AHP}$ has not been determined, recent studies have suggested that SK3 channels are the major contributors to the $mI_{AHP}$ in neurons of the rat dorsal motor nucleus of the vagus (DMV) (Pedarzani et al., 2000), midbrain dopaminergic neurons (Wolfart et al., 2001), and superior cervical ganglion neurons (Hosseini et al., 2001).

The slow AHP (sAHP) has much slower kinetics than mAHP and is solely mediated by a slow $Ca^{2+}$ activated $K^+$ current known as $sI_{AHP}$. The time course of activation of $sI_{AHP}$ lasts up to ~500 ms, its time constant of decay is in the range of 1-4 s. The kinetics of the sAHP current are strongly temperature-dependent (Sah, 1996). The $sI_{AHP}$ is voltage-independent and activated by $Ca^{2+}$ either directly or through $Ca^{2+}$ induced $Ca^{2+}$ release depending on the neuronal subtypes (Sah and McLachlan, 2001). The $sI_{AHP}$ is not blocked by apamin or TEA, while $sI_{AHP}$ is modulated by a range of neurotransmitters and second messenger pathways (Sah,

1996). The identity of the channels that underlie the $sI_{AHP}$ remains unclear although SK1 was initially reported to be apamin-insensitive, and suggested that these channels could underlie the $sI_{AHP}$ (Marrion and Tavalin, 1998). Recent studies have reported that the accumulation of $Na^+$ during a burst of action potentials that leads to a prolonged sAHP also progressively increases $Na^+$ activated $K^+$ ($K_{Na}$) currents during the burst itself, leading to adaptation of firing rate during the burst in neurons of the visual cortex (Sanchez et al., 2000). Physiologically, the sAHP is responsible for spike frequency adaptation in a number of neuronal cell. The presence of the sAHP leads to a progressive slowing of the discharge frequency and eventual cessation of action potentials (Madison and Nicoll, 1982; Sah, 1996; Faber and Sah, 2002). Thus, the presence of $sI_{AHP}$ allows for a greater level of control over the firing properties of neurons.

## 1.6. Characteristics of $Ca^{2+}$-activated $Cl^-$ channels

$Ca^{2+}$-activated $Cl^-$ channels (CaCC) are expressed in a variety of cell types, including epithelium, cardiac, smooth muscle, and central and peripheral neurons. Recent studies have demonstrated that $Cl^-$ channels are involved in regulation of physiological functions, including cellular excitability, cell volume homeostasis, intracellular organells acidification, cell migration, proliferation, differentiation, and apoptosis. Although CaCC have been studied for more than 20 years, their physiological roles and mechanisms of regulation have remained unclear because specific blockers are not available yet. Electrophysiological studies suggest there may be several kinds of CaCC, but their molecular identities also remain in question. Therefore, the $Ca^{2+}$-activated $Cl^-$ channel family (CLCA) remains a highly contentious candidate for CaCCs. The first reported clone of candidates for CaCCs from bovine tracheal epithelium, was bCLCA (Cunningham et al., 1995). This prototype was

followed by cloning of other members of the CLCA family : the endothelial adhesion protein Lu-ECAM-1 (bCLCA2), the bovine bCLCA1,2, murine mCLCA1-4, pig pCLCA1, human hCLCA1-4, and rat rCACL1 proteins (Yamazaki et al., 2005; Jeong et al., 2005).

Even though the function of CaCCs in neurons remain poorly established, it has been suggested that they are involved in action potential repolarization, generation of afterdepolarization, and membrane oscillatory behavior. For examples, in cultured spinal cord neurons, CaCCs were first identified (Owen et al., 1987). CaCCs conductances in spinal neurons are shown 50 nS. $E_{Cl}$ in spinal neurons is near −60 mV (Barker and Ramson, 1978; Hussy, 1992) so that activation of $Cl^-$ currents tends to stabilize the resting voltage or, if activated during the action potential, to hyperpolarize the membrane. Accordingly, CaCCs accelerate repolarization and, because of the slow inactivation kinetics, prevent repetitive firing and prolonged trains of action potentials in spinal neurons (Barker and Ransom, 1978; Bixby and Spitzer, 1984). A number of studies have shown that a subset of DRG neurons expresses CaCCs. The CaCCs conductance in DRG neurons is quite large; roughly 5 - 30 nS has been measured in cells loaded with $Cl^-$ (Mayer; 1985). Such a profound change of membrane conductance is expected to significantly modulate electrical excitability of the cell. $E_{Cl}$ of DRG neurons was about −30 mV (Deschenes et al., 1975) and, consequently, depolarize upon activation of CaCCs. Previously studies repoted that slow, depolarizing after-potentials have been described for DRG neurons (Crain, 1956) and are probably mediated by CaCCs that open during action potentials when $[Ca^{2+}]_i$ is raised (Mayer, 1985; Scott et al., 1994). In addition many studies have suggested correlation between neuronal excitability and afterdepolarization by activation of CaCCs in postnatal rat sensory neurons, sympathetic ganglion cells, rat nodose ganglion neurons and pituitary cells (Mayer, 1985; De Castro et al., 1997; Lancaster et al., 2002; Korn et al., 1991).

Specific pharmacological tools, often in the form of biological toxin with a high affinity and selectivity, have been an invaluable asset in the identification of channels

and in the study of their structure and function. Unfortunately, there are no equivalent tools for CaCCs. Most of chemical compounds that block CaCCs suffer from lack of selectivity and/or low affinity. However, in spite of potential difficulties, a wide variety of $Cl^-$ channel blockers have been used to identify $Ca^{2+}$ activated $Cl^-$ current including niflumic acid, DIDS, SITS, NPPB, 9-AC, NPA (N-phenylanthracilic) and mibefradil.

# II. PURPOSES

The MPG neurons very very a useful model system for studying the autonomic control of pelvic organs during normal and pathological conditions. Therefore, studies on $Ca^{2+}$ channels and their modulation in the MPG is necessary for understanding the physiology and pathophysiology of the urogenital system. To date, it still remains unknown which isoforms of HVA $Ca^{2+}$ channels are functionally expressed in the MPG neurons. More importantly, functional roles of HVA $Ca^{2+}$ channels in regulation of on excitability still remains unanswered. Therefore, the purposes of this study was to investigate expression and function of HVA $Ca^{2+}$ channels in MPG neurons innervating urogenital system. At first, 1) to investigate functional expression of HVA $Ca^{2+}$ channel isoforms in the MPG neurons using pharmacological and molecular biological tools. To understand function of HVA $Ca^{2+}$ channel in regulation of excitability in the MPG neurons, it was necessary 2) to investigate basic mechanism underlying spike firing in sympathetic and parasympathetic MPG neurons. Finally, 3) to investigate functional roles of the particular HVA $Ca^{2+}$ channels subtypes in neuronal excitability of the MPG neurons.

# III. MATERIALS & METHODS

## 3.1. Isolation of the MPG neurons.

Single neurons of the MPG were enzymatically dissociated as described previously (Lee et al. 2002). Briefly, male Sprague-Dawley rats (150-200g) were anesthetized with pentobarbital sodium (50 mg/kg i.p.). The MPG were dissected out from the lateral surfaces of the prostate gland and placed in cold Hank's balanced salt solution. The ganglia were then desheathed, cut into small pieces, and incubated in the modified Earle's balanced salt solution (EBSS, pH 7.4) containing 0.7 mg/ml collagenase type D, 0.1 mg/ml trypsin (all from Boehringer Mannheim Biochemicals, Indianapolis, IN), and 0.1 mg/ml DNase Type I (Sigma Chemical Co., St Louis, MO, USA) in a 25 $cm^2$ tissue culture flask. The flask was then placed in a shaking water bath at 35 ℃ for 55 min. The EBSS was modified by adding 3.6 mg/L glucose, and 10 mM HEPES. After incubation, ganglia were dispersed into single neurons by vigorous shaking of the flask. After centrifugation at 50 × g for 5 min, the dissociated neurons were resuspended in minimum essential medium (MEM) containing 10% fetal bovine serum (FBS) and 1% penicillin-streptomycin (all from Cambrex Bio Science, Inc, Walkersville, MD, USA). For measurement of currents, neurons were then plated onto polystyrene culture dishes (35mm) coated with poly-D-lysine and maintained in a humidified 95% air-5% $CO_2$ incubator at 37 ℃ until use.

## 3.2. Transient expression of $Ca^{2+}$ channel α1E in Human Embryonic Kidney (HEK) 293 cells.

The plasmid cDNAs encoding rat α1E (rbEII, GenBank accession number L15453) were in pMT2 (Genetics Institute, Cambridge, MA, USA), rat $\beta_2$a (M 80545) (Perez-Reyes et al., 1992) and rat $\alpha_2\delta_1$ (M 86621) (Kim et al. 1992) in pCDNA3 (Invitrogen, Carlsbad, CA, USA), and green fluorescence protein (GFP) in pEGFP-N1 (Clontech, Cambridge, UK). The human embryonic kidney (HEK) 293 cells were grown in standard Dulbecco's modified Eagle's medium (Invitrogen) supplemented with 10% FBS (Cambrex), 100 mg/mL streptomycin, and 100 units/mL penicillin (Cambrex). HEK 293 cells in 90% confluence were split with 0.25% trypsin-EDTA and replated on 35 mm dishes (Corning Inc. Corning, New York, USA) in a density of $2\times10^5$ cells/dish. One day after plating, these cells were transfected with 1, 0.5, 1, and 0.7 μg of α1E, $\beta_2$a, $\alpha_2\delta$, and GFP cDNAs, respectively, using a calcium phosphate transfection kit (Invitrogen), and incubated for at least 24 hours in the $CO_2$ incubator at 37°C. Successfully transfected cells were easily identified by observation of the fluorescence induced by the GFP, and electrophysiological recordings were made between 2 and 4 days after transfection.

## 3.3. RT-PCR analysis

Total RNA of the dissociated the MPG neurons was extracted using Trizol reagent (Invitrogen, Carlsbad, CA, USA). The concentration and purity of the total RNA were measured with ultraviolet spectrophotometer. The first strand cDNA was synthesized from 1 μg of total RNA using 50 U M-MLV (Moloney Murine Leukemia Virus) reverse transcriptase (PerkinElmer Life Sciences, Shelton, CT, USA) by incubating at 42°C for 1 hour. The polymerase chain reaction (PCR) to detect transcripts of $Ca^{2+}$

channel and SK and BK channel isoforms was performed by following steps; initiated by a first denaturation at 95°C, followed by 35～40 cycles consisting of denaturation, annealing and polymerization. PCR conditions are shown in Table 2,3,4 and 5 particularly. The PCR reaction was terminated by maintaining temperatures at 72°C for several minitues. As an internal reference, β-actin or GapDh (Glyceraldehyde-3-phosphate dehydrogenase) gene was amplified. The resultant PCR products were separated on a 1.5% agarose gel and visualized by ethidium bromide staining. Specific primer pairs are listed in Tables 2,3,4 and 5.

## 3.4. Identification of splice variants of α1E

Total RNA was isolated from cerebellum, cerebrum and the MPG neurons using Trizol reagent. After reverse transcription of total RNA, fragments of α1E splice variant were amplified by PCR. Specific primer pairs for different splicing loci and PCR conditions were listed in Table 3. The resultant PCR products were separated on a 1.5% agarose gel and visualized by ethidium bromide staining. The PCR products were excised from the agarose gel and purified using MiniElute Gel extraction kit (Qiagen). Purified PCR products were sequenced at TAKARA Korea Sequencing Center. Sequencing reactions were performed on a MEGABACE 1000 (GE healthcare, Waukesha, WI) sequencer using the ET Dye terminator B.1.1 chemistry. Sequence data were analyzed using the cimarron 3.12 analysis program.

## 3.5. Western blot analysis of $Ca^{2+}$ channel isoforms.

The dissociated MPG neurons and rat whole brain were homogenized in ice-cold hypotonic buffer (10 mM Tris, pH 7.4) containing protease inhibitor mixture (Sigma), and then centrifuged at 13,000 rpm for 10 min. The precipitated samples were

resolved in a lysis buffer (50 mM Tris-HCl, 150 mM NaCl, 1% NP-40, and protease inhibitors, pH 8.0), incubated for 40 min on ice, and then centrifuged at 13,000 rpm for 15 min to remove any insoluble material. Aliquots were taken to quantify total lysate protein using the Bradford method (Kruger, 1994). After boiling in SDS buffer for 5 min, samples (40 mg protein/lane) were separated by SDS-polyacrylamide gel electrophoresis using 8% acrylamide gel and then transferred (at 150 V for 1 hour) to polyvinylidene difluoride membrane (BioTrace$^{TM}$ PVDF, Pall Corporation, East Hills, NY, USA). The membrane was blocked with Tris-buffered saline/Tween 20 containing 2% BSA (bovine serum albumin, SIGMA) for 30 min, incubated overnight at 4°C with rabbit polyclonal antibodies directed against the Ⅱ-Ⅲ linker of $Ca^{2+}$ channel α1A, α1B, α1C, α1D, and α1E subunits (all from Alomone Labs, Jerusalem, Israel) at working dilution of 1 : 200, and washed several times with cold Tris-buffered saline/Tween 20 containing 2% BSA. Horseradish-peroxidase conjugated secondary antibody was added and then membranes were incubated for 1 hour at room temperature. After intensive washing, bound antibodies were detected by ECL (Enhanced chemiluminescence) Western blot detection reagents (Amersham Biosciences, Little Chalfont, UK) on X-ray film.

## 3.6. SiRNA silencing of α1E

### 3.6.1. Preparation of siRNA

All of the siRNA duplex sequences used in this study were designed according to the guidelines described before (Elbashir, et al, 2001). The siRNA targeting α1E of MPG neurons designed using Bioneer's proprietary siRNA design program called Turbo si-Designer (www.bioneer.co.kr). RNA oligonucleotides were synthesized by Bioneer (Daejeon, Republic of Korea) using standard phosphoramidite chemistry. The siRNA

sequence was designed target for the C-terminus (nucleotide position 4007-4027) of the α1E (GenBank Accession Number: L15453) and sequence of this position was homologous to C-terminus of the MPG α1E splice variant. SiRNA sequence were as follows; α1E-siRNA-sense: CGACAGUUCCAAGGACACA(dTdT), α1E-siRNA-antisense: UGUGUCCUUGGAACUGUCG(dTdT). The following ds/siRNA construct was used as a fluorescein-labeled-negative-control ; negative-control-sense-fluorescein : CCUACGCC ACCAAUUUCGU(dTdT), negative-control-antisense-fluorescein: ACGAAAUUGGUGG CGUAGG(dTdT). Fluorescein-labelled negative control siRNA was used to demonstrate that the target-specific siRNA did not induce a nonspecific effect on gene expression. Fluorescein-labelled negative control siRNA consisted of a 19 bp scrambled sequence with 3' dT overhanged and had no significant homology to any known gene sequence from rat. Two stabilizing deoxythymidine overhanged and a terminal hydroxyl group was present at 3' ends of each strand, and each strand is phosphorylated at its 5' end. After synthesizing and purifying each strand of siRNAs by HPLC, the equimolar amounts of sense and antisense strands were mixed together and annealed by heating the mixture at 90°C for 1 min and subsequently incubating at 37°C for 1-2 hr. The successful formation of siRNA duplexes was confirmed by 15% nondenaturing polyacrylamide gels. ds/siRNA transfection was performed using Lipofectamine$^{TM}$2000 (Invitrogen Corp. Carlsbad, CA) according to the manufacturer's instructions. The ratio of ds/siRNA:Lipofectamine$^{TM}$2000 was 1:5. Three hours before transfection, MEM containing 10% FBS was replaced by on antibiotics-free medium containing serum. Six hours after the transfection, the medium was replaced by the MEM again. Forty eight hours after the transfection, expression of fluorescein in the MPG neurons was observed under an inverse fluorescence microscope and then expression of α1E transcript was analyzed molecularity and electrophysiologically in the MPG neurons.

### 3.6.2. Evaluation of knock-down of α1E mRNA by semi-quantitative RT-PCR

Forty eight hours after the transfection, the target-specific ds/siRNA or negative ds/siRNA-FITC transfected the MPG neurons were collected from the culture dishes using 0.25% trypsin-EDTA and total RNA was extracted using the Trizol reagent according to the manufacturer's instructions. The first strand cDNA was synthesized from 1 μg of total RNA as above described. PCR reaction was initiated by a first denaturation at 95°C for 5 min, followed by 30 cycles consisting of denaturation at 94°C for 60 s, annealing at 55°C for 60 s and polymerization at 72°C for 45 s. The PCR was terminated by maintaining temperatures at 72°C for 10 min. GapDh was an internal standard. Specific primer pairs for α1E isoform is listed in Table 2. The PCR products were separated in 1.5% agarose gels, visualized by staining with ethidium bromide (EtBr). Semi-quantitative analysis was performed with the Quantity One (Bio-rad, Ver.4.2.3) software. The expression level of α1E was denoted after normalized with the intensity of GapDh.

## 3.7. Electrophysiology

### 3.7.1. Patch-clamp recordings

$Ca^{2+}$ currents were recorded under the whole cell-ruptured configuration of the patch clamp technique (Hamill et al. 1981) as described previously (Ikeda 1991; Jeong and Ikeda, 1998). Patch electrodes were fabricated from a borosilicate glass capillary (Corning 8250, Garner Glass Co. Claremont, CA, USA). The electrodes were coated with Sylgard 184 (Dow corning, Midland, MI, USA), fire polished on microforge, and had resistances of 1.5-2.5 MΩ when filled with the internal solution described below.

An Ag/AgCl pellet connected via a 0.15 M NaCl/agar bridge was used to ground the bath. The cell membrane capacitance and series resistance were compensated (> 80%) electronically using an Axopatch-1D amplifier (Axon Instruments, Foster City, CA, USA). Voltage protocol generation and data acquisition were performed using the S5 data acquisition software (written by Dr. Stephen R. Ikeda, National Institute on Alcohol Abuse and Alcoholism, National Institutes of Health, Bethesda, Maryland) on a Macintosh G4 computer equipped with an ITC18 data acquisition board (Instrutech, Port Washington, NY, USA). Current traces were generally low-pass filtered at 5 KHz using the 4-pole Bessel filter in the clamp amplifier, digitized at 2 KHz, and stored on the computer hard drive for later analysis. An Ag/AgCl pellet connected via a 0.15 M NaCl/agar bridge was used to ground the bath. $Ca^{2+}$-activated $K^+$ current ($I_{AHP}$) and current clamp recordings to investigate excitability were performed under the amphotericin B-perforated whole cell configuration of the patch clamp technique using EPC-10 amplifier and pulse/pulsefit (v 8.50) software (HEKA Electronik, Lambrecht, Germany). The resistance of the filled pipettes ranged from 3 to 5 MΩ, and junction potential was less than 1 mV. Electrophysiological recordings began 8-10 min after formation of a GΩ seal when the series resistance was stabilized between 10 and 20 MΩ in the perforated patch. Cells with a stable resting membrane potential below -45 mV were included for data analysis. All experiments were performed at room temperature (20～24°C).

### 3.7.2. Solutions and drugs.

To isolate $Ca^{2+}$ currents, patch pipettes were filled with an internal solution containing (in mM) : 120 N-methyl-D-glucamine (NMG)-methanesulfonate (MS), 20 tetraethylammonium (TEA)-MS, 20 HCl, 11 EGTA, 1 $CaCl_2$, 10 HEPES, 4 Mg-ATP, 0.3 $Na_2$-GTP, and 14 creatine phosphate (pH 7.2, 290 mOsm/kg). External recording

solution contained (in mM) : 145 TEA-MS, 10 HEPES, 10 $CaCl_2$, 15 glucose, and 0.0003 tetrodotoxin (TTX) (pH 7.4, 325 mOsm/kg). For the perforated patch clamp to measure $K^+$ current and current clamp, amphotericin B (SIGMA) stock was dissolved in demethylsulfoxide (DMSO, 50 mg/ml), and stored for up one week at -20°C. Just before use the stock solution was siluted in pipette solution and sonicated for 10 seconds to yield a final amphotericin B concentration of 50 μg/ml). Perforated patch clamp internal solution containing (in mM) : 120 K-gluconate, 20 KCl, 10 HEPES (pH 7.2, 295 mOsm/kg). External recoding solution for perforated patch clamp contained (in mM) : 137 NaCl, 5.4 KCl, 2 $CaCl_2 \cdot 2H_2O$, 1 $MgCl_2 \cdot 6H_2O$, 10 Glucose, 10 HEPES (pH 7.4, 325 mOsm/kg). Drugs were applied to single neurons via a gravity-fed fused silica capillary tube connected to an array of seven polyethylene tubes. Stock solutions (0.1-10 mM) were made for the following drugs : nimodipine (Sigma), ω-agatoxin IVA, ω-conotoxin GVIA, SNX-482, mibefradil, apamin, 1-EBIO, paxillin, Iberiotoxin, charybdotoxin, DIDS, niflumic acid (all from Alomone Labs, Jerusalem, Israel), $CdCl_2$ and $NiCl_2$. All peptides were stored at -20°C or -80°C. All of the drugs were dissolved in distilled water, except for nimodipine, paxillin, DIDS, and niflumic acid dissolved in DMSO. For experiments with toxins, the external solution was supplemented with 0.1 mg/ml cytochrome C or BSA (bovain serum albumin) to minimize non-specific peptide binding to tubings. Cytochrome C and BSA itself had little effect on currents.

## 3.8. Data analysis.

Current traces were corrected for linear leakage current as determined by hyperpolarizing pulses. The membrane capacitance was measured by application of a 10 mV hyperpolarizing pulse from a holding potential of -80 mV and calculated according to the following equation : $C_m = \tau_c I_o/\Delta V_m (1 - I_\infty/I_o)$, where $C_m$ is the membrane capacitance, c is the time constant of membrane capacitance, $I_o$ is the maximum capacitive current value, $\Delta V_m$ is the amplitude of test pulse, and $I_\infty$ is the amplitude of steady-state current (Jeong and Wurster, 1997). Concentration-response curves were constructed by fitting experimental data to the Hill equation : $B = B_{max}/(1 + (IC_{50}/[drug])^{nH})$, where B is the fraction blocked, $B_{max}$ is the maximal block, $IC_{50}$ is the half-maximal inhibitory concentration of the drug applied, and $n_H$ is the Hill slope. Threshold was defined as the potential at which an action potential begins to be generated. Amount of current injection to elicit single action potential or spike firing was determined by threshold current size. The current block was defined as $[1-(I_{test})/(I_{control})] \times 100$ and the fold change defined as [test values/control values]. Data analysis and curve fitting were performed with the IGOR data analysis package (Wave-Metrics, Lake Oswego, OR) or GraphPad Prism (ver.4.0, GraphPad software Inc.) All results were presented as means ± SEM. Unpaired student t tests were used to test for effects of drugs on current or excitability and for difference between two groups. The threshold for statistical significance was set to a P value of 0.05. If P value set to less than 0.01 or 0.001, data was considered highly significant.

**Table 2. $Ca^{2+}$ channel isoform-specific primer pairs used for RT-PCR analysis**

| Primer | Accession # | Sequence | Predicted size |
|---|---|---|---|
| **α1A** | NM_012918 | F GATGAACAAGAAGAGGAAGAGG<br>R CTTGTTGGTGTTGTTGTTACGG | 332 bp |
| **α1B** | AF055477 | F TGGAGGGCTGGACTGACAT<br>R GCGTTCTTGTCCTCCTCTGC | 282 bp |
| **α1C** | M59786 | F AAGATGACTCCAACGCCACC<br>R GATGATGACGAAGAGCACGAGG | 394 bp |
| **α1D** | M57682 | F TGAGACACAGACGAAGCGAAGC<br>R GTTGTCACTGTTGGCTATCTGG | 366 bp |
| **α1E** | L15453 | F ATCTTACTGTGGACCTTCGTGC<br>R CTCAGTGTAATGGATGCGCG | 506 bp |
| **α1H** | AF290213 | F GCTCTCACCCGTCTACTTCG<br>R AGATACTTTTCGCACGACCAGG | 256 bp |
| **β-actin** | NM_031144 | F GGGAAATCGTGCGTGACATT<br>R CGGATGTCAACGTCACACTT | 253 bp |

F : forward, R : reverse

**PCR Condition**

1) 5 min at 95°C, 2) 45 sec at 95°C, 3) 40 sec at 55°C, 4) 60 sec at 72°C

5) 7 min at 72°C, repeating from step 2 to 4 at 35 times.

**Table 3. α1E splice variant specific primers used for RT-PCR analysis**

| Primer | | Sequence | Predicted size |
|---|---|---|---|
| **N-terminus (for rat type)** | F | TGGAGCGATTCATACCTGTTC | 272 bp |
| | R | GCGGCCAATCGATGAGTTTC | |
| **N-terminus (for H/M type)** | F | ATGGCTCGCTTCGGGGAGGC | 899 bp |
| | R | GCCGATCCAGTCCTTACATTCA | |
| **II-III loop** | F | GGAGGTCAGCCCGATGTC | 420 bp |
| | R | GGGCTCCTCTGGTTGTCC | 399 bp<br>363 bp |
| **C-terminus** | F | CTGAGTGGTCGGAGTGGATAC | 369 bp |
| | R | AGAGAGGAGATGCTTTCGTTC | 498 bp* |

F : forward, R : reverse

Accession Number

- Mouse : L29346, Human : L27745, Rat : L15453

* In the presence of the 129 bp insertion the expected size 498 bp.

**PCR Condition**

1) 15 min at 95°C, 2) 60 sec at 95°C, 3) 50 sec at 57°C, 4) 60 sec at 72°C

5) 10 min at 72°C, repeating from step 2 to 4 at 35 times.

**Table 4. $Ca^{2+}$-activated $K^+$ channel subunits-specific primer pairs used for RT-PCR analysis.**

| Primer | Accession # | Sequence | Predicted size |
|---|---|---|---|
| **BK-α** | AF135265 | F CAAGATGGATGCGCTCATCA<br>R TAGAAATTCTGGCAGGATTC | 438 bp |
| **BK-β** | U54495 | F AAGCTGGTGATGGCCCAGAA<br>R TGGTTTTGATCCCGAGTGTC | 293 bp |
| **SK1** | NM019313 | F GCTCTTTTGCTCTGAAATGCC<br>R CAGTCGTCGGCACCATTGTCC | 118 bp |
| **SK2** | NM019314 | F GTCGCTGTATTCTTTAGCTCTG<br>R ACGCTCATAAGTCATGGC | 151 bp |
| **SK3** | NM019315 | F GCTCTGATTTTTGGGATGTTTG<br>R CGATGATCAAACCAAGCAGGATGA | 148 bp |

F : forward, R : reverse

**PCR Condition for BK subunits**

1) 15 min at 95°C, 2) 45 sec at 95°C, 3) 40 sec at 54°C, 4) 45 sec at 72°C

5) 7 min at 72°C, repeating from step 2 to 4 at 35 times.

**PCR Condition for SK subunits**

1) 5 min at 95°C, 2) 50 sec at 95°C, 3) 45 sec at 60°C, 4) 45 sec at 72°C

5) 5 min at 72°C, repeating from step 2 to 4 at 40 times.

**Table 5. BK channel β subunit specific primers used for RT-PCR analysis**

| Primer | Accession # | Sequence | Predicted size |
|---|---|---|---|
| **BK-β1** | NM_019273 | F TGGAGACCAA ACTTCCTGCT<br>R CCTGGTCCTT GATGTTGGTT | 314 bp |
| **BK-β2** | NM_176861 | F ACCATGACCT CCTGGACAAA<br>R ACGTTGGCCA GAAGAGAGAA | 710 bp |
| **BK-β4** | NM_023960 | F CCCAGCCATT CACTTGCTAT<br>R GAGGGTTTCC CAAACAGTCA | 459 bp |

F : forward, R : reverse

**PCR Condition for BK β subunits**

1) 5 min at 95°C, 2) 45 sec at 95°C, 3) 40 sec at 57°C, 4) 60 sec at 72°C

5) 10 min at 72°C, repeating from step 2 to 4 at 35 times.

# IV. RESULTS

## 4.1. Criteria for distinguishing cell-types of the MPG neurons

Cell types of the MPG neurons could be easily recognized in according to the previously established criteria: cell size measured in electrical capacitance, and expression of T-type $Ca^{2+}$ channels (Zhu and Yakel 1997, Zhu et al. 1995, Lee et al. 2002). As illustrated in Figure 3, sympathetic MPG neurons are identified by presence of T-type $Ca^{2+}$ currents detected as a prominent hump at low-voltage range (-50 to -20 mV) or fast-inactivating peak currents evoked by test pulses to -30 mV. Conversely, the parasympathetic MPG neurons lack the hump and the transient T-type $Ca^{2+}$ currents. Figure 4 shows that correlations between cell membrane capacitance (pF) and T-current existence (Fig. 4A) or T-current amplitude (Fig. 4B). On average, cells having 62.5±5.3 pF capacitance showed T-current (about 3.1 pA/pF), frequently, while small cells having 28.6±2.6 pF of capacitance did not show T-current. To make sure of the distinguishing between sympathetic and parsympathetic MPG neurons, investigated cell-type responses to 100 μM γ-amino butyric acid (GABA) and 10 μM 5-HT. Under the experimental conditions (i.e. when both external and internal solutions contain 20 mM $Cl^-$) for measurement of $Ca^{2+}$ currents, GABA and 5-HT evoked a large inward currents exclusively in sympathetic and parasympathetic MPG neurons, respectively (Fig. 5). Figure 6A showed that most of cells having small membrane capacitance (solid line) represent high density of 5-HT current, while most of large membrane capacitance cells (dashed line) had GABA induced inward current. Overall, sympathetic MPG neurons could be distinguished with large cell capacitance (more than on average 62.5±5.3 pF) and existence of GABA and T-current from parasympathetic ones showing small cell capacitance (less than on average 28.6±2.6 pF), 5-HT current and no T-current (Fig. 6). Another criteria to distinguish sympathetic

and parasympathetic MPG neurons was investigated. As illustrated in figure 7, sympathetic and parasympathetic MPG neurons produced tonic and phasic firing, respectively in response to injection of supra-threshold current for 400 ms. Figure 8A showed correlation between firing patterns and cell membrane capacitance in MPG neurons. Figure 8B illustrated that most of sympathetic cells (dashed line) having large capacitance and GABA current showed tonic firing pattern, while majority of parasympathetic cells having small capacitance and 5-HT current appeared phasic firing pattern.

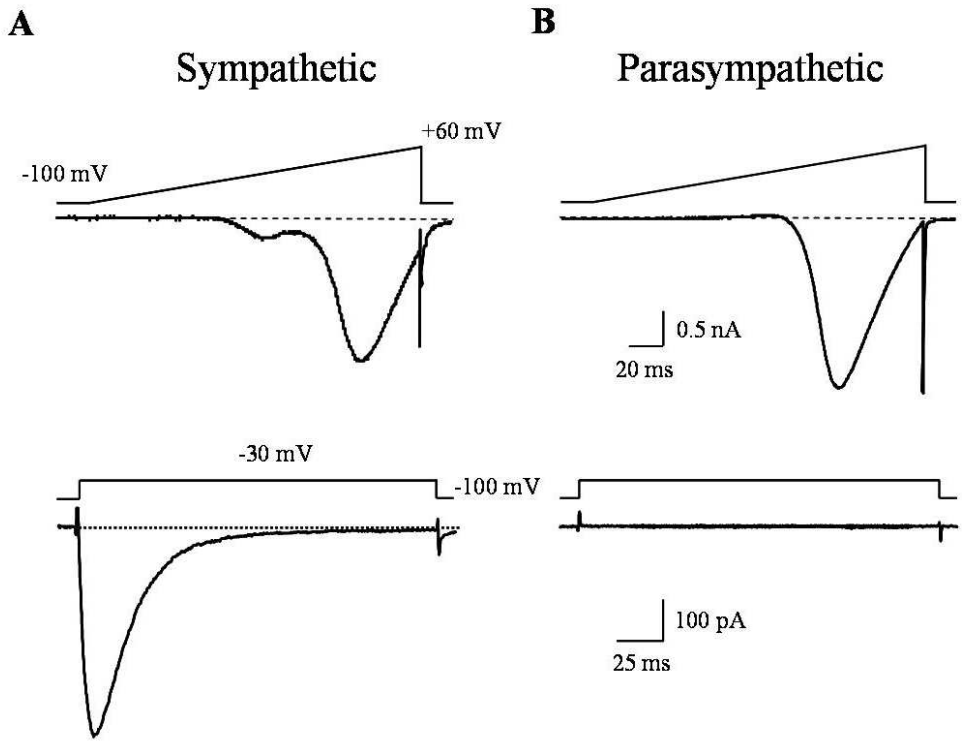


**Fig. 3. Cell type-specific characteristics of the MPG neurons - I.**

Representative traces of inward $Ca^{2+}$ currents in the (A) sympathetic and (B) parasympathetic MPG neurons recorded using whole cell patch clamp method. $Ca^{2+}$ currents were evoked by a ramp from -100 mV to +60 mV for 180 ms (upper traces) and test pulses to -30 mV from a holding potential of -100 mV (lower traces). LVA T-type $Ca^{2+}$ currents were detected as a hump (upper) or a transiently activation current (lower) exclusively in sympathetic MPG neurons.

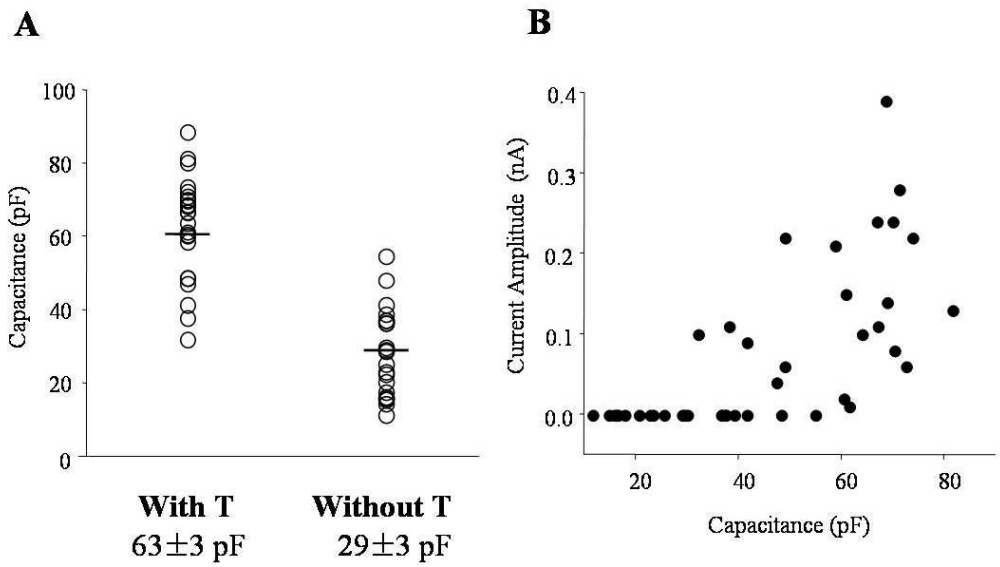


**Fig. 4. Relationship between cell size and expression of the T-type $Ca^{2+}$ channel.**

Plots showing the correlation between membrane capacitance (pF) and (A) T-current existence or (B) T-current amplitude. Data are presented as means ± SEM.

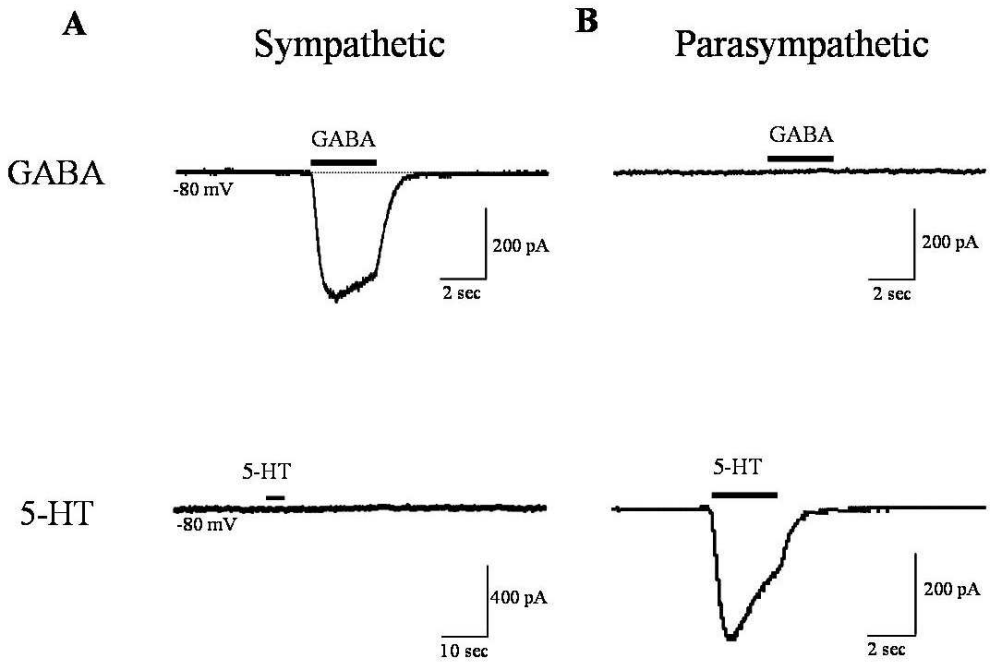


**Fig. 5. Cell type-specific characteristics of the MPG neurons - Ⅱ.**

Representative traces of inward currents evoked by application of GABA (100 μM) or 5-HT (10 μM) in (A) the sympathetic and (B) parasympathetic MPG neurons. Note that the GABA and 5-HT currents are hallmarks of the sympathetic and parasympathetic MPG neurons, respectively. Cells were held at -80 mV.

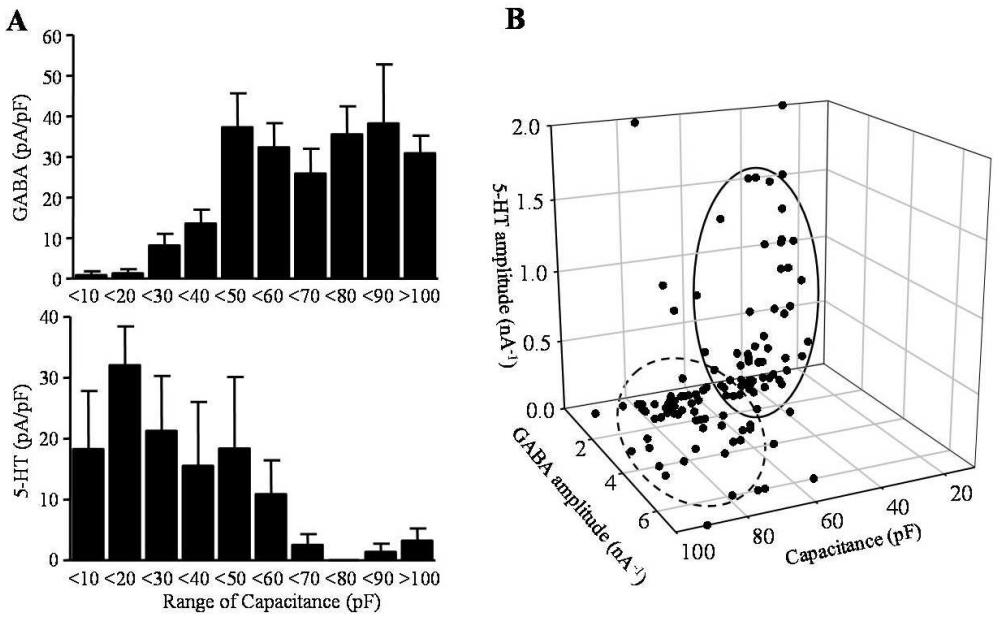


**Fig. 6. Relationship between cell size and expression of a specific ligand gated channel.**

(A) : Bar graphs showing the correlation between GABA or 5-HT induced inward current density (pA/pF) and membrane capacitance (pF). (B) : Three-dimensional plot of membrane capacitance, an amplitude of GABA, and 5-HT currents. The MPG neurons distributed within solid line and considered as parasympathetic and these with the dot line are as sympathetic. Data are presented as means ± SEM

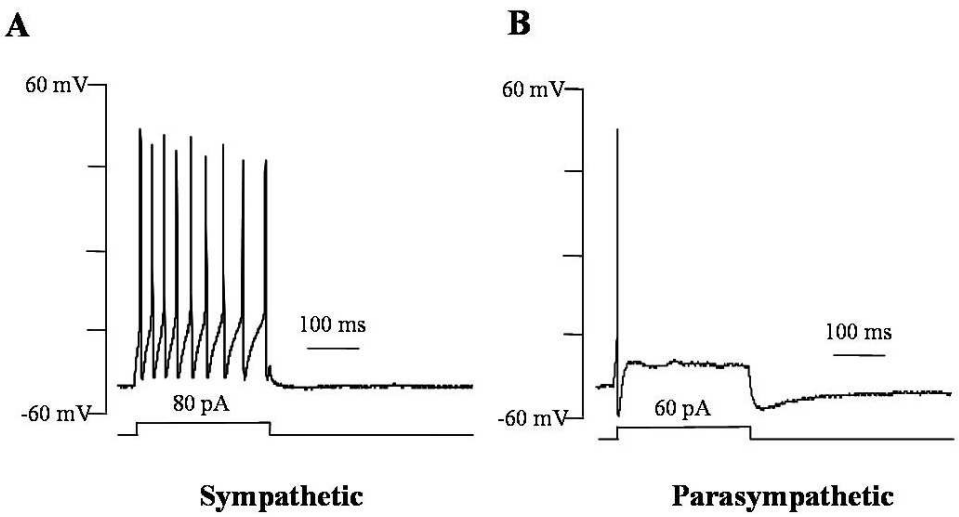


**Fig. 7. Cell type-specific characteristics of the MPG neurons - Ⅲ.**

Representative traces of action potentials in (A) a tonic and sympathetic and (B) a phasic and parasympathetic MPG neurons. The action potentials were evoked by injection of supre-threshold current for 400 ms.

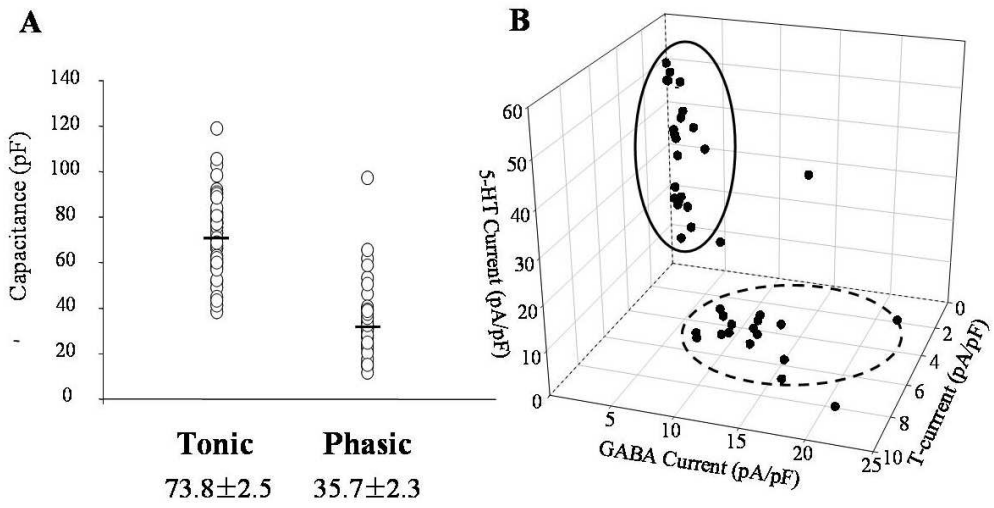


**Fig. 8. Relationship between cell size and spike firing pattern**

(A) : Plots showing the correlation between membrane capacitance (pF) and firing pattern (tonic or phasic) in the MPG neurons. B : Three-dimensional plot of T-type Ca2+ and ligand-gated channel (GABA and 5-HT) current density. The MPG neurons distributed within solid line and showed as phasic firing and these with the dot line are shown tonic firing pattern. Data are presented as means ± SEM

## 4.2. Molecular identification of HVA $Ca^{2+}$ channel isoforms expressed in the MPG neurons.

To determine the expression profile of transcripts encoding HVA $Ca^{2+}$ channel α1 subunits, RT-PCR analysis was performed on mRNA isolated from dissociated the MPG neurons. As a positive control, mRNA from rat whole-brain tissues were RT-PCR amplified. As illustrated in Figure 9, the MPG neurons expressed transcripts for all of the HVA $Ca^{2+}$ channel α1 subunits (i.e., α1B, α1C, α1D and α1E) with the exception of α1A. When the RT-PCR process was run without reverse transcriptase, no PCR products were observed, indicating no contamination of genomic DNA. The mRNA transcript for α1A was clearly detected in RT-PCR products of the positive control as a band of the expected size (lane1, 332 bp).

Next, Western blot analysis was carried out to examine whether all of the detected mRNA transcripts were translated into the corresponding $Ca^{2+}$ channel α1 subunits in the MPG neurons. All of the primary antibodies applied in these experiments have been proven to be highly specific (Saegusa et al. 2000; Latour et al. 2003). As positive controls, proteins extracted from whole brain (for α1A, α1B, α1C, and α1D) and cerebellar tissues (for α1E) were employed. Consistent with the RT-PCR results, the MPG neurons expressed α1B, α1C, α1D, and α1E, but not α1A proteins (Fig. 10).

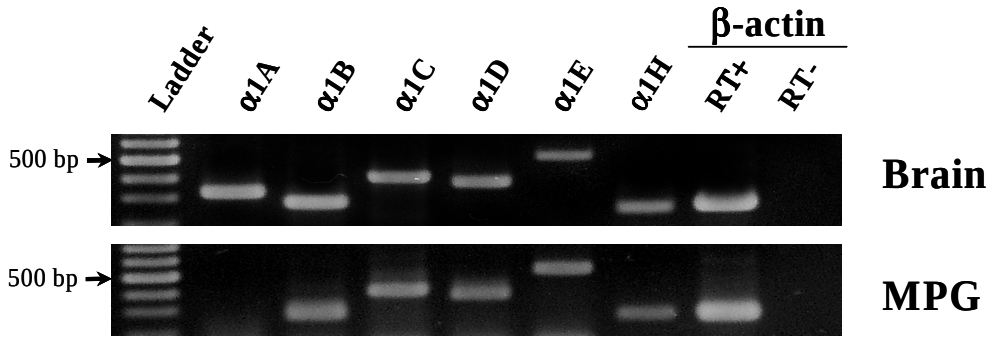


**Fig. 9. RT-PCR analysis of mRNA encoding $Ca^{2+}$ channel α1 subunits expressed in the MPG neurons.**

Total RNA isolated from dissociated the MPG neurons was reverse transcribed, and amplified by PCR with $Ca^{2+}$ channel α1 subunit (α1A, α1B, α1C, α1D, α1E, and α1H) specific primers (Table 1). The resultant PCR product were separated and visualized on an agarose gel containing ethidium bromide (EtBr). β-actin RNA as an internal control and whole brain RNA as a positive control were used. When the RT-PCR process was run without reverse transcriptase (RT-), no PCR products were observed indicating no contamination of genomic DNAs

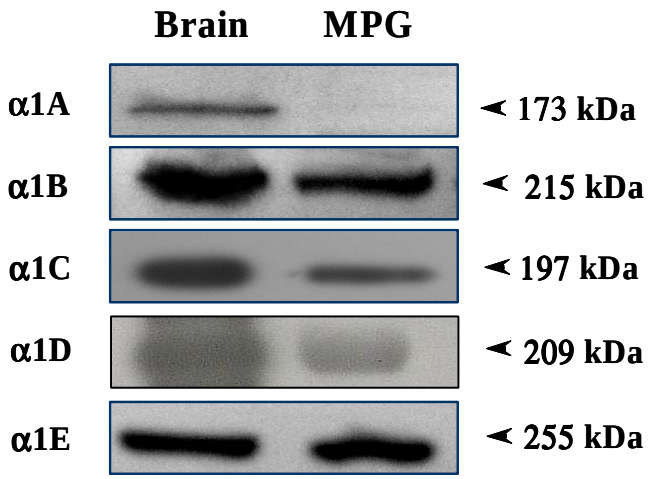


**Fig. 10. HVA $Ca^{2+}$ channel α1 subunits identified by western blot analysis in the MPG neurons.**

Proteins extracted from the MPG neurons and rat brain were probed with rabbit polyclonal antibodies directed against the II-III linkers of $Ca^{2+}$ channel α1A, α1B, α1C, α1D, and α1E subunits. The MPG neurons express all $Ca^{2+}$ channel α1 subunits with the exception of α1A. The α1A antibody was able to reveal an appropriate band when applied to the brain proteins.

## 4.3. Pharmacological identification of HVA $Ca^{2+}$ channel isoforms expressed in sympathetic and parasympathetic MPG neurons.

Next, the following two questions were addressed: what subtypes of HVA $Ca^{2+}$ channels were functionally expressed and whether the expression is cell type-specific as determined by measure of T-type $Ca^{2+}$ channel current (Lee et al. 2002). In this regard, HVA $Ca^{2+}$ currents were pharmacologically dissected out in sympathetic and parasympathetic MPG neurons by sequential application of different toxins and drugs (Adams et al. 1993; Randall and Tsien, 1995; Jeong and Wurster, 1997). To evoke the peak $Ca^{2+}$ currents, test pulses to +10 mV were applied from a holding potential of -80 mV at 0.1 Hz. During current measurements for 10 min, no significant rundown in the peak $Ca^{2+}$ current was detected. Figure 11A represents time-dependent reductions in $Ca^{2+}$ currents by different subtype-specific antagonists in a sympathetic MPG neuron. Application of nimodipine (10 μM), a DHP L-type antagonist, blocked 21% total of $Ca^{2+}$ currents. The N-type current was identified with the use of ω-conotoxin GVIA isolated from the venom of the fish-hunting snail, *Conus geographus* (Olivera et al. 1984). In the presence of w-conotoxin GVIA at a saturating concentration (2 μM), 54% of $Ca^{2+}$ currents were slowly blocked. After successively blocking L- and N-type $Ca^{2+}$ currents, tested with a high concentration of ω-agatoxin IVA (1 μM), which was large enough to block both P- and Q-types of currents (Randall and Tsien, 1995; Jeong and Wurster, 1997). However, no currents were affected by ω-agatoxin IVA in the sympathetic neuron. In addition, application of 1 μM ω-conotoxin MVIIC, an N- and P/Q-type antagonist, failed to block the $Ca^{2+}$ currents further in presence of nimodipine and ω-conotoxin GVIA (data not shown). These results were consistent with the absence of the α1A transcript and protein as revealed by RT-PCR and Western blot analyses. There remained significant residual currents resistant to the combined application of the organic antagonists. These residual currents were fully

blocked by $CdCl_2$ (0.1 mM), a non-selective $Ca^{2+}$ channel antagonist, indicating the presence of R-type $Ca^{2+}$ currents (Fig. 11A). Taken together, the sympathetic MPG neuron was found to functionally express three types (L, N, and R) of HVA $Ca^{2+}$ channels but not the P/Q-types. Next, also examined inhibitory effects of 10 μM nimodipine, 2 μM ω-conotoxin GVIA, 1 μM agatoxin IVA, and 0.1 mM $CdCl_2$ on HVA $Ca^{2+}$ currents in the parasympathetic neurons showing no T-type $Ca^{2+}$ and GABA currents (Fig. 11B). Like the sympathetic MPG neurons, the parasympathetic MPG neurons functionally expressed L-, N-, and R-type, but not P/Q-type, $Ca^{2+}$ currents. As summarized in Fig. 12, there was no cell-specific difference in the relative contribution of the $Ca^{2+}$ channel isoforms to total $Ca^{2+}$ currents. On average, L-type $Ca^{2+}$ channels contribute to 17 ± 4% and 14 ± 2%, N-type to 57 ± 5% and 60 ± 3%, and R-type to 25 ± 3% and 22 ± 2% of the total currents, respectively, in sympathetic (n = 16) and parasympathetic (n = 13) MPG neurons. It should be mentioned that the current kinetics were not further analyzed to characterize the pharmacologically identified $Ca^{2+}$ channel subtypes because the kinetics appeared to be variable from one cell to the next.

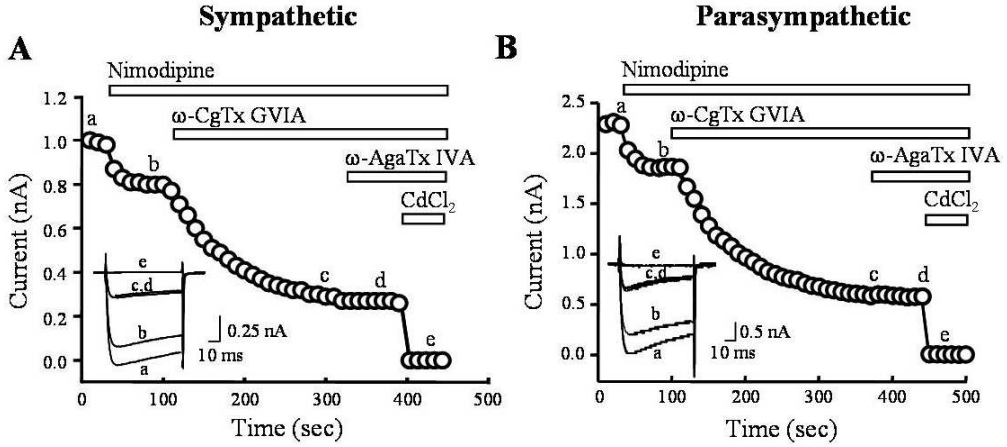


**Fig. 11. Pharmacological dissection of HVA $Ca^{2+}$ channel currents in the MPG neurons.**

(A) and (B), time course of $Ca^{2+}$ current block by serial application of nimodipine (10 μM), ω-conotoxin GVIA (2 μM), ω-agatoxin IVA (1 μM), and $CdCl_2$ (0.1 mM) in the sympathetic and parasympathetic MPG neurons, respectively. The peak $Ca^{2+}$ current was evoked every 10 s by test pulses to +10 mV for 75 ms from a holding potential of -80 mV. *Inset:* current traces obtained at different time points (labeled a-e).

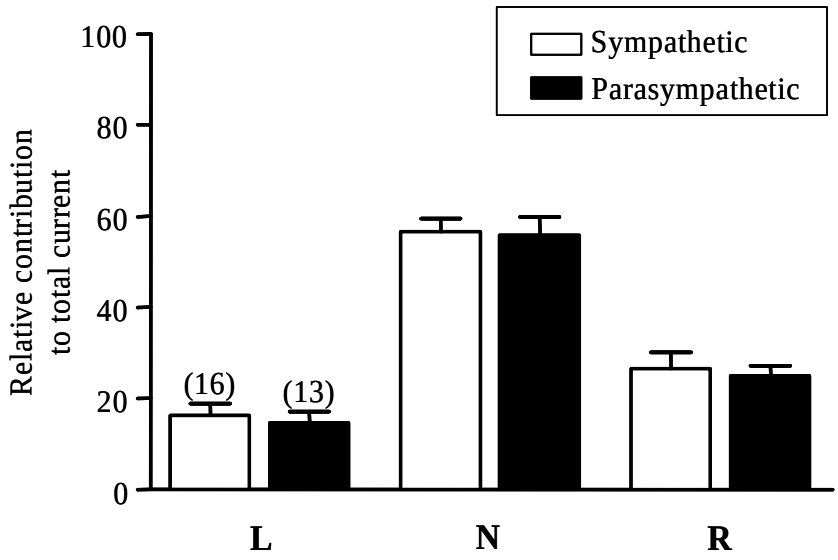


**Fig. 12. Summary of relative contribution of L-, N-, and R-type currents to total $Ca^{2+}$ currents in the sympathetic and parasympathetic MPG neurons.**

Bar graph represents relative contribution of L-, N-, and R-type $Ca^{2+}$ currents to total HVA $Ca^{2+}$ current. Data are presented as means ± SEM. Numbers of cells tested is indicated in parentheses.

## 4.4. Pharmacological characteristics of R-type $Ca^{2+}$ currents in the MPG neurons.

A previous study has shown that native R-type $Ca^{2+}$ currents could be potently blocked by nickel (Tottene et al, 1996). Accordingly, effects of nickel on R-type $Ca^{2+}$ currents were tested. When 0.3 mM nickel was applied after blocking L- and N-types with 10 μM nimodipine and 2 μM ω-conotoxin GVIA, the R-type $Ca^{2+}$ currents were significantly blocked in a sympathetic MPG neuron (Fig. 13A). On average, nickel at 0.3 mM blocked 72 ± 4% (n = 3) of the MPG R-type $Ca^{2+}$ currents. Interestingly, 500 nM SNX-482, a selective antagonist of recombinant α1E channels, failed to produce effective block of the native R-type currents (n = 16). Likewise, in parasympathetic MPG neurons, R-type currents were sensitive to nickel but not to SNX-482. Next, to compare the pharmacological properties of the MPG R-type $Ca^{2+}$ currents with those of the prototype α1E (rbEII), heterologously expressed in HEK 293 cells (Fig. 5B). No endogenous $Ca^{2+}$ currents were detected in control cells expressing only GFP, whereas large peak $Ca^{2+}$ currents were developed in cells coexpressing rat α1E, $\beta_2$a, and $\alpha_2\delta_1$ subunits (Fig. 14). The peak $Ca^{2+}$ currents of the recombinant α1E were very sensitive to nickel and SNX-482, which is consistent with the previous findings (Soong et al., 1993; Zamponi et al., 1996; Newcomb et al., 1998). On average, 0.3 mM nickel and 300 nM SNX-482 blocked 70 ± 5 % (n = 3) and 94 ± 3 % (n = 3) of the recombinant α1E $Ca^{2+}$ currents, respectively. As defined from concentration-response curves (Fig. 15), the potency ($IC_{50}$) of $Ni^{2+}$ block was similar for the MPG R-type (22 ± 1.1 μM; slope factor, 0.81 ± 0.11) and the recombinant α1E (21 ± 0.2 μM; slope factor, 0.75 ± 0.13) $Ca^{2+}$ currents. More importantly, unlike the MPG R-type, the recombinant α1E $Ca^{2+}$ currents expressed in HEK 293 cells were highly sensitive to SNX-482 ($IC_{50}$ = 76 ± 0.4 nM; slope factor, 1.71 ± 0.25) (Fig. 15). The Hill slope factor suggests that the recombinant α1E may have more than SNX-482 site as reported previously

(Tottene et al., 2000). Taken together, these data suggest that MPG neurons express $Ni^{2+}$-sensitive and SNX-482-resistant R-type $Ca^{2+}$ currents.

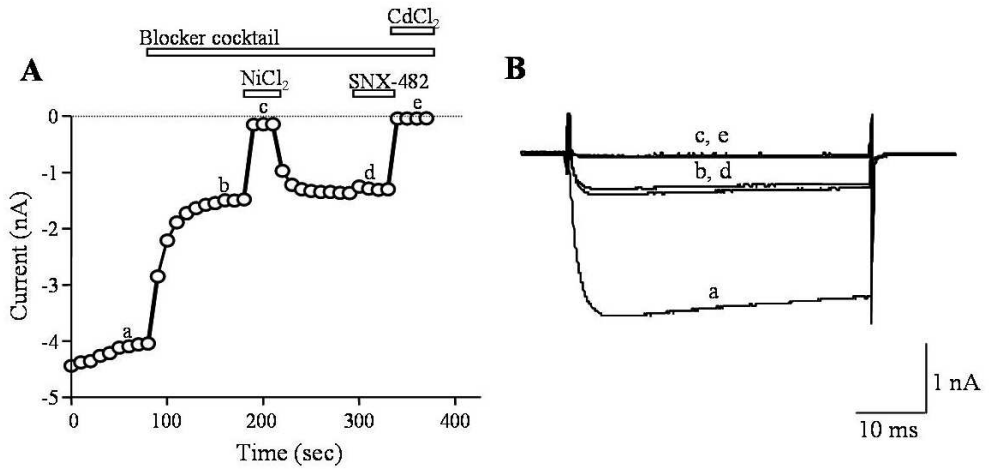


**Fig. 13. Effects of nickel and SNX-482 on R-type $Ca^{2+}$ currents in the MPG neurons.** (A) : L- and N-type $Ca^{2+}$ currents were completely eliminated by application of nimodipine (10 μM) and ω-conotoxin GVIA (2 μM) prior to testing $NiCl_2$ (300 μM) and SNX-482 (500 nM). The peak $Ca^{2+}$ current was evoked every 10 s by a test pulse to +10 mV for 75 ms from a holding potential of -80 mV. Blocker cocktail contained nimodipine (10 μM), ω-conotoxin GVIA (2 μM), and ω-agatoxin GIVA (1μM). (B) : current traces obtained at different time points (labeled a-e).

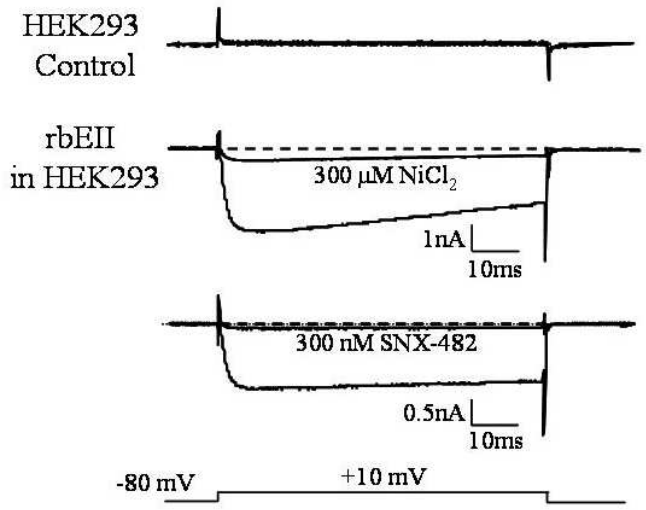


**Fig. 14. Effects of Nickel and SNX-482 on peak currents of the recombinant α1E $Ca^{2+}$ channel.**

HEK 293 cells were transfected with 1, 0.5, 1, and 0.7 μg of rat α1E, $\beta_2$a, $\alpha_2\delta$, and GFP (green fluorescent protein) cDNAs, respectively, using the calcium phosphate transfection method. After 48 hour, effects of nickel (0.3 mM) and SNX-482 (300 mM) on recombinant α1E (rbEII) were tested. $Ca^{2+}$ currents evoked by a test pulse to +10 mV for 75 ms from a holding potential of -80 mV. Note that no endogenous currents were detected in the HEK 293 cells expressing only GFP.

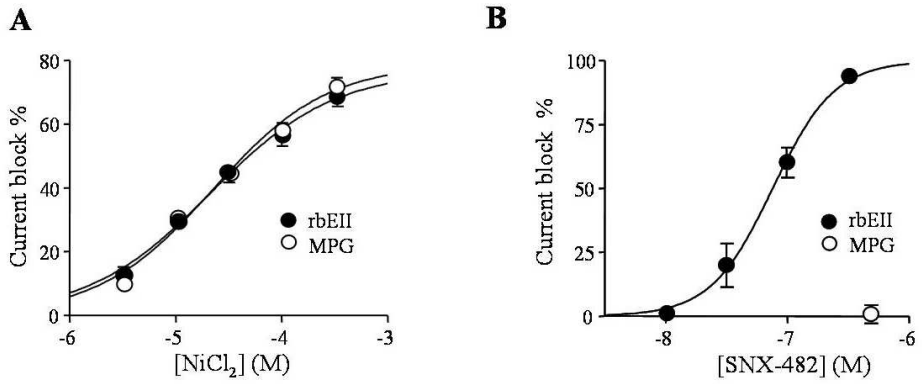


**Fig. 15. Concentration-response curves for block of the MPG R-type and the recombinant α1E $Ca^{2+}$ currents by nickel and SNX-482.**

Concentration-response curve of (A) nickel and (B) SNX-482 block. Note that the MPG R-type currents were little blocked by SNX-482 (500 nM). Absolute current block (%) was plotted as a function of drug concentration. Solid lines represent fits of data points by the Hill equation (see Material and Methods). For nickel block of the MPG R-type and rbEII $Ca^{2+}$ currents, $IC_{50}$ values (Hill slope) were 22 ± 0.1 μM (0.81 ± 0.11) and 21 ± 0.2 μM (0.91 ± 0.1), respectively. For SNX-482 block of the rbEII $Ca^{2+}$ currents, the $IC_{50}$ (Hill slope) was 76 ± 0.4 nM (1.71 ± 0.25). Data are presented means ± SEM.

## 4.5. Molecular characterization of R-type $Ca^{2+}$ currents in the MPG neurons.

Recent studies have revealed heterogeneity of the R-type $Ca^{2+}$ channel (Tottene et al., 2000; Wilson et al., 2000; Joux et al., 2001; Sochivko et al., 2002) which may arise from alternative splicing in the gene encoding the α1E subunit. Distribution and functions of the α1E variants appear to be tissue-specific and determine neuronal functions. (Marubio et al., 1996; Pereverzev A., 2002). As mentioned above, the MPG neurons expressed SNX-482-resistant R-type $Ca^{2+}$ currents. Recently, splicing variants of α1E, which is comparable with those observed in some central neurons such as retinal ganglion neurons, hippocampal CA1 neurons, and cerebellar granule neurons (Newcomb et al. 1998; Tottene et al. 2000; Sochivko et al. 2002). Next, therefore, the molecular nature of SNX-482-resistant R-type $Ca^{2+}$ currents was examined in the MPG neurons.

### 4.5.1 Overview on spice variants of α1E ($Ca_v2.3$)

As illustrated in Figure 16, eight splicing variants of the α1E can be deduced from sequence comparison among rat, rabbit and human α1E clones. In 1993, the rat rbEII (Soong et al., 1993) was cloned and functionally expressed. Its deduced amino acid terminus from the hippocampus of adult rats was shorter by 50 amino acids than other mammalian α1E subunits, which was explained by an alternative exon present in the rbEII, lacking the first methionine residue. During consecutive investigations, the 5' end of the α1E was amplified from adult rat brain RNA and was found to contain the homologous sequence as the major transcript detected in mouse and human fetal brain. Therefore, only three loci that were insert 1 and 2 in the intracellular connecting domains II and III (II-III loop) and insert 3 of C-terminus were included in the

systematic investigation of structural variants from $Ca_v2.3$. As illustrated in figure 16, seven mutants representing putative splice variants of human α1E ($Ca_v2.3$) were generated by PCR using the cloned variant $Ca_v2.3d$ as a template. To date, $Ca_v2.3d$ represents the longest transcript derived from a human fetal brain cDNA library (Schneider et al., 1994). It contains insert I (19 amino acid), insert 2 (7 amino acid), and insert 3 (43 amino acid). Four variants of a II-III loop having different size were investigated either within the cloned $Ca_v2.3d$ backbone or after transferring them into the $Ca_v2.3c$ variant formerly called a1Ed-DEL, which was lacking of the insert 3 (exon 45) in the carboxy terminus. These eight constructs, the neuronal $Ca_v2.3c$ (Williams et al., 1994) and the endocrine $Ca_v2.3e$ (Vajna et al., 1998) are the predominant splice variants detected *in vivo*, while $Ca_v2.3d$ could be a splice variant restricted to the fetal brain. $Ca_v2.3a$, $Ca_v2.3b$ and $Ca_v2.3f$ are deduced from the cerebellar granule cells (Schramm et al., 1999), and α1E-4 and α1Ef variants have never been found in tissues, yet.

### 4.5.2. Identification of α1E splice variant in the MPG neurons

To difine the splicing variant of the α1E expressed in the MPG neurons, systemic examination was applicated to four loci: the amino-terminus, two segments (insert 1 and 2) of the II-III loop and the carboxy terminus. The cDNA fragments from MPG neurons were amplified by RT-PCR using region-specific primer pairs (Table 3). RT-PCR amplification in the II-III loop of α1E subunit from the MPG neurons with specific primer yielded a major 363 bp product. For positive controls, cDNA fragments of the α1E splice variants expressed in the cerebellum and cerebrum were also amplified (Williams ME. et al 1994; Rolf Vajna et al. 1998). The rat cerebrum, a major of about 420 bp product amplified. In the rat cerebellum, two types of splice variant detected about 420 bp, and 363 bp by RT-PCR analysis in the Ⅱ-Ⅲ loop

region. PCR amplification in C-terminus region of α1E from the MPG neurons produced a 498 bp single fragment. The rat cerebrum yielded about a major 369 bp fragment, while the rat cerebellum, both types of products about of 369 bp and 420 bp were detected. An additional faint band above 500 bp was also detected in the cerebellum and cerebellum of C-terminus specific region. It was unclear whether non specific product or another splice variant in C-terminus region of cerebrum and cerebellum (Fig 17). Unexpectively, PCR product with specific primers for N-terminus could not be detected from the MPG neurons, while, N-terminal fragment of 272 bp was amplified in rat cerebrum and cerebellum. Recently which is a new isoform of rat α1E subunit has been found to have long N-terminus, which is similar to the human/mouse form (Schramm, et al. 1999). Therefore, a pair of specific primers for human/mouse 5'-end (Table 3) was employed to identify the N-terminus of MPG α1E. As result of RT-PCR analysis using human/mouse 5'-end specific primer pairs, a cDNA fragment of 899 bp was amplified from cerebrum, cerebellum and MPG neurons (Fig. 17). Figure 18 shows sequence alignment of the prototype rat α1E (rbEII) and MPG α1E. Compared with the rbEII, the the MPG α1E have additional 50 amino acid in N-terminus like human/mouse α1E and contains short II-III loop lacking 19 amino acid (Insert 1) and longer C-terminus containing additional 43 amino acid. Taken together, these results suggested the molecular structure of the α1E splice variant expressed in the MPG neurons (Fig. 19). The MPG α1E was quite similar to one of the cerebellum α1E isoform (Rolf Vajna et al. 1998).

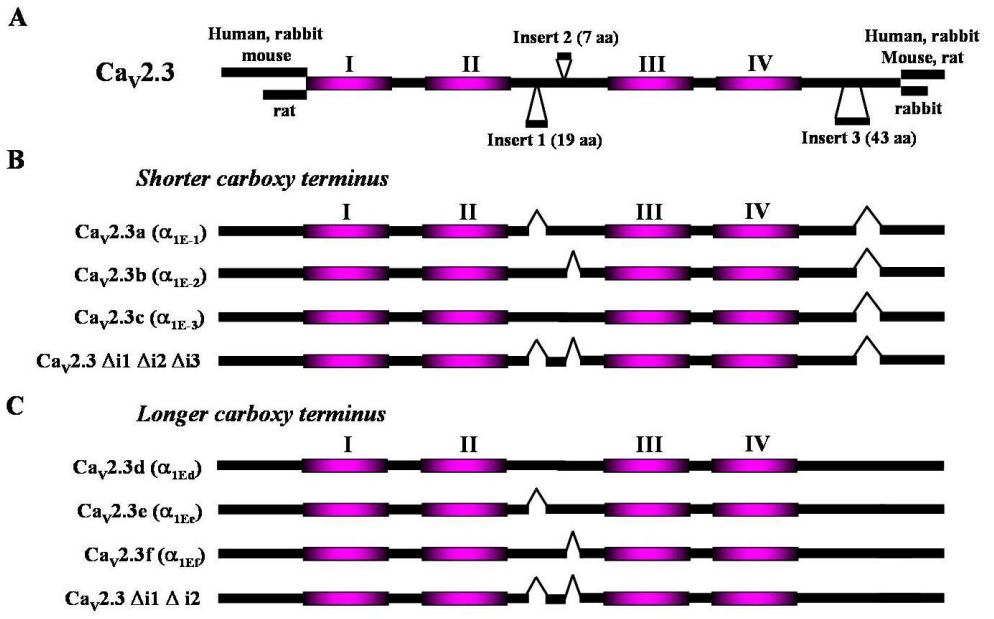


**Fig. 16. Splice variants of the α1E deduced from comparison of cloned mammalian $Ca_v2.3$ subunits.**

The primary structure of cloned α1E is shown in a linear form hight-lighted for the four intramolecular domain I-IV. alternate ends or insertions and deletions are symbolized by separate bars or gaps (Λ), respectively. (A) : Amino terminus, the cytosolic II-III linker, and the carboxy terminus contain major structural variation within the $Ca_v2.3$ subunits from different species. (B) : Four structural variants were deduced for the $Ca_v2.3$ subunits lacking the insert 3 (exon 45) from the carboxy terminus. C: Similar to (B), four variants were deduced for $Ca_v2.3$ subunits containing the insert 3.

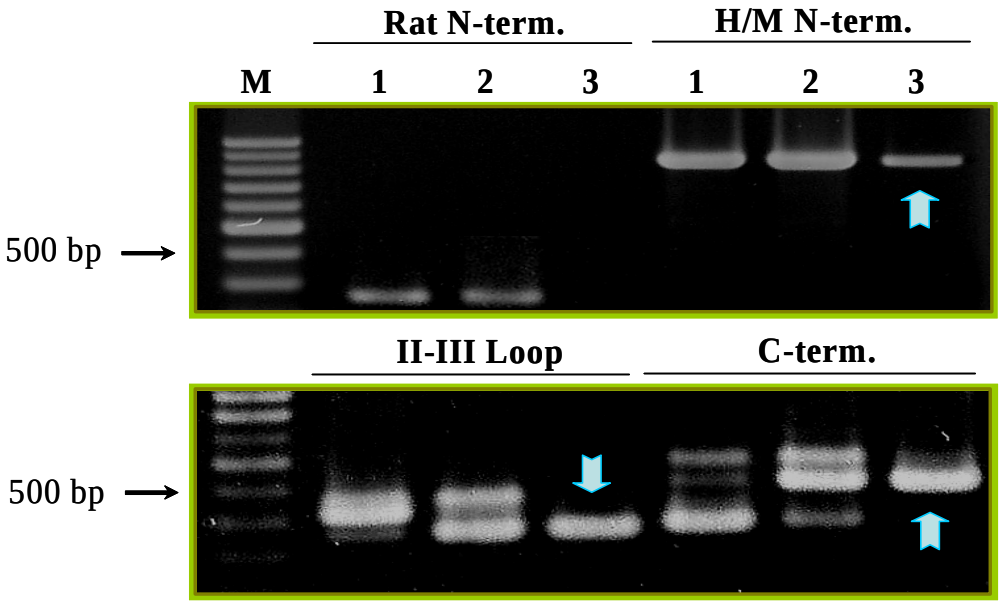


**Fig. 17. Identification of α1E splice variants in brain and the MPG neurons by RT-PCR analysis.**

Total RNA from rat cerebrum, cerebellum and MPG neurons was isolated and the cDNA fragment derived from α1E mRNA were amplified. With the specific primers for splice regions (table 2), the PCR fragments of the II-III loop and C-terminus were amplified in the MPG neurons. No transcript was detected in the MPG neurons (lane 3) with the rat N-terminus-specific primer. With the primer pairs for the human/mouse α1E N-terminus (H/M N-term), the specific fragments of the N-terminus was amplified in the MPG neurons. Cerebrum (lane 1) and cerebellum (lane 2) were used as positive controls for specific primers. Note that, only a single PCR fragment was detected in the MPG neurons.

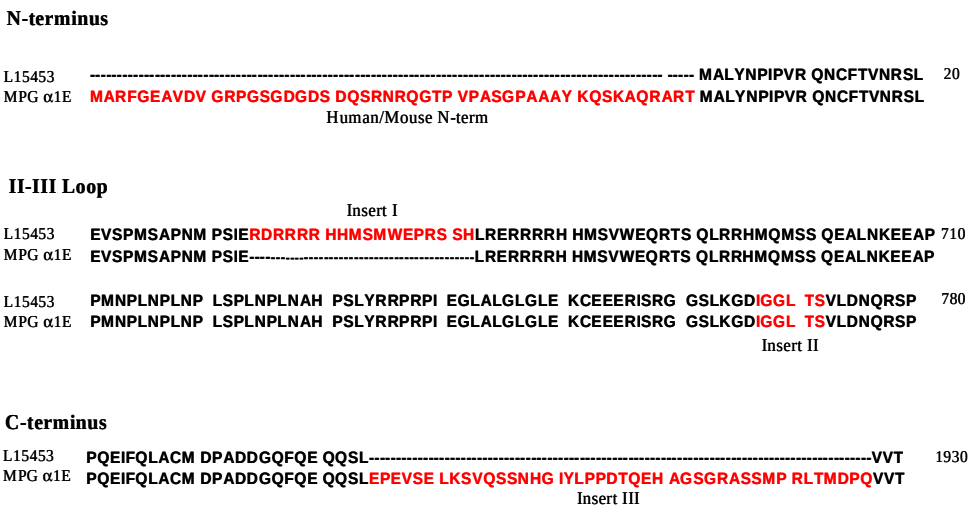


**Fig. 18. Comparison of the MPG α1E splice variant and the prototype α1E clones by alignment sequences of amino acid.**

Alignment of amino acid sequences show that the MPG α1E have additional 50 amino acids in the amino terminus as the human/mouse α1E clones. The MPG neurons α1E contains a shorter II-III loop lacking Insert 1 and longer C-terminus contains the additional 43 amino acid.

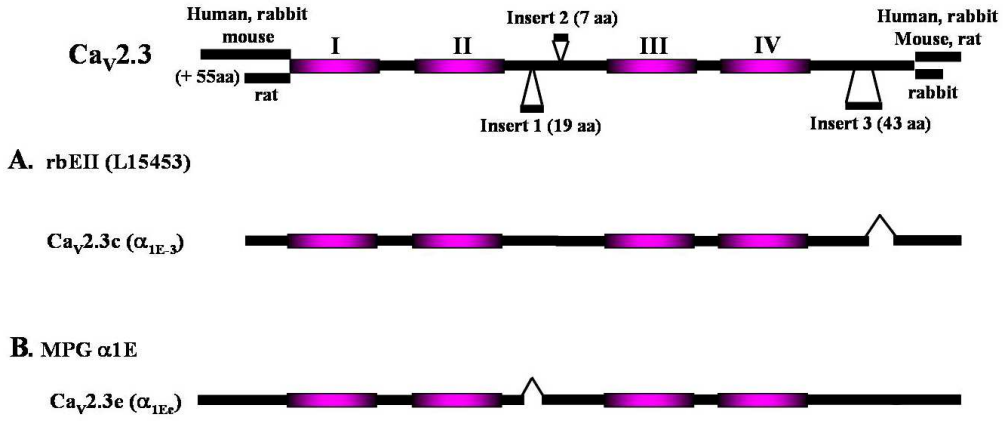


**Fig. 19. Splice variant isoform of the α1E identified in the MPG neurons.**

The primary structure of cloned α1E is shown in a linear form (upper). When the MPG α1E (B) was compared with rbEII (A), the splice variant of α1E in the MPG neurons has a longer N-, C- terminus and the shorter II-III loop.

## 4.6. Knock-out of R-type $Ca^{2+}$ currents in the MPG neurons by siRNA strategy.

To test whether the α1E splice variant encodes R-type $Ca^{2+}$ channels in the MPG neurons, ds/siRNA targetted to the MPG α1E was designed. Fluorescein-labeled scrambled ds/siRNA was used for negative control. the MPG neurons were transfected with either scrambled ds/siRNA or a mixture of scramble ds/siRNA and target ds/siRNA (1:1). Forty eight hours after transfection, fluorescein-positive the MPG neurons were observed under an inverse fluorescence microscope (Fig. 20).

To evaluate the effect of siRNA on transcript levels of the α1E subunit, semi-quantitative RT-PCR analysis was performed. When the expression level of α1E was normalized to that of GapDh, α1E transcript intensity level was greatly reduced by target ds/siRNA from 0.33 to 0.10. Inhibition of the MPG α1E mRNA levels by target ds/siRNA was about 70 % (Fig. 21). These data suggest that the target siRNA was specific for the α1E of the MPG neurons.

Finally, R-type currents were recorded in the MPG neurons transfected with the ds/siRNAs. As described above, the expression profile of HVA $Ca^{2+}$ channels was pharmacologically assessed. On average. nimodipine-sensitive L-type $Ca^{2+}$ channels contribute to 12 ± 6 % and 12 ± 4 %, N-type to 62 ± 11 % and 72 ± 6 %, and R-type to 17 ± 8 % and 5 ± 6 % of the total current, respectively, in the control group transfected with scrambled ds/siRNA (n=5) and the experimental group with the target ds/siRNA (n=6). It should be noted that the relative contribution of N-type currents was slightly increased as that of R-type currents was decreased (Fig. 22). Taken together, these data strongly suggested that R-type currents are encoded by the α1E splice variant in the MPG neurons.

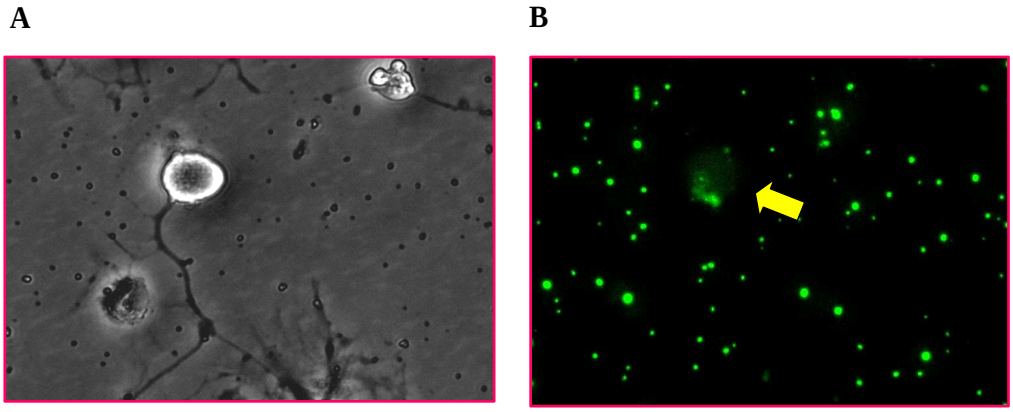


**Fig. 20. Transfection of the MPG neurons with fluorescein labeled siRNA.**

(A) : Microscopic image of the MPG neurons. (B) : Fluorescence microscopic image showing the MPG neurons transfected with fluorescein labeled siRNA. Transfection was performed using lipofectamine (1 mg/ml ; 100 μM RNA) at 37°C for 48 hours.

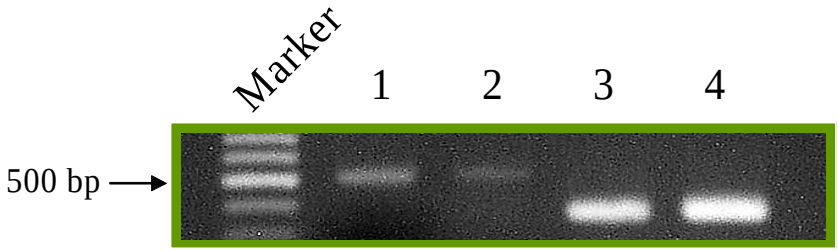


**Fig. 21. Semi-quantitative RT-PCR analysis of α1E transcript level in the MPG neurons transfected with α1E-specific siRNA.**

The MPG neurons was transfected with fluorescein-labeled scrambled ds/siRNA (lane 1) or a mixture of fluorescein-labeled ds/siRNA and α1E targeted ds/siRNA (lane 2) as described in the Materials and Methods. Total RNA was isolated from cell lysate after 48 hours transfection. The synthesis of α1E cDNA was carried out by semi-quantitative PCR and the product was analyzed by electrophoresis on 1.5% agarose gel with EtBr. lane 1 : fluorescein-labeled scrambled ds/siRNA, lane 2 : a mixture of fluorescein-labeled ds/siRNA and α1E targeted ds/siRNAlane 3, 4 : GapDh transcripts of lane 1 and 2 as an internal control were used, respectively.

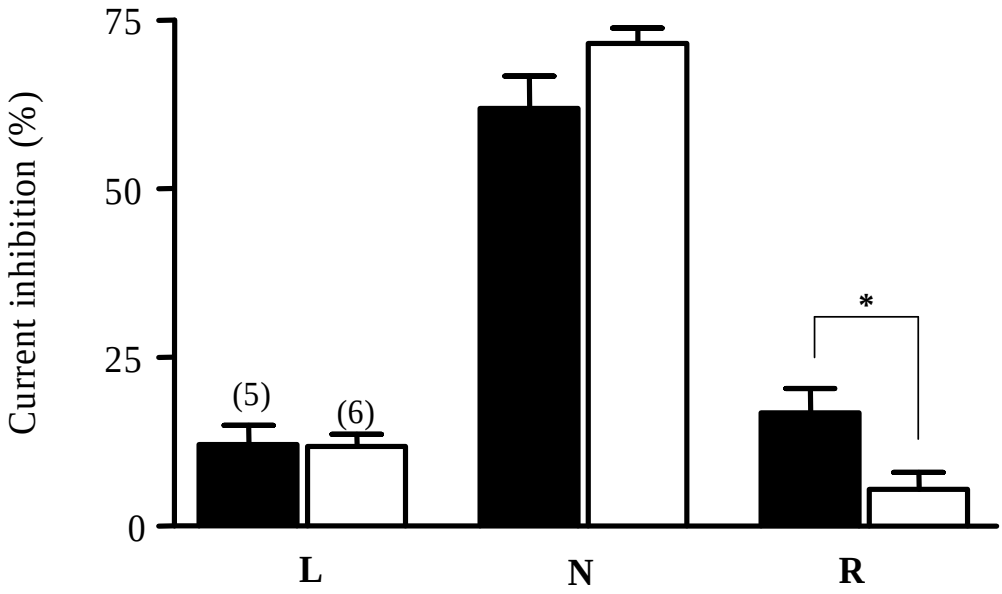


**Fig. 22. SiRNA silencing of SNX-482-insensitive R-type current in the MPG neurons.** The MPG neurons were transfected with fluorescein-labeling scrambled ds/siRNA (closed bar) or mixed fluorescein-labeling ds/siRNA and α1E targeted ds/siRNA (open bar) for 48 hours. Pharmacological dissection of $Ca^{2+}$ currents using isoform-specific toxins was described in the text. Note that inhibition of the N-type $Ca^{2+}$ channels was slightly increased after silencing of th α1E in the MPG neurons. Data are presented as means ± SEM. Numbers of cells tested is indicated in parentheses.

* $p < 0.05$

## 4.7. Characteristics of afterhyperpolarization (AHP) in the MPG neurons

As mentioned above, sympathetic and parasympathetic MPG neurons showed tonic and phasic firing patterns, respectively when supra-threshold current for 400 ms was intracellularly injected (Fig. 23A). On average, the firing frequency in sympathetic and parasympathetic MPG neurons, were $18.7 \pm 1.8$ Hz, (n=22) and $5.1 \pm 2.0$ Hz, (n=18), respectively (Fig. 23 C Top). To identify mechanisms underlying the difference in spike firing between the sympathetic and parasympathetic MPG neurons, afterhyperpolarization (AHP) following a single action potential was compared. In this regard, AHP following a single action potential was recorded and analyzed for acquiring two parameters, amplitude and duration as illustrated in Figure 24 (Greffrath et al., 2004). In general, sympathetic MPG neurons generated AHP with high amplitude and short duration in response to a depolarizing current injection for 10 ms, while parasympathetic ones showed AHP with low amplitude and long duration (Fig. 23B). On average, AHP amplitudes were $-14.9 \pm 3.0$ mV (n=17) and $-10.4 \pm 3.3$ mV (n=16), and AHP durations were $119.8 \pm 3.0$ ms (n=17) and $223.7 \pm 3.3$ ms (n=16) in sympathetic and parasympathetic MPG neurons, respectively (Fig 23C, middle and bottom).

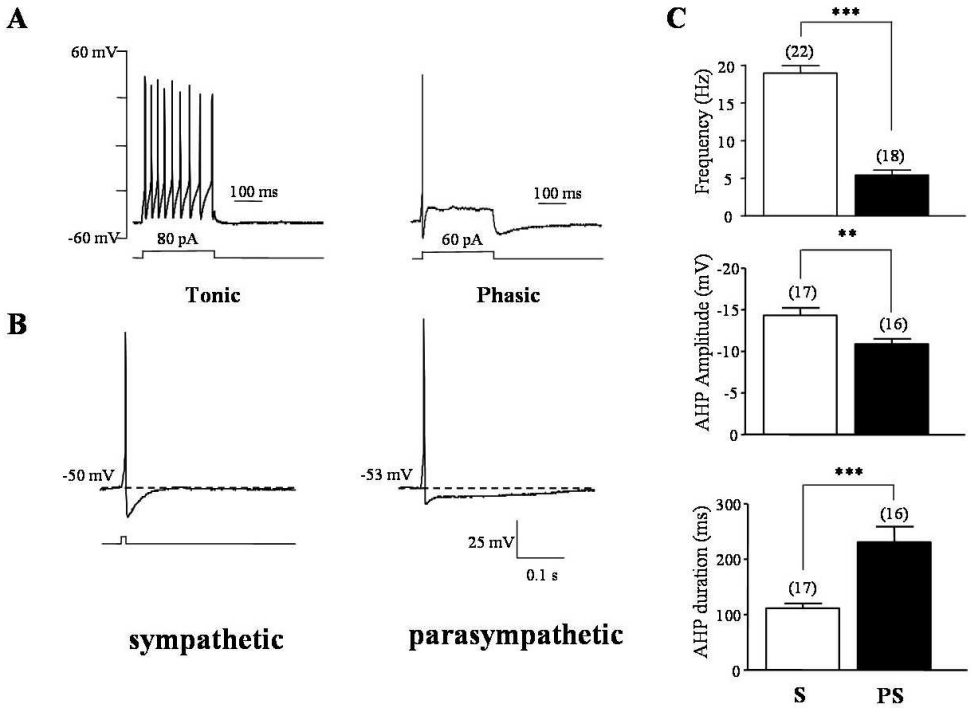


**Fig. 23. Cell type specific firing patterns and AHP properties in the MPG neurons.**

(A) : Representative traces of tonic and phasic spike firing in the sympathetic and parasympathetic MPG neurons was induced by injection of supra-threshold current for 400 ms, respectively. (B) : A single action potential is followed by AHP (afterhyperpolarization) that differs from the one found sympathetic and parasympathetic MPG neurons. AHP of the tonic and sympathetic MPG neurons showed a larger amplitude and a shorter duration than that of the phasic and parasympathetic ones. (C) : Bar graph showing differences in the firing frequency (top), AHP amplitude (middle) and AHP duration (bottom) between the sympathetic and parasympathetic MPG neurons. Data are presented as means±SEM. Numbers of cells tested is indicated in parentheses. ** $p < 0.01$, *** $p < 0.001$

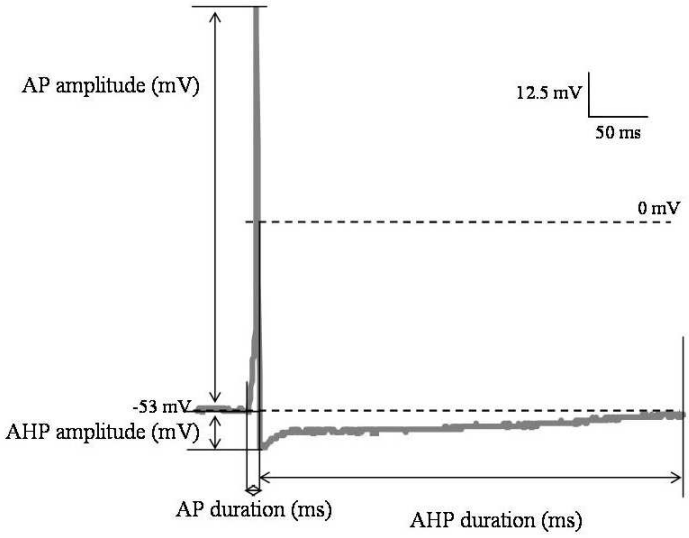


**Fig. 24. Analysis of AHP following a single action potential.**

The amplitude of AHP components was determined as the voltage difference between the firing level of the spike and the negative peak of the AHP. The duration of action potential was determined as the width between the start point of spike and the negative peak of the action potential. AHP duration was width between the negative peak of the AHP and end point of the AP train to the resting membrane potential level. Action potential amplitude was determined as the voltage difference between the resting level and the positive peak of the action potential.

## 4.8. Contribution of $Ca^{2+}$-activated $K^+$ channels to AHP in the MPG neurons

### 4.8.1. Molecular identification of the $Ca^{2+}$-activated $K^+$ channels in the MPG neurons

Previous studies have shown that $Ca^{2+}$-activated $K^+$ channels are responsible for generation of AHP (Blank, et al., 2004; Maylie, et al., 2003; Sah, et al., 2002). Therefore, expression profile of $Ca^{2+}$ activated $K^+$ channel mRNA subunits was determined by RT-PCR analysis with specific primer pairs (Table. 4) in the MPG neurons. Figure 25 showed that the MPG neurons express BK-α (438 bp), BK-β (293 bp), SK2 (151 bp) and SK3 (148 bp) transcripts but not SK1 (118 bp). In addition, the MPG neurons were found to express all of BK subunits β1, β2, and β4. Whole brain cDNA was used as a positive control for specific primer pairs (Table. 5) and GapDh was used as an internal standard. Smooth muscle cDNA was used as a positive control for BK β1 subunit (Fig. 26).

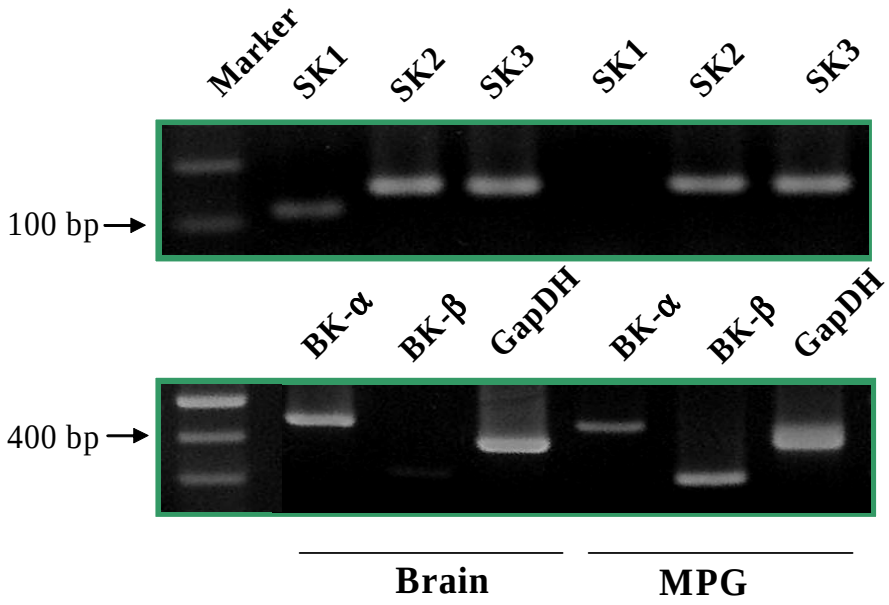


**Fig. 25. RT-PCR analysis of transcripts encoding $Ca^{2+}$-activated $K^{+}$ channel subunits (BK and SK channels) in the MPG neurons.**

Total RNA isolated from dissociated the MPG neurons was reverse transcribed, and amplified by PCR with specific primer pairs (Table 3). The resultant PCR products were separated and visualized on an agarose gel containing ethidium bromide (EtBr). GapDh RNA as an internal control and whole brain RNA as a positive control were used.

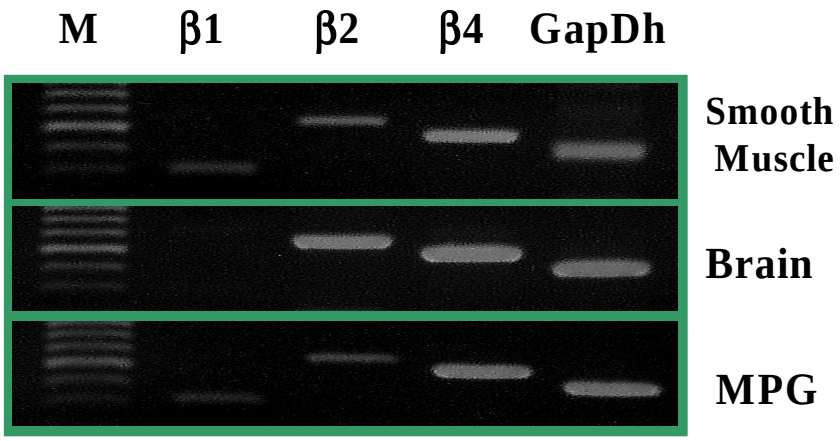


**Fig. 26. RT-PCR analysis of mRNA encoding the BK channel β subunit isoforms in the MPG neurons.**

Total RNA isolated from dissociated MPG neurons and RT-PCR analysis with specific primer pairs (Table 4) performed previously described. The resultant PCR product were separated and visualized on an agarose gel containing ethidium bromide (EtBr). GapDh RNA as an internal control and whole brain or smooth muscle RNA as positive controls were used.

### 4.8.2. Functional roles of the SK channels in generation of AHP in the MPG neurons

In many neurons, SK channels are responsible for generation of AHP (Sah 1996). Therefore, to elucidate functional roles of the SK channels in generation of AHP in sympathetic (Fig. 27A) and parasympathetic (Fig. 27B) MPG neurons were tested using apamin, a SK channel blocker and 1-EBIO, an activator. In a parasympathetic neuron, apamin (500 nM) and 1-EBIO (100 μM) significantly reduced and increased AHP duration, respectively without affecting AHP amplitude. On average, apamin reduced AHP durations from 119.8 ± 12.2 ms to 114.2 ± 11.3 ms and from 223.7 ± 27.9 ms to 89.5 ± 16.2 ms in sympathetic (n=9) and parasympathetic (n=11) MPG neurons, respectively. While, 100 μM 1-EBIO increased AHP duration from 119.8 ± 12.2 to 167.4 ± 10.0 and from 223.7 ± 27.9 to 290.7±37.1 in sympathetic (n=5) and parasympathetic MPG neurons (n=6), respectively (Fig. 28). To confirm the existence of the apamin-sensitive current components in the MPG neurons, outward tail current ($I_{AHP}$) evoked following a step from a holding potential of -50 mV to +10 mV was recorded under the amphotericin-perforated configuration of the patch clamp technique. In many other studies, a long duration (100 ms) of depolarizing step pulse procotol was used to maximize AHP amplitude. However, the protocol was not suitable in this study because $Ca^{2+}$ independent slow currents which generate burst firing were activated in AHP potential with SK current during 100 ms step pulse. Therefore 100 ms duration step pulse usually accepted by studies about burst firing or spontaneous burst firing neurons to identify potentiation next bursting. Therefore in this study accepted above describing 10 ms duration protocol. As illustrated in Fig. 29A and 29B, a phasic parasympathetic MPG neurons displayed $I_{AHP}$ that was longer in duration and shorter in peak amplitude when compared with those of a sympathetic ones. On average, durations of $I_{AHP}$ were 86.4 ± 2.3 ms (n=8) and 313.8 ± 3.3 ms (n=11), and

amplitudes of $I_{AHP}$ were 555.3 ± 2.8 mV (n=8) and 134.8 ± 3.3 mV (n=11) in sympathetic and parasympathetic MPG neurons, respectively. Apamin (500 nM) reduced the $I_{AHP}$ duration by 73 ± 2 % without affecting amplitude in parasympathetic MPG neurons. In sympathetic MPG neurons, apamin reduced 39 ± 7 % of duration and 14 ± 6 % of amplitude (Fig. 30A, B). Taken together, these data suggest that SK channels are responsible for generation of mAHP blocking by apamin in the MPG neurons. However, relative contribution of SK channels to the mAHP is much larger in parasympathetic neurons than sympathetic neurons.

### 4.8.3. Functional roles of mAHP in excitability of the MPG neurons.

Finally, the functional roles of SK channels were investigated in the spike firing of the MPG neurons. Apamin (500 mM) greatly increased the firing frequency in parasympathetic MPG neurons (% of change: 170 ± 3, n=10) but not in sympathetic MPG neurons (% of change: 110 ± 1, n=8). The SK channel activator 1-EBIO (100 μM) failed to change the firing frequency in both sympathetic and parasympathetic MPG neurons (Fig. 31). Taken together, these data suggest that SK channel determine the firing patterns in sympathetic and parasympathetic MPG neurons by generating mAHP.

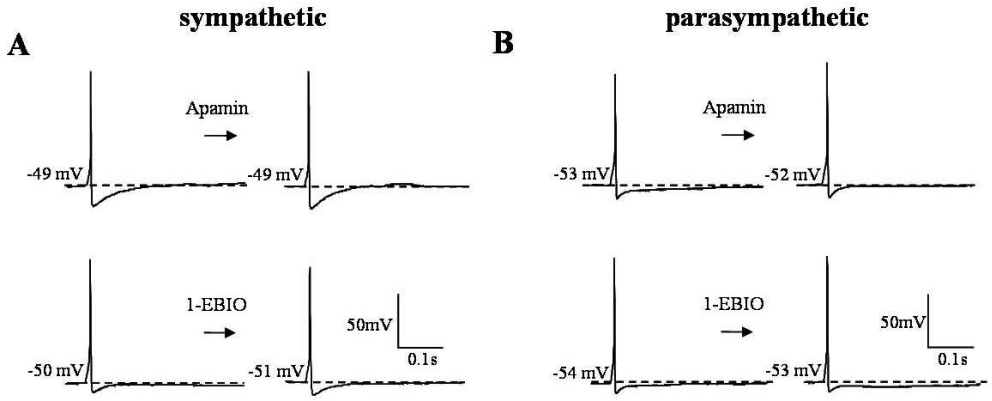


**Fig. 27. Contribution of apamin-sensitive $Ca^{2+}$-activated $K^+$ channels to AHP in the MPG neurons.**

AHP duration and amplitude measured before and after the application of $SK_{Ca}$ channel specific blocker apamin (500 nM) and activator 1-EBIO (100 μM) in (A) sympathetic and (B) parasympathetic MPG neurons. A single action potentials was triggered by 10 ms supra-threshold current injection from resting membrane potential in the MPG neurons.

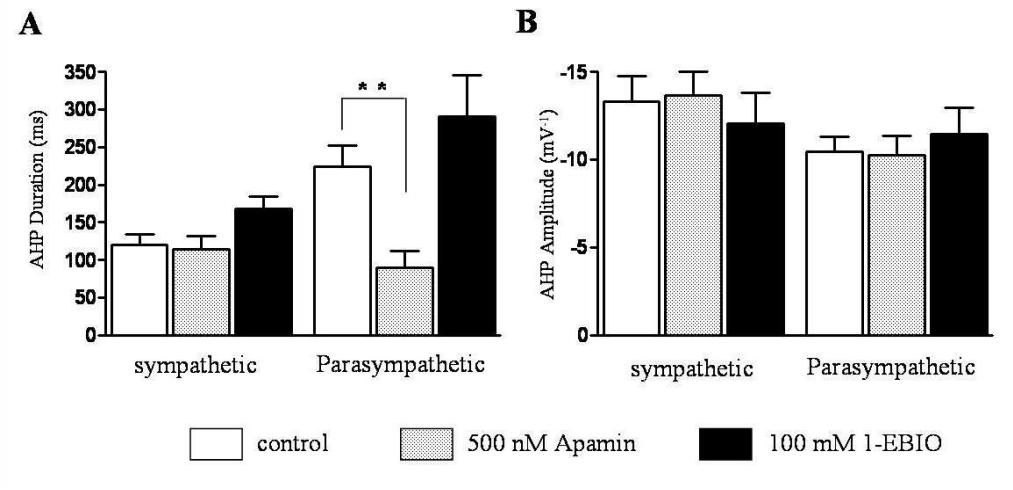


**Fig. 28. Summary of contribution of apamin-sensitive SK channels to AHP in the MPG neurons.**

Effects of SK channel modulators on (A) AHP duration and (B) amplitude of AHP in sympathetic and parasympathetic MPG neurons. ** $p < 0.01$

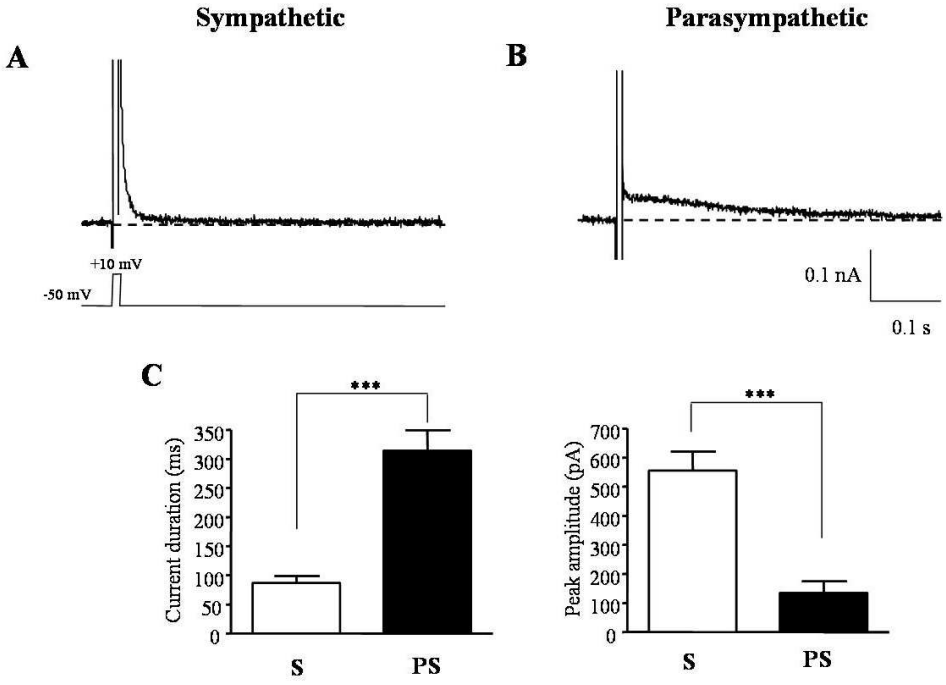


**Fig. 29. Measurement of $I_{AHP}$ in the MPG neurons.**

Representative traces of $I_{AHP}$ measured in the (A) sympathetic and (B) parasympathetic MPG neurons. $I_{AHP}$ was evoked to depolarizing pulses +10 mV for 10 ms from a holding potential of -50 mV. (C) : Bar graphs showing the differences in the current duration (left) and peak amplitude (right) between the sympathetic and parasympathetic MPG neurons. Numbers of cells tested is indicated in parentheses. *** P< 0.001

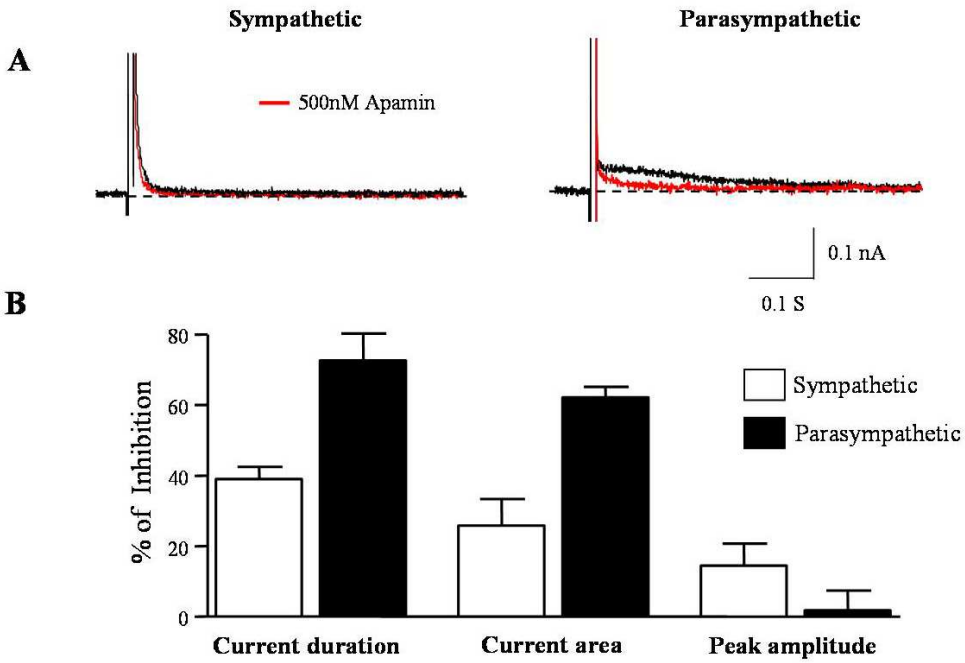


**Fig. 30. Effect of a $SK_{Ca}$ channel-specific blocker, apamin on $I_{AHP}$ in the MPG neurons.**

(A) : Representative trace of $I_{AHP}$ in the presence of 500 nM apamin. Note that the majority of outward current in the parasympathetic MPG neurons was inhibited by apamin-induced $I_{AHP}$ unlike the sympathetic ones. (B) : Bar graphs showing the percentage of inhibition of duration, area, and peak amplitude in the sympathetic and parasympathetic MPG neurons. $I_{AHP}$ was measured in the MPG neurons evoked by depolarizing pulses to +10 mV for 10 ms from a holding potential of -50 mV. Data are presented as means ± SEM. Numbers of cells tested is indicated in parentheses.

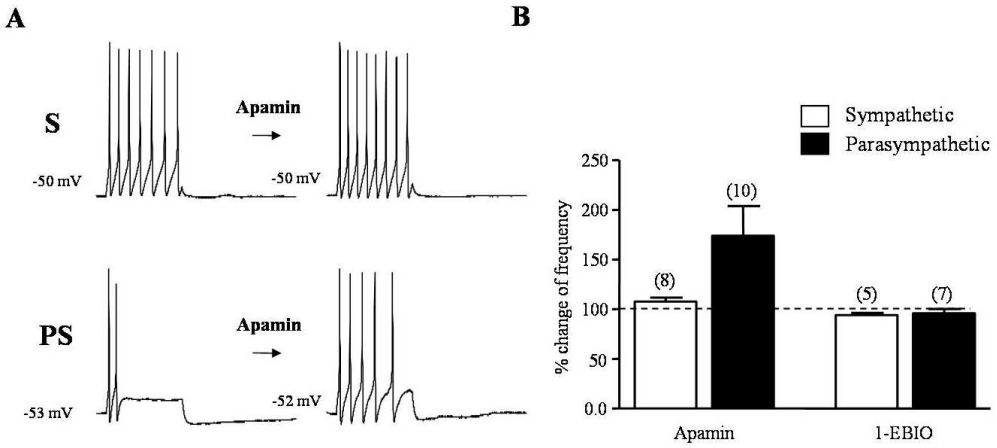


**Fig. 31. Effects of $SK_{Ca}$ channel modulators on firing frequency in the MPG neurons.** (A) : Representative traces of action potential recorded before and after application of apamin (100 nM) in the sympathetic (upper) and parasympathetic (bottom) MPG neurons. Firing frequency increased in the presence of apamin. (B) : Bar graph showing the % change of firing frequency when applicated the drugs (apamin and 1-EBIO) in sympathetic and parasympathetic MPG neurons. $K_{Ca}$ activator 1-EBIO (100 μM) did not affect the change of firing frequency. Trains of action potentials evoked by 400 ms supra-threshold current injection from the resting membrane potentil. Numbers of cells tested is indicated in parentheses.

### 4.8.4. Functional roles of BK channels in the MPG neurons

BK channels are known to be sensitive to tetraethylammonium (TEA) in a low micro molar range (Blatz and Magleby, 1987), the scorpion-derived peptides, charybdotoxin and iberiotoxin (Galvez et al., 1990). Recently, the mycotoxins paxilline and penitrem A have also been described to block BK channels (Strobaek et al., 2000). Of these blockers, iberiotoxin and paxilline are selective for BK channels, while the others non-selectively block different potassium channels. To examine the role of the BK channel in regulation of excitability in the MPG neurons, the BK channel blockers were tested under the current clamp mode. Application of 1 mM TEA-Cl or 10 μM paxilline resulted in slow repolarization of action potential in the parasympathetic MPG neurons (Fig. 32 Top). In the sympathetic MPG neurons, those blockers was less effective for slowing repolarization of action potential. When measured at 0 mV, the % changes of action potential duration by 1 mM TEA-Cl or 10 μM paxillin were 110 ± 28 % or 110 ± 10 % and 150 ± 20 % or 160 ± 30 % in sympathetic and parasympathetic MPG neurons, respectively (Fig. 32 bottom). Iberiotoxin (100 nM) and charybdotoxin (100 nM) had no effect on relaxation of action potential. These results are consistent with the finding that the MPG neurons express the β4 subunit of BK channels.

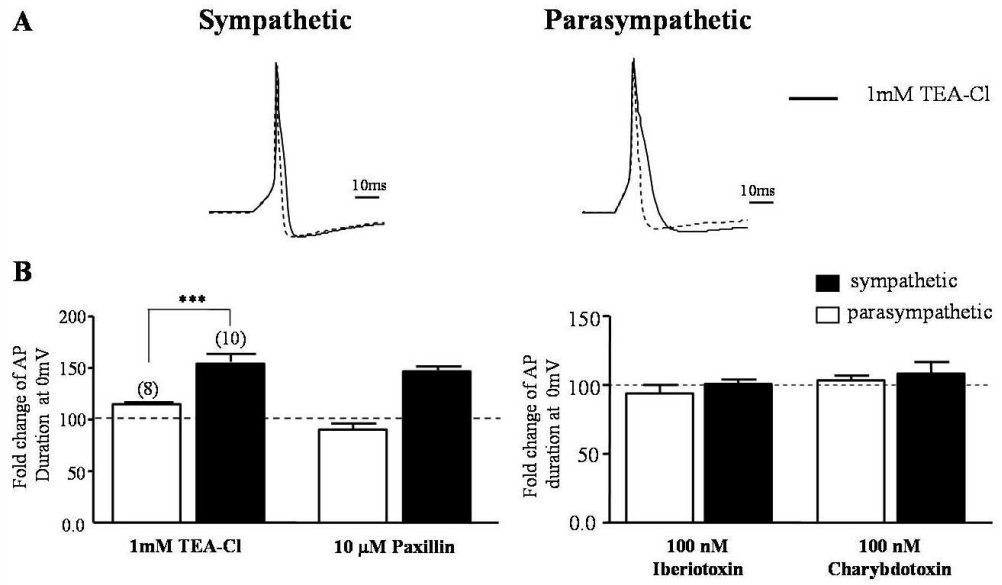


**Fig. 32. Effects of $BK_{Ca}$ channel blockers on action potential repolarization in the MPG neurons.**

(A) : Action potential wave-forms before (dotted line) and after (solid line) bath application of 1 mM TEA-Cl in the MPG neurons. (B) : Bar graphs showing % change of the action potential determined different BK channel blockers were applicated. Note that repolarization of action potential was sensitive to TEA and paxillin but not to iberiotoxin and charybdotoxin. There was no effect on the action potential duration when bath applicated $BK_{Ca}$ channel specific blocker Iberiotoxin (100 nM) and charybdotoxin (100 nM). Numbers of cells tested is indicated in parentheses. *** $P < 0.001$

## 4.9. Effects of $Ca^{2+}$ ion on excitability in the MPG neurons

In general, $Ca^{2+}$ influx through VACCs may be critical for activation of SK channels to regulate spike firing. First of all, therefore effects of extracellular $Ca^{2+}$ on excitability of the MPG neurons were tested. As illustrated Figure 33, removal of extracellular $Ca^{2+}$ (i.e. 0 mM $Ca^{2+}$) increased firing frequency in both sympathetic and parasympathetic MPG neurons. On average, in the absence of extracellular $Ca^{2+}$, the firing frequency was increased from $17 \pm 3$ to $24 \pm 3$ (% change of frequency was 140 $\pm 5$ ) in sympathetic MPG neurons, and increased firing frequency from $6 \pm 1$ to $15 \pm 2$ (% change of frequency was $253 \pm 32$) in parasympathetic MPG neurons. Chelation of intracellular $Ca^{2+}$ by BAPTA-AM (20 μM) produced the same effect as 0 mM $Ca^{2+}$ did. On average, BAPTA/AM increased the firing frequency from $17 \pm 4$ to $18 \pm 2$ in sympathetic MPG neurons (% change of frequency was $109 \pm 11$ ) and from $5 \pm 1$ to $12 \pm 1$ (% change of frequency was $307 \pm 77$ ) in parasympathetic MPG neurons (Fig. 34). Taken together, these results suggested that extracellular $Ca^{2+}$ ion is critical for regulating excitability of the MPG neurons.

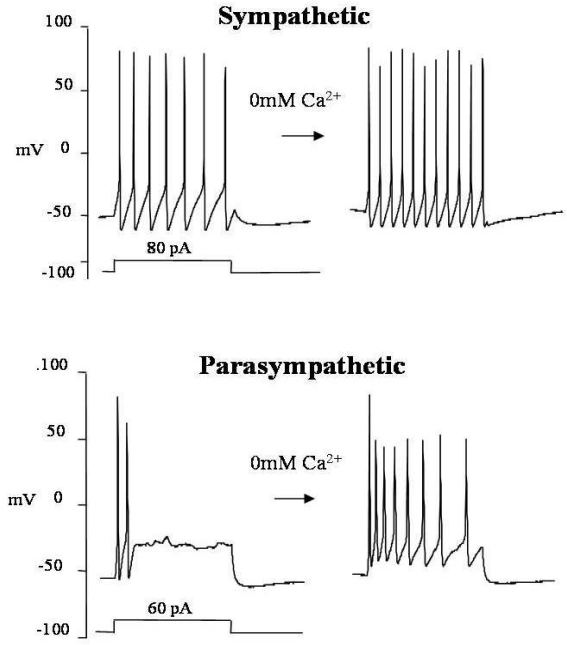


**Fig. 33. Effects of extracellular $Ca^{2+}$ ion on excitability in the MPG neurons.**

Representation traces of spike firings eviked by a prolonged injection of supra-threshold current before and after removal of extracellular $Ca^{2+}$ (0 mM) in (A) the sympathetic and (B) parasymapthetic neurons.

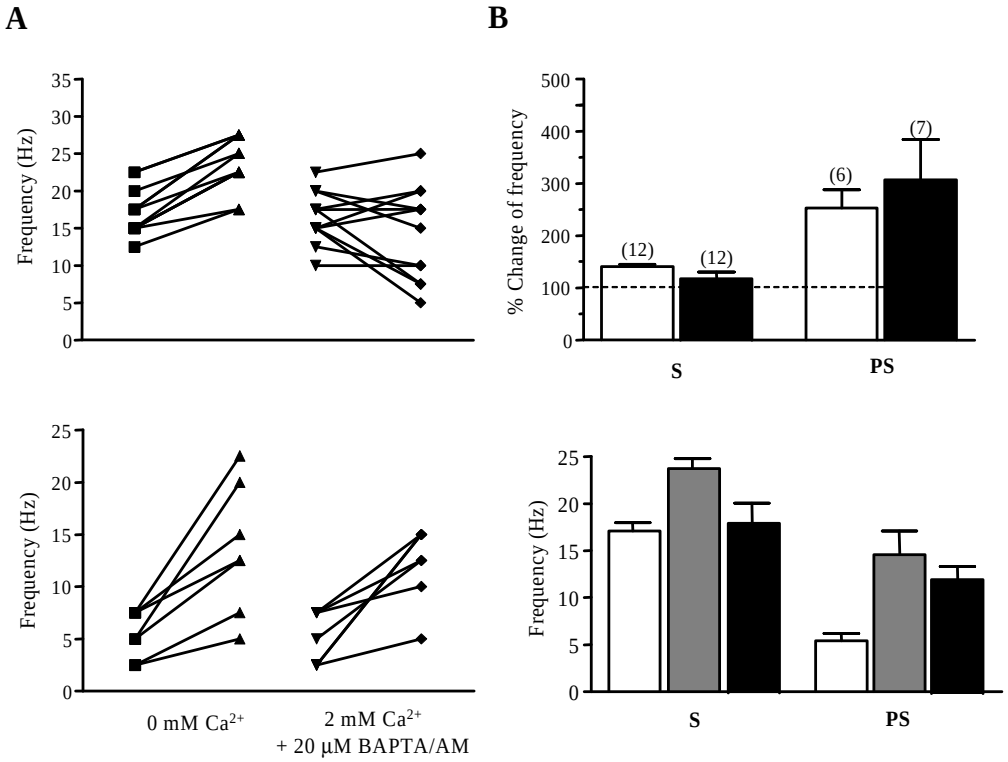


**Fig. 34. Summary of effects of extracellular $Ca^{2+}$ ion on excitability in the MPG neurons.**

(A) : Effects of removal of extracellular $Ca^{2+}$ and BAPTA/AM on the spike frequency in the sympathetic and parasympathetic neurons. (B) : Summary. Bar graphs showing with % change of frequency (upper) or the absolute values of frequency (bottom). Upper white bar; 0 mM $Ca^{2+}$ solution, black bar; 20 μM BAPTA/AM, Bottom white bar; 2 mM $Ca^{2+}$ solution (normal PSS), gray bar; 0 mM $Ca^{2+}$ solution, black bar; 2 mM $Ca^{2+}$ solution containing 20 μM BAPTA/AM. Numbers of cells tested is indicated in parentheses.

## 4.10. Contribution of HVA $Ca^{2+}$ channel isoforms on spike firing in the MPG neurons.

$Ca^{2+}$ influx through voltage-activated $Ca^{2+}$ channels during the action potential influences the firing properties of many types of neurons either directly or through $Ca^{2+}$-activated $K^{+}$ channels (Sah, 1996). Contribution of HVA $Ca^{2+}$ channel isoforms to spike firing was examined in the MPG neurons using $Ca^{2+}$ channel blockers including $CdCl_2$, (a non-specific $Ca^{2+}$ channel blocker), nimodipine (an L-type $Ca^{2+}$ channel blocker) and ω-conotoxin GVIA (an N-type $Ca^{2+}$ channel blocker). $CdCl_2$ markedly increased firing frequency in the parasympathetic MPG neurons, but not in the sympathetic ones. Interestingly, application of 10 μM nimodipine significantly reduced firing frequency in the sympathetic MPG neurons without affecting that in the parasympathetic ones. Application of 3 μM ω-conotoxin GVIA increased firing frequency in both sympathetic and parasympathetic MPG neurons (Fig. 35). On average, $CdCl_2$, Nimodipine and ω-conotoxin GVIA changed % change in firing frequency by 112 ± 8 %, 40 ± 6 %, and 152 ± 15 %, respectively in the sympathetic MPG neurons. and by 333 ± 48 %, 106 ±11 %, and 243 ± 23 %, respectively in the parasympathetic MPG neurons. Application of 300 μM $NiCl_2$ and 10 μM Mibefradil slightly decreased firing frequency in the sympathetic MPG neurons (% change in firing frequency were 79 ± 8 % and 84 ± 6 %, respectively), while little affected that in parasympathetic ones (% change in firing frequency were 105 ±12 % and 93 ±15 %, respectively). Taken together, these data suggest that L-and N-type HVA $Ca^{2+}$ channel have opposite roles in regulating spike firing in the sympathetic MPG neurons while, in parasympathetic ones, both L- and N-type HVA $Ca^{2+}$ channels same roles regulating spike firing. In addition, R-type Ca2+ channels appeared to be not implicated in regulating excitability in both types of neurons

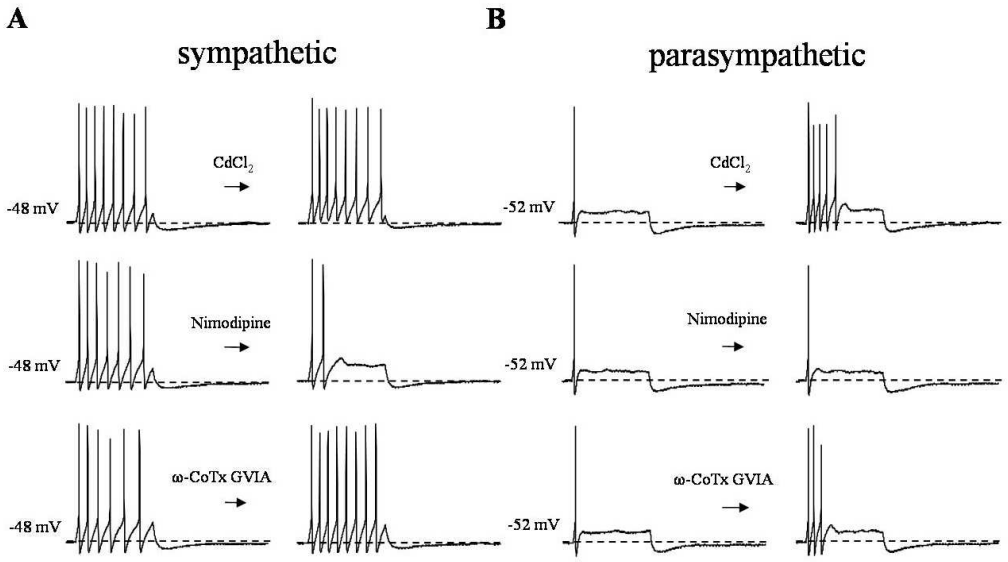


**Fig. 35. Differential contribution of HVA $Ca^{2+}$ channel isoforms to excitability in the MPG neurons.**

Representative traces showing effects of $Ca^{2+}$ channel blockers on firing frequency in (A) the tonic and sympathetic and (B) the phasic and parasympathetic MPG neurons. Tonic and phasic firing were induced by injection of supra-threshold current for 400 ms in the (A) sympathetic and (B) parasympathetic MPG neurons, respectively. Firing frequency was measured before and after bath application $CdCl_2$ (300 μM), Nimodipine (10 μM), and ω-conotoxin GVIA (3 μM)

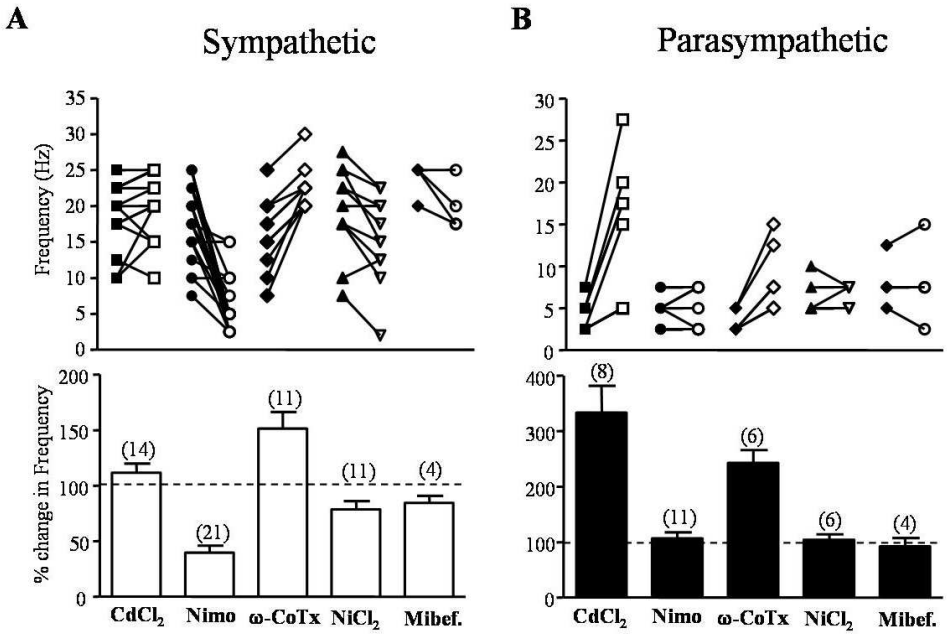


**Fig. 36. Summary of HVA $Ca^{2+}$ channel blockers on excitability in the MPG neurons.** Effects of different HVA $Ca^{2+}$ channel blockers on firing frequency in (A) sympathetic and (B) parasympathetic MPG neurons. Concentrations of blockers used are as follow : $CdCl_2$ (300 μM), Nimodipine (10 μM), ω-conotoxin GVIA (3 μM), $NiCl_2$ (300 μM), and Mibefradil (10 μM). Closed and open symbols in the upper line graphs represent control and toxin-treatment, respectively. Numbers of cells tested is indicated in parentheses. Data are presented as means±SEM

## 4.11. Effect of L-and N-type $Ca^{2+}$ channels on AHP and $I_{AHP}$ in the MPG neurons.

To explain the differential contribution of L-and N-type $Ca^{2+}$ channels on the spike firing, it was tested whether HVA $Ca^{2+}$ channel are specifically coupled with SK or BK channels. 300 μM $CdCl_2$ greatly reduced AHP size in the MPG neurons. On average, % change of AHP durations were $64 \pm 6$ % and $21 \pm 5$ % and % change of AHP amplitude at 150 ms (peak of mAHP) were $60 \pm 10$ % and $65 \pm 10$ % in sympathetic and parasympathetic MPG neurons, respectively (Fig. 37, 38). 10 μM nimodipine increased AHP duration and amplitude, on average, % change of AHP duration was $210 \pm 30$ % (n=8), and % change of AHP amplitude at 150 ms was 190 $\pm$ 40 %, (n=8) in sympathetic MPG neurons. Conversely, 3 μM ω-conotoxin GVIA slightly decreased AHP duration and amplitude, on average, % change of AHP duration was $90 \pm 10$ % (n=7) and % change of AHP amplitude at 150 ms was $40 \pm 2$ % (n=7) in sympathetic MPG neurons. In parasympathetic MPG neurons, nimodipine slightly increased AHP size. On average, % change of AHP durations and amplitude were $120 \pm 10$ %, and $120 \pm 20$ %, respectively, while ω-conotoxin GVIA greatly decreased AHP, on average, % change of AHP duration and amplitude were $40 \pm 2$ %, and $30 \pm 1$ %, respectively (Fig. 37, 38).

Next, effects of $Ca^{2+}$ channel blockers on $mI_{AHP}$ were examined in the MPG neurons. As described above, $mI_{AHP}$ of the MPG neurons was evoked depolarizing pulses to +10 mV for 10 ms from a holding potential of -50 mV. Nimodipine enhanced $mI_{AHP}$ in sympathetic MPG neurons on average, % change of $mI_{AHP}$ amplitude and duration were $40 \pm 4$ % and $52 \pm 4$ %, respectively. While, nimodipine slightly reduced $mI_{AHP}$, on average % change of reducing $mI_{AHP}$ amplitude and duration were $18 \pm 3$ % and $25 \pm 3$ %, respectively. Omega-conotoxin GVIA slightly reduced $I_{AHP}$ in sympathetic neurons on average % change of reducing $mI_{AHP}$ amplitude

and duration were 25 ± 2 % and 20 ± 2 %, respectively. Conversely, greatly decreased $mI_{AHP}$ in parasympathetic MPG neurons, on average % change of reducing $mI_{AHP}$ amplitude and duration were 73 ± 2 % and 77 ± 2 %, respectively (Fig. 39, 40). This finding indicated $mI_{AHP}$ was exclusively coupled to N-type $Ca^{2+}$ channel in phasic parasympathetic MPG neurons. Taken together, these data suggest that each $Ca^{2+}$ channel isoform makes a specific coupling to SK channels in the MPG neurons.

Finally, to investigate correlation between $Ca^{2+}$ channel isoforms and BK channels, examined effects of $Ca^{2+}$ channel blocker on transient outward current in the MPG neurons (Fig. 41). As previously described, $mI_{AHP}$ was measured by evoked to +10 mV depolarizing pulses for 10 ms from a holding potential of -50 mV. Even though, most of this transient outward peak current blocked by $CdCl_2$ by % of inhibition were 63 ± 7 % and 50 ± 8 % in sympathetic and parasympathetic MPG neurons, respectively, there was remaining apamin insensitive transient peak current. Application of nimodipine particularly reduced transient peak current in sympathetic MPG neurons (% of inhibition : 42 ± 7 %), while less affected in parasympathetic ones (% of inhibition : 15 ± 7 %). Omega-conotoxin GVIA slightly decreased transient peak current in sympathetic and parasympathetic MPG neurons (% of inhibition : 4 ± 2 % and 21 ± 8 %, respectively). These data suggested that transient outward current induced by BK channels coupled with L-type $Ca^{2+}$ channel in sympathetic MPG neuron.

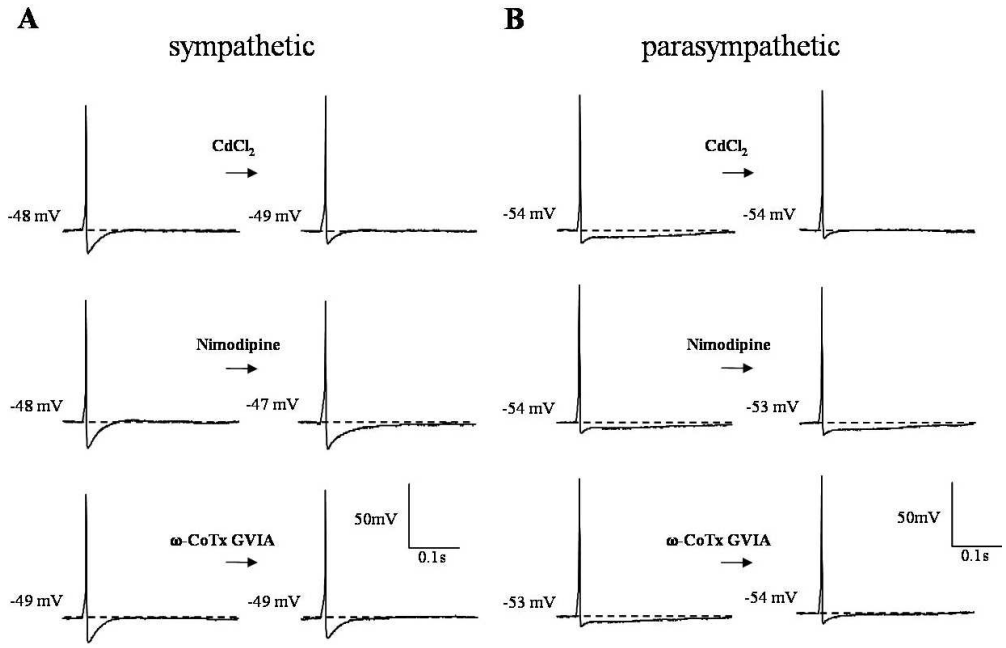


**Fig. 37. Effects of HVA $Ca^{2+}$ channel blockers on AHP in the MPG neurons.**

Representative traces showing AHPs before and after application of $Ca^{2+}$ channel blockers, Nimodipine (10 μM), ω-conotoxin GVIA (3 μM), and $CdCl_2$ (300 μM) in (A) the sympathetic and (B) parasympathetic MPG neurons. A single action potentials were evoked by 10 ms supra-threshold current injections from resting membrane potential to monitor the AHP. HVA $Ca^{2+}$ channel blockers differentially contribute to the AHP in sympathetic and parasympathetic MPG neurons.

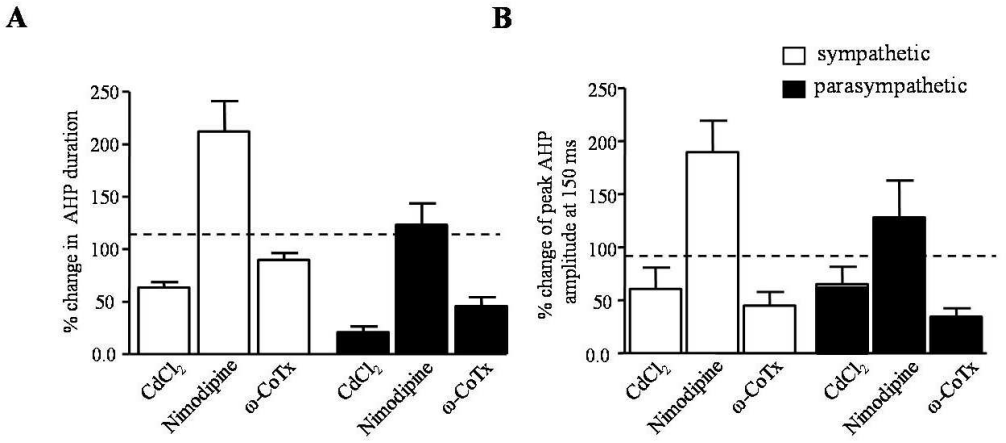


**Fig. 38. Summary of the effects of HVA $Ca^{2+}$ channel blockers on AHP in the MPG neurons.**

Bar graphs comparing the % change of AHP (A) duration or (B) AHP amplitude with the sympathetic and parasympathetic MPG neurons after bath application of HVA $Ca^{2+}$ channel blockers. Data are presented as means±SEM. Numbers of cells tested is indicated in parentheses.

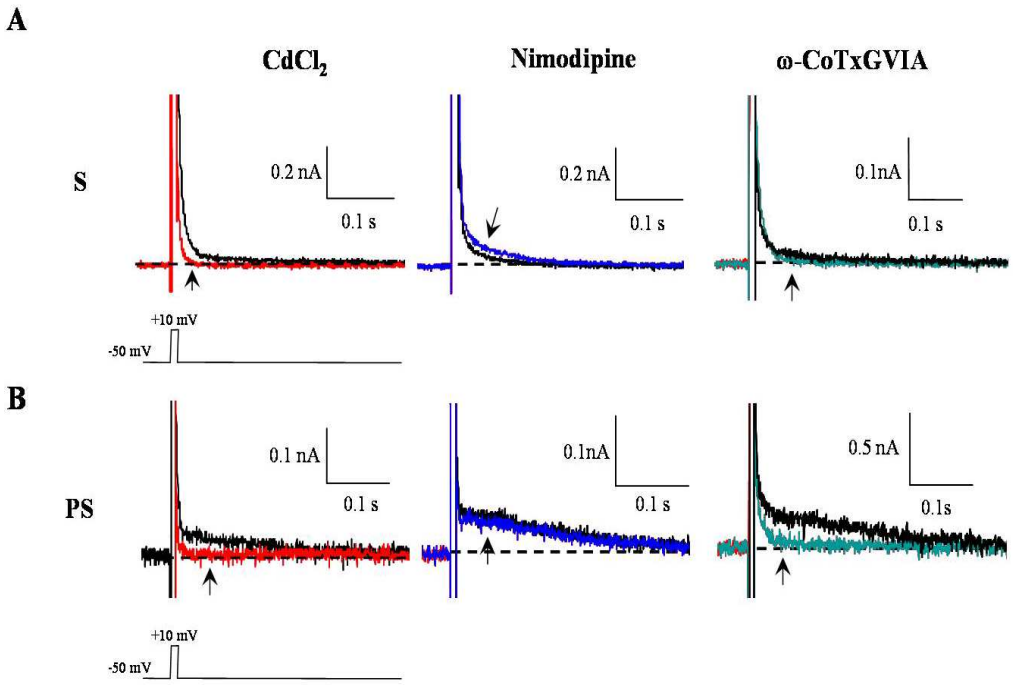


**Fig. 39. Effects of HVA $Ca^{2+}$ channel blockers on $mI_{AHP}$ in the MPG neurons.**

Representative traces showing effects of $Ca^{2+}$ channel blockers on $I_{AHP}$ in the (A) sympathetic and (B) parasympathetic MPG neurons. The tail currents ($mI_{AHP}$) were recorded after depolarizing pulses to +10 mV for 10 ms from a holding potential of -50 mV.

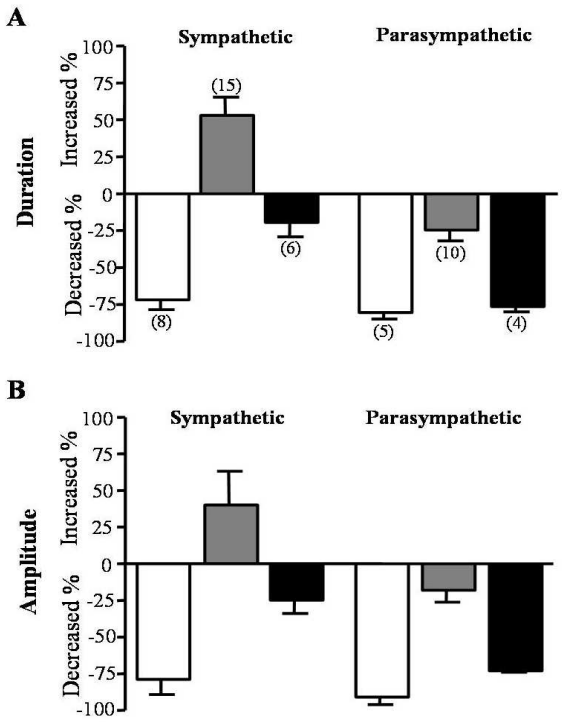


**Fig. 40. Summary of the effects of HVA $Ca^{2+}$ channel blockers on $mI_{AHP}$ in the MPG neurons.**

Bar graph showing changes in percentage of $mI_{AHP}$ (A) duration and (B) amplitude in the sympathetic and parasympathetic MPG neurons by HVA $Ca^{2+}$ channel blockers. Numbers of cells tested is indicated in parentheses. Data are presented as means ± SEM

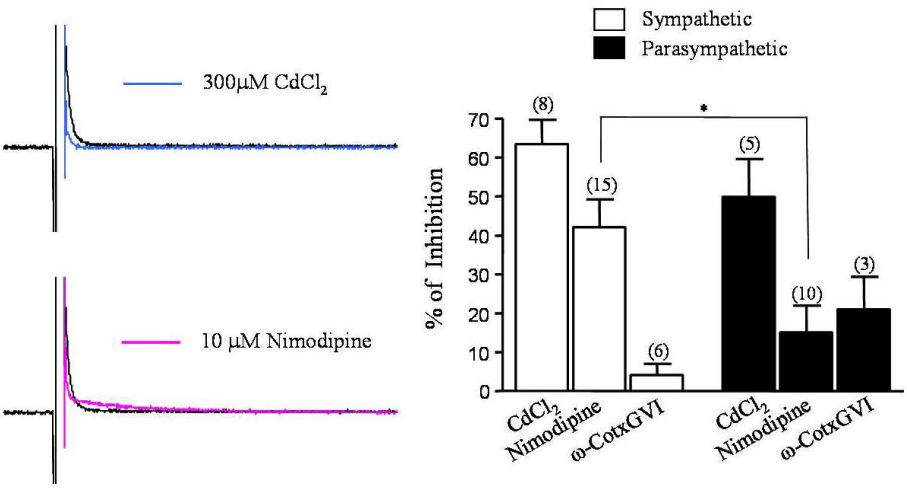


**Fig. 41. Effects of $Ca^{2+}$ channel blockers on fast transient outward current in the MPG neurons.**

(Left) : Representative traces showing $fI_{AHP}$ in the absence or presence of $CdCl_2$ (300 μM), Nimodipine (10 μM) and ω-conotoxin GVIA (3 μM). (Right) : Summary of the effects of $Ca^{2+}$ channel blockers on $fI_{AHP}$ in the sympathetic and parasympathetic MPG neurons. The amplitude of $fI_{AHP}$ was measured 3 ms after depolarizing pulses to +10 mV. * $P< 0.05$.

## 4.12. Effects of $Ca^{2+}$-activated $Cl^-$ channels on firing frequency in the sympathetic MPG neurons

In many types of neurons, a transient outward current contributes to the initial phase of repolarization during the action potential. Recent studies have suggested that $Ca^{2+}$-activated $Cl^-$ channels (CaCCs) is also involved in the processed of repolarization and afterdepolarization (Yanfang Xu et al. 2002; Hartzell C. et al., 2005). To investigate the relationship between CaCCs and excitability in the MPG neurons, CaCC blockers (300 μM Niflumic acid or 100 μM DIDS) were tested in the sympathetic MPG neurons. Bath application of niflumic acid or DIDS significantly reduced firing frequency in the sympathetic MPG neurons, which was reminiscent of nimodipine effect (Fig. 42). In addition, these blockers increased $I_{AHP}$ in the sympathetic MPG neurons (Fig. 43), On average, niflumic acid increased % change of peak amplitude and $mI_{AHP}$ amplitude to $130 \pm 10$ % and $350 \pm 60$ %, respectively in sympathetic MPG neurons. In parasympathetic MPG neurons, niflumic acid or DIDS had no effects on firing frequency (data not shown), and slightly reduced outward current amplitude ($mI_{AHP}$) about $20 \pm 1$%, while slight increase in peak current about $150 \pm 30$ % (Fig. 43). Taken together, these results suggest that firing properties of sympathetic MPG neurons was partially affected by the CaCC and effect of this channel was reminiscent of L-type $Ca^{2+}$ channel.

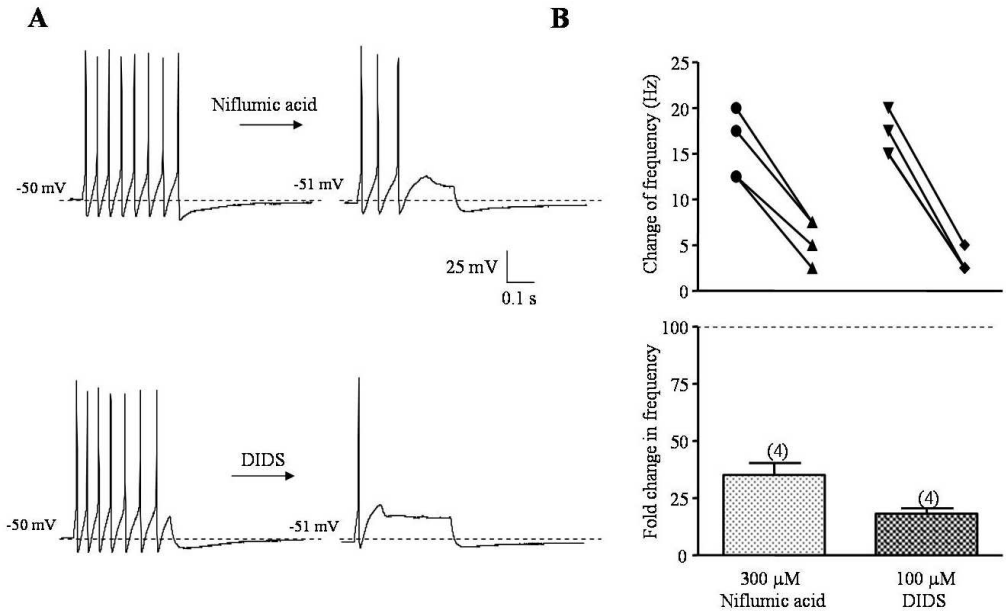


**Fig. 42. $Ca^{2+}$-activated $Cl^-$ channel blockers decreased firing frequency in the sympathetic MPG neurons.**

(A) : Representative traces showing spike firing before and after application of niflumic acid (300 μM) and DIDS (100 μ). (B) : Graphs showing the change of firing frequency (Hz), (upper) and fold change in frequency (lower) before and after CaCC blockers in the sympathetic MPG neurons. Numbers of cells tested is indicated in parentheses. Data were presented as means ± SEM

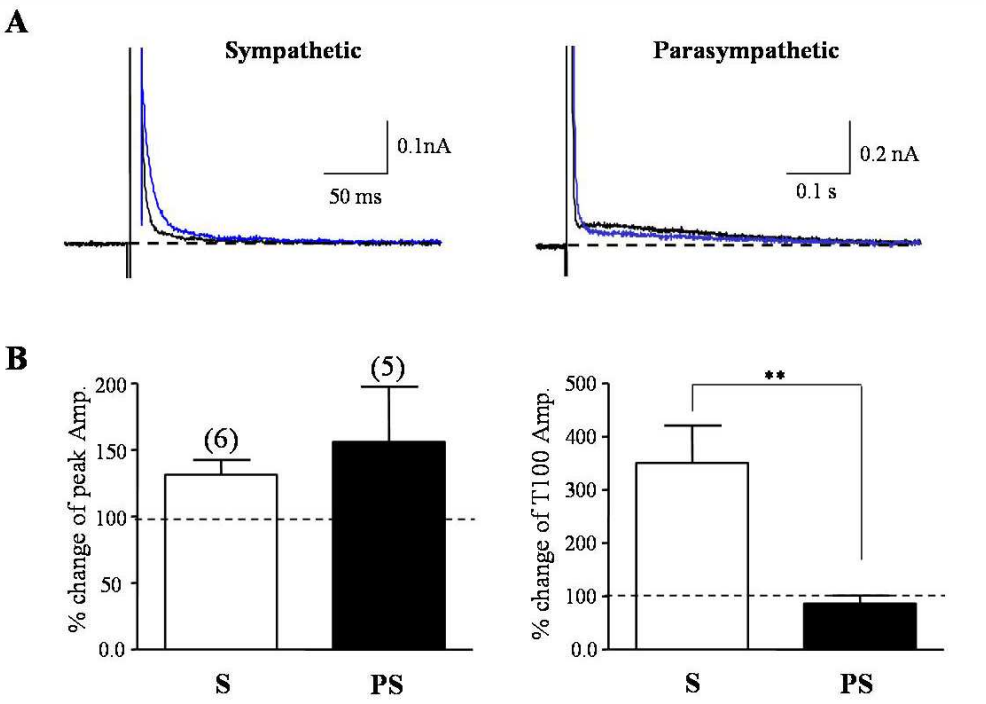


**Fig. 43. Effects of niflumic acid on $I_{AHP}$ amplitude in the MPG neurons.**

(A) : Representative traces showing changes $I_{AHP}$ in induced by niflumic acid (300 μM) in the MPG neurons. (B) : Bar graphs showing % changes in peak amplitude of $mI_{AHP}$ (left) and % changes of $mI_{AHP}$ amplitude measured at 100 ms point after depolarizing step pulse (right) in the sympathetic and parasympathetic MPG neurons. Numbers of cells tested is indicated in parentheses. Data were presented as means ± SEM **P< 0.01

## 4.13. Effects of intracellular stores on excitability in the MPG neurons.

Finally, contribution of $Ca^{2+}$-induced $Ca^{2+}$ release (CICR) on excitability was examined. Using ryanodine (10 μM) was a blocker of specific $Ca^{2+}$ release from the endoplasimc reticulum (ER), and thapsigargin (100 nM), a specific bloaker of the sarcoendoplasmic reticulum $Ca^{2+}$-ATPase (SERCA) on ER, which depletes the intracellular $Ca^{2+}$ store. Both ryanodine and thapsigargin had no effect on spike firing pattern in both sympathetic and parasympathetic MPG neurons (Fig. 44 and 45). In control experiments, nimodipine decreased firing frequency in the sympathetic MPG neurons after treatment of ryanodine or thapsigargin for 10 minitues in the cells (Fig. 45). Therefore, these data suggest that intracellular $Ca^{2+}$ store is not relevant to spike firing in both type of MPG neurons.

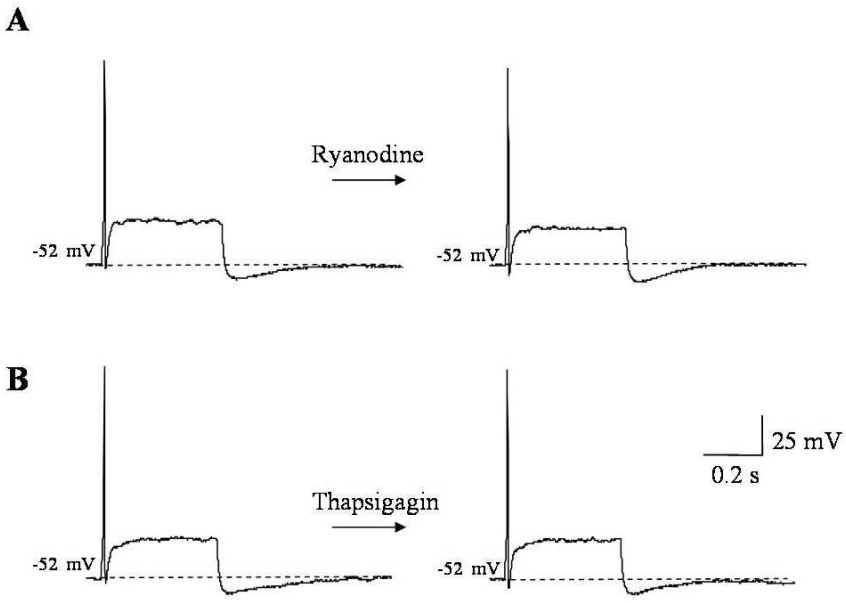


**Fig. 44. Test of intracellular $Ca^{2+}$ store in regulation of excitability in a parasympathetic MPG neuron.**

To investigate involvement of intracellular $Ca^{2+}$, 10 μM ryanodine (A) and 100 nM thapsigagin (B) were applied for 10 min to a parasympathetic MPG neurons. Note that no changes in firing frequency occurred in the parasympathetic MPG neurons.

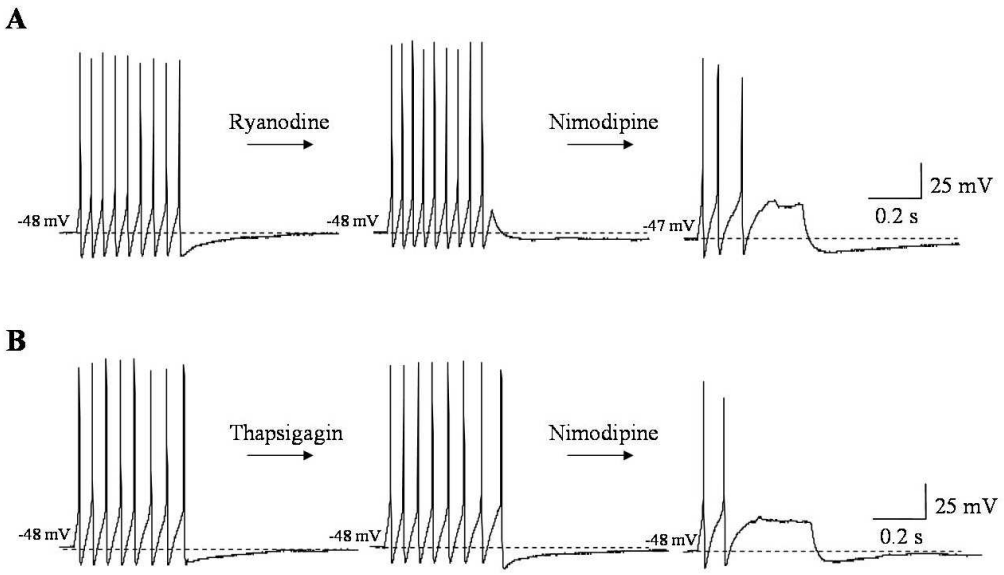


**Fig. 45. Test of intracellular $Ca^{2+}$ store in regulation of excitability in a sympathetic MPG neuron**

To investigate involvement of intracellular $Ca^{2+}$, 10 μM ryanodine (A) and 100 nM thapsigagin (B) were applied for 10 min to a sympathetic MPG neurons. Note that no changes in firing frequency occurred in the sympathetic MPG neurons.

# V. DISCUSSION

The purposes of the present study were to investigate 1) expression profile of HVA $Ca^{2+}$ channel isoforms, 2) the basic mechanisms underlying spike firing properties, and 3) functional roles of the HVA $Ca^{2+}$ channel isoforms in regulation of excitability in the sympathetic and parasympathetic MPG neurons.

## 5.1. Expression profile of HVA $Ca^{2+}$ channel isoforms in the MPG neurons

The MPG provides a good model system for studying cell-specific gene expression and functions (e.g., tonic versus phasic firing patterns) in the autonomic nervous system because one ganglion capsule possesses both sympathetic and parasympathetic neurons (Dail, 1996). The impetus for the present study arose from previous findings that LVA T-type $Ca^{2+}$ channels encoded by the α1H are exclusively expressed in the sympathetic MPG neurons (Zhu et al., 1995; Lee et al., 2002). Accordingly, one may speculate that expression profile of HVA $Ca^{2+}$ channel subtypes could be different between sympathetic and parasympathetic MPG neurons, which may affect functions of the neurons and eventually of their innervating urogenital organs. In conjunction with the RT-PCR and Western blot analyses, however, the pharmacological studies with nimodipine, ω-conotoxin GVIA, and ω-agatoxin IVA indicate that the expression profile of HVA $Ca^{2+}$ channels is identical for two populations of MPG neurons, although functional roles of certain subtypes appear to be cell-specific (see below).

The total $Ca^{2+}$ channel currents commonly comprise L-, N-, and R-type currents in the MPG neurons: N-type $Ca^{2+}$ channel is the most dominant subtype responsible for 60% of the total currents, which is comparable with other mammalian autonomic

neurons, including sympathetic superior cervical (Boland et al., 1994; Zhu et al., 1995), celiac-superior mesenteric (Carrier and Ikeda, 1992), parasympathetic intracardiac (Xu and Adams, 1992; Jeong and Wurster, 1997), and paratrachial (Aibara et al., 1992) neurons. L-type $Ca^{2+}$ currents mediate approximately 15% of total $Ca^{2+}$ currents and appear to arise from both α1C and α1D isoforms. In the MPG neurons, substantial currents (25% of total currents) were resistant to application of nimodipine and ω-conotoxin GVIA. Most autonomic neurons are known to display the non-L- and non-N-type currents (Adams and Harper, 1995). However, so far, the nature of these currents has been poorly defined, although they are expected to consist of P-, Q-, and R-type $Ca^{2+}$ currents. Although P- and Q-type $Ca^{2+}$ channels are the α1A gene products, biophysical and pharmacological phenotypes are quite different. This may be because of the differential splicing of the α1A subunit (Bourinet et al., 1999) and/or its association with different β subunits (Moreno et al., 1997; Mermelstein et al., 1999). Noninactivating P-type $Ca^{2+}$ channels are potently blocked by ω-agatoxin IVA ($IC_{50}$ = ~1 nM), whereas Q-type $Ca^{2+}$ channels with fast kinetics are less sensitive to the toxin ($IC_{50}$ = ~100 nM) (Randall and Tsien, 1995). In the present experiments, RT-PCR and Western blot analyses failed to detect the α1A transcript and protein. Consistent with these results, 1 μM ω-agatoxin IVA blocked none of the currents remaining in the presence of nimodipine and ω-conotoxin GVIA. Taken together, it was concluded that P/Q-type $Ca^{2+}$ channels are absent in the MPG neurons. Previous studies have shown that P/Q-type $Ca^{2+}$ channels together with N-type channels mediate sympathetic and parasympathetic neurotransmission in rat vas deferens (Wright and Angus, 1996; Tran and Boot, 1997) and bladder detrusor, respectively (Frew and Lundy, 1995; for review, see also Waterman, 2000). Accordingly, it is likely that the P/Q-type $Ca^{2+}$ channels are exclusively localized in synaptic terminals but not in cell bodies of the MPG neurons.

Overall, R-type $Ca^{2+}$ currents appear to solely constitute the $Cd^{2+}$-sensitive non-L- and non-N-type currents in the MPG neurons. Western blot analysis revealed

expression of α1E proteins in the MPG neurons. Similar to the recombinant α1E (rbEII) channels expressed in HEK 293 cells (Zamponi et al., 1996) and Xenopus oocytes (Soong et al., 1993), R-type $Ca^{2+}$ currents in the MPG neurons were highly sensitive to $Ni^{2+}$ block ($IC_{50}$ = 22 ± 0.1 μM). Accordingly, it is likely that the α1E underlies R-type $Ca^{2+}$ currents in the MPG neurons. The $Ni^{2+}$ sensitivity of the R-type $Ca^{2+}$ channels is similar to that of T-type $Ca^{2+}$ channels previously reported (Lee et al., 2002; Jeong et al., 2003) and appears to be much higher than that of L- and N-type $Ca^{2+}$ channels (Jeong et al., 2003). Interestingly, SNX-482, a selective antagonist of the recombinant α1E channels (See Figs. 14 and 15), failed to block R-type $Ca^{2+}$ currents in the MPG neurons, which is also observed in several types of central neurons including rat cerebellar granule neurons (Newcomb et al., 1998). Recent studies using antisense or transgenic strategies have shown that the α1E gives rise to SNX-482-sensitive and -resistant components (Piedras-Renteria and Tsien, 1998; Tottene et al., 2000; Sochivko et al., 2002), whose relative contribution to R-type $Ca^{2+}$ currents may vary from one cell to another cell. In the MPG neurons, likewise, the majority of SNX-482-insensitive R-type currents were proved to be encoded by α1E using the siRNA silencing technique. Like P/Q-type $Ca^{2+}$ currents as explained above (Moreno et al., 1997; Bourinet et al., 1999), the R-type $Ca^{2+}$ currents with a different toxin sensitivity may also arise from alternative splicing and/or heterogeneity of $Ca^{2+}$ channel auxiliary subunits. Indeed, some studies using RT-PCR analysis have revealed multiple splicing variants of the α1E gene in rat cerebellar granule neurons (Schramm et al., 1999) and human cerebellum (Pereverzev et al., 1998). On the other hand, it has been found that sensitivity of the recombinant α1E channel to SNX-482 is independent of $Ca^{2+}$ channel β subunits (Bourinet et al., 2001), although effects of other auxiliary subunits (i.e. $\alpha_2\delta$ and γ subunits) remain unknown. RT-PCR analysis of mRNA isolated from the MPG neurons revealed only a single splice variant containing a shorter II-III loop and longer N- and C-termini compared with the cloned rat version (rbEII). This is reminiscent of rat cerebellar variants corresponding to SNX-482

resistant R-type $Ca^{2+}$ currents (called "G3" or "Rc" or "$\alpha 1_{Ee}$" form) (Schramm et al., 1999). Taken together, the most plausible explanation for resistance of R-type $Ca^{2+}$ currents to SNX-482 in the MPG neurons may use alternative splicing of the prototype $\alpha$1E. However, one should note that the spliced loop and terminal regions cannot interact with externally applied SNX-482. Recent study of Bourinet et al. (2001) has suggested that candidate binding sites of SNX-482 may be the domain III and IV S3-S4 linker of the $\alpha$1E subunit. Thus, it may be interesting to identify the splicing variant responsible for resistance to SNX-482 in the MPG neurons.

## 5.2. The basic mechanisms underlying spike firing properties in the MPG neurons

The sympathetic and parasympathetic MPG neurons have tonic and phasic firing patterns, respectively. In many neurons, $Ca^{2+}$-activated ion channels play important roles in controlling spike firing by forming prolonged AHP of the membrane potential. More importantly, these $Ca^{2+}$-dependent currents rely on $Ca^{2+}$ influx through the VACCs (Sah, 1995; Williams et al., 1997). In general, the medium AHP controls the tonic firing of neurons, whereas the slow AHP is responsible for spike frequency adaptation, a prominent reduction in the firing frequency in the late phase of responses to prolonged depolarizing stimuli (Sah, 1996). Accordingly, in the present study, $Ca^{2+}$-activated $K^+$ channels were considered as the major ion channels responsible for neuronal excitability, because of their implication in generation of the medium and slow AHPs. The MPG neurons also displayed the mAHP following a single action potential. However, the shape of the mAHP was quite different in the sympathetic and parasympathetic MPG neurons. That is the former, the amplitude and duration of the mAHP was large and short, respectively, while in the latter, vice versa, suggesting the ionic mechanisms underlying the mAHP may be different between the two types of

the MPG neurons. Consistent with the notion, the SK channels underlie most of the mAHP in the parasympathetic MPG neurons, while they contribute minimally to that in the sympathetic ones. A pharmacological study has shown that the SK2 and SK3 channels are very sensitive to apamin, while the SK1 channels are apamin insensitive (Kohler et al., 1996). Together with the RT-PCR data that the MPG neurons expressed transcripts of SK2 and SK3 subunits with an exception of SK1 subunit, it is suggested that the mAHP arises from SK2 and/or SK3 channels in the parasympathetic MPG neurons.

Unlike the SK channels, the BK channels contribute minimally to setting firing rates in the MPG neurons as reported previously (Faber et al., 2002). Because BK channels require for activation coincident $Ca^{2+}$ influx and membrane depolarization to open channels under physiological conditions (Cui et al., 1997), it is unlikely that they are active during the interspike interval. Conversely, the BK channels are responsible for action potential repolarization in the MPG neurons. Several studies have shown that different β subunits determine the pharmacological properties of the BK channels (McManus et al., 1995; Dworetzky et al., 1996; Meera et al., 2000), and alters the voltage-dependence (Wallner et al., 1995), apparent $Ca^{2+}$ sensitivity (Ramanathan et al., 2000), and kinetics of the assembled channels (Meera et al., 1996). For examples, the BK channels formed by the α- and β4-subunits, which are found in the brain, are resistant to charybdotoxin and iberiotoxin (Meera et al., 2000). This resistance is thought to be due to the extracellular loop of the β4-subunit that forms a part of the toxin receptor and prevents the transport of the toxin from the binding site. Co-expression of α- and β1-subunits in rat insulinoma tumor (RINm5f) cells and adrenal chromaffin cells confers a reduced sensitivity to charybdotoxin and also causes an inactivation of the channel (Ding et al., 1998; Xia et al., 1999). It is likely that the BK channels expressed in the MPG neurons containing the β4-subunit since repolarization of action potential were affected by TEA-Cl at low concentrations and paxillin, but not charybdotoxin and iberiotoxin. This notion is additionally supported by

the RT-PCR result that the MPG neurons mainly express BK-β4 subunit. The relative contribution of the BK channels on the fAHP (as judged by the repolarization speed) was more prominent in the parasympathetic neurons than the sympathetic neruons. In the sympathetic MPG neurons, other types of ion channels such as the M-type $K^+$ channels appear to be important for repolarization of action potential . Considering that these BK blockers barely affect firing frequency in both sympathetic and parasympathetic MPG neurons, the SK channels may be more important for spike firing properties in the MPG neurons. However, many studies have shown that AHP was induced by other ion channels beside $Ca^{2+}$-activated $K^+$ channels, which control the inter-action potential trajectory. For examples, a hyperpolarization activated non-selective cation current ($I_h$) (Mercuri et al., 1995), rapidly inactivating $K^+$ current ($I_A$) (Liss et al., 2001), $Na^+$-activated $K^+$ channels (Bhattacharjee and Kaczmazek, 2005), and KCNQ channels (Forti et al., 2006) are capable of triggering mAHP or sAHP through $Ca^{2+}$-independent mechanisms. Therefore, $Ca^{2+}$-independent mechanism in the MPG neurons await to be examined. It was generally assumed that an AHP with a large amplitude results in a slow rate of spontaneous action potential generation, and vice versa. However, some studies have reported that AHP duration is also important for regulation of firing frequency (Susumu et al., 2005). In the MPG neurons, however, AHP duration rather than AHP amplitude is the critical determinant of the tonic and phasic spike firing properties.

## 5.3. Functional roles of the HVA $Ca^{2+}$ channel isoforms in regulation of excitability in the MPG neurons.

It is obvious that $Ca^{2+}$ entry, but not $Ca^{2+}$ release from the internal stores in critical for controlling spike firing in the MPG neurons. Although there are many routes for $Ca^{2+}$ entry, the VACCs may be the most popularly used in the MPG

neurons. In the MPG neurons, the VACCs are implicated in transmitter release in the synaptic terminals as well as spike firing in the cell bodies. Several studies have suggested that N- and P/Q-types, but not L-type $Ca^{2+}$ channels mediate synaptic transmission between postganglionic neurons and effectors such as the urinary detrusor and the vas deferens (Waterman, 2000). The roles of R-type $Ca^{2+}$ channels in transmitter release are yet unclear. A previous study has shown that LVA T-type $Ca^{2+}$ channels are implicated in generation of low-threshold spikes in the sympathetic MPG neurons (Lee et al., 2002). Likewise, the HVA $Ca^{2+}$ channel subtypes expressed in cell bodies of the MPG neurons appear to contribute to spike adaptation in cell-specific ways. Among the HVA $Ca^{2+}$ channel isoforms, N-type $Ca^{2+}$ channel, the most abundant one in the MPG neurons, plays a negative regulator of spike firing in both sympathetic and parasympathetic neurons. $Ca^{2+}$ influx through N-type $Ca^{2+}$ channels was responsible for AHP and $I_{AHP}$ in both types of MPG neurons. Therefore, block of N-type $Ca^{2+}$ channel increased spike firing frequency through decreasing AHP and $I_{AHP}$ in the MPG neurons. This is quite comparable with other types of neurons. For examples, Davies et al. (1996) have been reported that $Ca^{2+}$ influx through N-type channels reduced excitability by selective activation of small conductance $Ca^{2+}$-activated $K^+$ channels (SK type) in rat superior cervical ganglion. In lamprey spinal cord motor- and interneurons, apamin-sensitive $Ca^{2+}$-activated $K^+$ channels underlying the AHP are activated primarily by $Ca^{2+}$ influx through N-type channels (Wikstrom and Manira, 1998). Unlike the N-type $Ca^{2+}$ channel, the L-type one acts as a positive regulator of spike firing especially in the sympathetic MPG neurons. The effects of $Ca^{2+}$ influx through L-type channels on the AHP and $I_{AHP}$ in sympathetic MPG neurons are different from those in parasympathetic ones. Accordingly, block of L-type $Ca^{2+}$ channels decreased spike firing through enhancing AHP and $I_{AHP}$ in sympathetic MPG neurons, without affecting that in the parasympathetic MPG neurons. These findings suggest that L-type ones unlike N-type $Ca^{2+}$ channels are coupled to the SK channels to allow the tonic firings in the sympathetic MPG neurons. Previous studies have

reported coupling between L-type $Ca^{2+}$ channels and $Ca^{2+}$-activated $K^+$ channels contribute to AHP in some neurons. For examples, in hippocampal neurons, L-type channels activate SK but not BK channels (Marrion and Tavalin, 1998). On the other hand, in rat SCG neurons (Davies et al., 1996), L-type $Ca^{2+}$ channels are coupled to the large conductance (BK type) $Ca^{2+}$-activated $K^+$ channels to accelerate repolarization of action potential. Especially, L-type $Ca^{2+}$ channel contribute to transient outward peak current (fAHP) but N-type ones did not contribute to this current in sympathetic MPG neurons. Brenner et al., (1995) proposed a hypothesis that the broader action potentials allow a greater $Ca^{2+}$ influx during each action potential. As a result $Ca^{2+}$ ions are accumulated to a level that sustain the SK-type channels, thereby prolonging the interspike interval and increasing spike frequency adaptation. Actually, a larger AHP associated with spike broadening has been observed in CA1 hippocampal cells (Kamal et al., 2003) and in the early component of an action potential train in the lateral amygdala (Faber et al., 2002). However, in this study, the correlation between action potential broadening and sustaining of SK channel could not define and remained further study.

In addition, $Ca^{2+}$ independent residual transient outward current also was elicited with $I_{AHP}$ in the MPG neurons. Those may be composed with different kinds of channels such as $Ca^{2+}$ activated $Cl^-$ channels or other cation channels. Taken together, these data suggested that fast transient current may be encoded by BK channel coupling with L-type $Ca^{2+}$ channel in sympathetic MPG neurons. In general, BK channels do not contribute to regulating of spike frequency. Therefore, the question arise what kinds of channels regulate to AHP beside $Ca^{2+}$ activated $K^+$ channels in MPG neurons. One of candidates may be anion channels, which can significantly alter resting membrance potential and the duration of the action potential. Previously, have reported that $Cl^-$ was the charege carrier of $Ca^{2+}$ activated current in some neurons (Andrew et al., 1992). Blockers of $Ca^{2+}$ activated $Cl^-$ channel significantly reduced firing frequency in sympathetic MPG neurons like a effects of L-type blocker. There

were some reported that niflumic acid inhibited firing frequency in myometrium (Jones et al., 2004) and other group reported that block of $Ca^{2+}$ activated $Cl^-$ channel inhibited action potential after-depolarizations in rat cultured DRG neurons (Ayar et al., 1999). Take together, these results suggested that $Ca^{2+}$ activated $Cl^-$ channel contribute to neuronal excitability through regulate AHP size in sympathetic MPG neurons.

Finally, several previous studies have reported that $K^+$ and $Cl^-$ conductances responsible for AHP and ADP, respectively were activated by $Ca^{2+}$ induced $Ca^{2+}$ release (CICR) from intracellualr stores (Martinez, 1994; Davies, et al., 1996; Ayar, et al., 1999). These findings are not comparable with the previous reports where the internal $Ca^{2+}$ releas regulates spike firing through activation of $Ca^{2+}$ dependent $K^+$ or $Cl^-$ channels.

## 5.4. Summary of differential roles of $Ca^{2+}$ channel isoforms in regulation of excitability in the MPG neurons.

This study suggests that $Ca^{2+}$ influx through L-, and N-type HVA $Ca^{2+}$ channels during action potential seems to directly activate certain types of $Ca^{2+}$-activated $K^+$ (BK and SK) and/or $Cl^-$ channels (CaCC) in the MPG neurons. In sympathetic MPG neurons, L-type $Ca^{2+}$ channels and BK channels are closely associated whereas N-type $Ca^{2+}$ channels are mainly linked to the SK channels (Fig. 46). The ADP produced by the CaCCs channels appear to be large enough to offset the mAHP by the SK channels, thus conferring the tonic firing property to the sympathetic MPG neurons. Block of L-type channel results decreases excitability and broadens action potential. Conversely block of the N-type $Ca^{2+}$ channel slightly increase excitability in the sympathetic MPG neurons (Fig. 47, left). In the parasympathetic MPG neurons, among the HVA $Ca^{2+}$ channel isoforms, N-type $Ca^{2+}$ channels play major roles in firing adaptation by coupling the SK channels (Fig. 46, right). Accordingly, block of N-type

$Ca^{2+}$ channels leads to augmentation of excitability by reducing the mAHP (Fig 47, right) L-type $Ca^{2+}$ channels and BK channel closely correlated in sympathetic MPG neurons, while L-type ones in parasympathetic neurons coupled with SK channels. As described above, the BK channels may exert negligible effects on firing frequency unlike the SK channels.

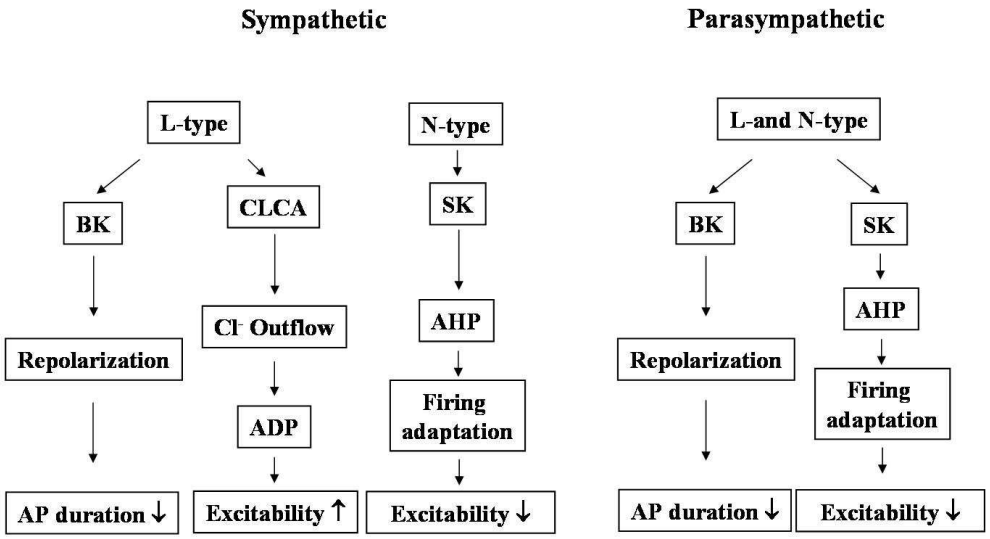


**Fig. 46. Proposed ionic mechanisms underlying regulation of excitability in MPG neurons.**

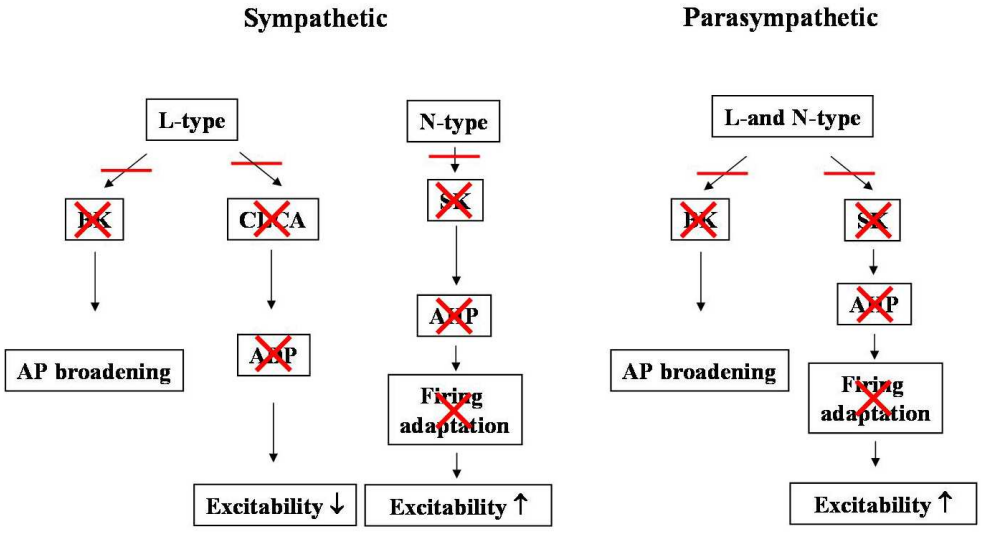


**Fig. 47. Effects of specific block of HVA L- and N-type $Ca^{2+}$ channel isoforms on excitability in the MPG neurons.**

# VI. SUMMARY

1. The MPG neurons functionally expressed all of the HVA $Ca^{2+}$ channel isoforms (N-, L- and R-type) with the exception of the P/Q-type encoded by the $\alpha$1A.

2. There was no significant difference in expression profiles of HVA $Ca^{2+}$ channels isoforms between sympathetic and parasympathetic MPG neurons.

3. The MPG neurons expressed SNX-482-resistant R-type $Ca^{2+}$ current encoded by a splice variant of the $\alpha$1E with long N- and C-terminus and short II-III loop (cerebellum type; SNX-482 resistant Rc, G3 or $\alpha 1_{Ee}$ form)

4. SK channel-induced medium AHP determines firing pattern of sympathetic and parasympathetic MPG neurons.

5. BK channel-induced fast AHP more contribute to action potential repolarization in the parasympathetic MPG neurons than the sympathetic ones.

6. $Ca^{2+}$ influx through L- and N-type $Ca^{2+}$ channels contributes to regulating excitability of sympathetic and parasympathetic MPG neurons in different ways.

7. N-type $Ca^{2+}$ channel plays a negative regulator of spike firing in both sympathetic and parasympathetic neurons. $Ca^{2+}$ influx through N-type $Ca^{2+}$ channels was responsible for AHP and $I_{AHP}$ in both types of MPG neurons. Therefore, block of N-type $Ca^{2+}$ channel increased spike firing frequency through decreasing AHP and $I_{AHP}$ in the MPG neurons.

8. The L-type $Ca^{2+}$ channels acts as a positive regulator of spike firing especially in the sympathetic MPG neurons. The effects of $Ca^{2+}$ influx through L-type channels on the AHP and $I_{AHP}$ in sympathetic MPG neurons are different from those in parasympathetic ones. Accordingly, block of L-type $Ca^{2+}$ channels decreased spike firing through enhancing AHP and $I_{AHP}$ in sympathetic MPG neurons, without affecting that in the parasympathetic MPG neurons.

9. These finding suggested that N-type $Ca^{2+}$ channels coupled with SK channel in both types of MPG neurons, while, L-type $Ca^{2+}$ channel correlated with CaCC and BK channel in sympathetic MPG neurons, and coincidence with SK channel in parasympathetic ones.

# VII. CONCLUSION

In conclusion, the MPG neurons from adult rats express three distinct subtypes of HVA $Ca^{2+}$ channels : L-, N-, and R- types. The P/Q-type $Ca^{2+}$ channels are not found in cell body, although they are suggested to be localized in the neuromuscular terminals. The expression profile of HVA $Ca^{2+}$ channels is identical in both sympathetic and parasympathetic neurons, and the SNX-482 resistant R-type currents encoded from alternative splicing of the α1E ("$\alpha 1_{Ee}$" or " Rc" type) and functionally expressed in the MPG neurons. Sympathetic and parsympathetic MPG neurons had different mechanism to modulate spike firing. Medium AHP mediated by SK channels and properties of action potential repolarization by BK-α and BK-β4 subunit determine the phasic firing pattern in parasympathetic MPG neurons. Conversely, less effective contribution of $Ca^{2+}$ activated $K^+$ channels and ADP by $Ca^{2+}$ activated $Cl^-$ channels determine the tonic firing pattern in sympathetic MPG neurons. Finally, $Ca^{2+}$ influx through L- and N- type $Ca^{2+}$ channels differently contribute to regulating excitability in sympathetic and parasympathetic MPG neurons. $Ca^{2+}$ influx through N-type channel reduced firing frequency in both sympathetic and parasympathetic neurons through enhancing $I_{AHP}$ and AHP, while $Ca^{2+}$ influx through L-type channel greatly enhanced the firing frequency through diminishing AHP and $I_{AHP}$ in sympathetic MPG neurons without affecting parasympathetic ones. These finding suggested that N-type $Ca^{2+}$ channels coupled with SK channel in both types of MPG neurons, while, L-type $Ca^{2+}$ channel correlated with CaCC and BK channel in sympathetic MPG neurons, and coincidence with SK channel in parasympathetic ones.

# VIII. REFERENCES


Adams PR., Constanti A., Brown DA. and Clark RB., Intracellular $Ca^{2+}$ activates a fast voltage-sensitive $K^{+}$ current in vertebrate sensory neurones. Nature. 1982, 296: 746–749.

Adams DJ. and Harper AA., Electrophysiological properties of autonomic ganglion neurons, In Autonomic Ganglia (McLachlan EM ed) 1995, pp153-212, Harwood, London

Aibara K., Ebihara S., and Akaike N., Voltage-dependent ionic currents in dissociated paratracheal ganglion cells of the rat. J Physiol (Lond) 1992, 457: 591–610.

Ayar A, Storer C, Tatham EL, Scott RH. The effects of changing intracellular $Ca^{2+}$ buffering on the excitability of cultured dorsal root ganglion neurones. Neurosci Lett. 1999,271(3):171-4.

Azouz R, Jensen MS, Yaari Y., Ionic basis of spike after-depolarization and burst generation in adult rat hippocampal CA1 pyramidal cells. J Physiol. 1996, 492 (Pt 1):211-23.

Barker JL, Ransom BR., Amino acid pharmacology of mammalian central neurones grown in tissue culture. J Physiol. 1978, 280:331-54.

Behrens R, Nolting A, Reimann F, Schwarz M, Waldschutz R, Pongs O., hKCNMB3 and hKCNMB4, cloning and characterization of two members of the large-conductance calcium-activated potassium channel beta subunit family. FEBS

Lett. 2000, 474(1):99-106.

Bean BP., Nitrendipine block of cardiac calcium channels: high-affinity binding to the inactivated state. Proc Natl Acad Sci USA 1984, 81: 6388–6392.

Bhattacharjee A, and Kaczmarek LK. For $K^+$ channels, $Na^+$ is the new $Ca^{2+}$. Trends Neurosci. 2005, 28(8):422-8.

Bixby JL, and Spitzer NC., The appearance and development of neurotransmitter sensitivity in Xenopus embryonic spinal neurones in vitro. J Physiol. 1984, 353:143-55.

Black JL 3rd., The voltage-gated calcium channel gamma subunits: a review of the literature. J Bioenerg Biomembr. 2003, 35(6):649-60.

Blank T, Nijholt I, Kye MJ, Spiess J. Small conductance $Ca^{2+}$-activated $K^+$ channels as targets of CNS drug development. Curr Drug Targets CNS Neurol Disord. 2004, 3(3):161-7.

Blatz AL., and Magleby, KL., Calcium-activated potassium channel. TINS 1987, 10: 463-467

Boland LM, Morrill JA, and Bean BP., ω-Conotoxin block of N-type calcium channels in frog and rat sympathetic neurons. J Neurosci 1994, 14:5011–5027.

Bourinet E, Soong TW, Sutton K, Slaymaker S, Mathews E, Monteil A, Zamponi GW, Nargeot J, and Snutch TP., Splicing of alpha α1A subunit gene generates phenotypic variants of P- and Q-type calcium channels. Nat Neurosci 1999, 2: 407–

415.

Bourinet E, Stotz SC, Spaetgens RL, Dayanithi G, Lemos J, Nargeot J, and Zamponi GW., Interaction of SNX-482 with domains III and IV inhibits activation gating of alpha1E ($Ca_V2.3$) calcium channels. Biophys J 2001, 81: 79–88.

Brenner R, Chen QH, Vilaythong A, Toney GM, Noebels JL, Aldrich RW., BK channel beta 4 subunit reduces dentate gyrus excitability and protects against temporal lobe seizures. Nat Neurosci. 2005, 8(12):1752-9.

Caeser M, Brown DA, Gahwiler BH, Knopfel T., Characterization of a calcium-dependent current generating a slow afterdepolarization of CA3 pyramidal cells in rat hippocampal slice cultures. Eur J Neurosci. 1993, 5(6):560-9.

Carrier GO and Ikeda SR., TTX-sensitive $Na^+$ channels and $Ca^{2+}$ channels of the L- and N-type underlie the inward current in acutely dispersed coeliacmesenteric ganglia neurons of adult rats. Eur J Physiol 1992, 421: 7–16.

Castro FD., Geijo-Barrientos E, Gallego R., Calcium-activated chloride current in normal mouse sympathetic ganglion cells. J Physiol. 1997, 498 (Pt 2):397-408

Catterall WA, Striessnig J, Snutch TP, and Perez-Reyes E., International Union of Pharmacology. XL. Compendium of voltage-gated ion channels: calcium channels. Pharmacol Rev 2003, 55: 579–581.

Charpak S, Gahwiler BH, Do KQ, Knopfel T., Potassium conductances in hippocampal neurons blocked by excitatory amino-acid transmitters. Nature. 1990, 347(6295):765-7.

Clozel JP, Ertel EA, Ertel SI. Voltage-gated T-type $Ca^{2+}$ channels and heart failure. Proc Assoc Am Physician 1999; 111: 429–37.

Cole AE, and Nicoll RA., Acetylcholine mediates a slow synaptic potential in hippocampal pyramidal cells. Science. 1983, 221(4617):1299-301.

Crain, SM., Resting and action potentials of cultured chick embryo spinal ganglion cells. J. Comp. Neurol. 1956, 104; 285–330.

Cui J, Cox DH, Aldrich RW., Intrinsic voltage dependence and $Ca^{2+}$ regulation of mslo large conductance $Ca^{2+}$-activated $K^{+}$ channels. J Gen Physiol. 1997, 109(5):647-73.

Cunningham SA, Awayda MS, Bubien JK, Ismailov II, Arrate MP, Berdiev BK, Benos DJ, Fuller CM., Cloning of an epithelial chloride channel from bovine trachea. J Biol Chem. 1995, 270(52):31016-26.

Czubayko U, Sultan F, Thier P, Schwarz C., Two types of neurons in the rat cerebellar nuclei as distinguished by membrane potentials and intracellular fillings. J Neurophysiol. 2001, 85(5):2017-29.

Dail WG., Moll MA., Weber K., Localization of vasoactive intestinal polypeptide in penile erectile tissue and in the major pelvic ganglion of the rat. Neuroscience. 1983, 10(4):1379-86.

Dail WG., The pelvic plexus: innervation of pelvic and extrapelvic visceral tissues. Microsc Res Tech. 1996, 35(2):95-106

Davies PJ., Ireland DR., McLachlan EM., Sources of $Ca^{2+}$ for different $Ca^{2+}$-activated $K^{+}$ conductances in neurones of the rat superior cervical ganglion. J Physiol. 1996, 495 (Pt 2):353-66.

Deschenes, M., Feltz, P. and Lamour, Y., A model for an estimate in vivo of the ionic basis of presynaptic inhibition: an intracellular analysis of the GABA-induced depolarization in rat dorsal root ganglia. Brain Res. 1976, 118, 486–493.

Diebold RJ., Koch WJ., Ellinor PT., Wang JJ, Muthuchamy M .and Wieczorek DF., Mutually exclusive exon splicing of the cardiac calcium channel alpha 1 subunit gene generates developmentally regulated isoforms in the rat heart. Proc Natl Acad Sci U S A 1992, 89: 1497–1501.

Ding JP., Li ZW. and Lingle CJ., Inactivating BK channels in rat chromaffin cells may arise from heteromultimeric assembly of distinct inactivation-competent and noninactivating subunits, Biophys. J. 74 (1998), pp. 268–289.

Dworetzky SI., Boissard CG., Lum-Ragan JT., McKay MC., Post-Munson DJ. and Trojnacki. T., Phenotypic alteration of a human BK (hSlo) channel by hSlo beta subunit coexpression: changes in blocker sensitivity, activation/relaxation and inactivation kinetics, and protein kinase A modulation, J Neurosci 16 (1996), pp. 4543–4550

Elbashir SM., Harborth J., Lendeckel W., Yalcin A., Weber K., Tuschl T., Duplexes of 21-nucleotide RNAs mediate RNA interference in cultured mammalian cells. Nature. 2001, 411(6836):494-8

Ellinor PT, Zhang JF, Randall AD, Zhou M, Schwarz TL, Tsien RW, Horne WA. Functional expression of a rapidly inactivating neuronal calcium channel. Nature. 1993, 363(6428):455-8.

Ertel SI, Ertel EA. Low-voltage-activated T-type $Ca^{2+}$ channels. TIPS 1997; 18: 37–42.

Faber ES., and Sah P., Physiological role of calcium-activated potassium currents in the rat lateral amygdala. J Neurosci. 2002, 22(5):1618-28.

Faber ES., and Sah P., $C^{2+}$-activated $K^{+}$ (BK) channel inactivation contributes to spike broadening during repetitive firing in the rat lateral amygdala. J Physiol. 2003, 552 (Pt 2):483-97

Felix R, Gurnett CA., De Waard M., Campbell K.P., Dissection of functional domains of the voltage-dependent $Ca^{2+}$ channel $\alpha_2\delta$ subunit. J Neurosci 1997, 17:6884-6891

Ferroni A, Mancinelli E, Camagni S, Wanke E. Two high voltage-activated calcium currents are present in isolation in adult rat spinal neurons. Biochem Bioph Res Commun 1989; 159: 379–84.

Flockerzi V, Oeken HJ., Hofmann F, Pelzer D., Cavalie A., Trautwein W., Purified dihydropyridine-binding site from skeletal muscle t-tubules is a functional calcium channel. Nature. 1986, 323(6083):66-8.

Forti L, Cesana E, Mapelli J, D'Angelo E. Ionic mechanisms of autorhythmic firing in cerebellar golgi cells.J Physiol. 2006, (Epub ahead of print)

Fox AP., Nowycky MC., Tsien RW., Single-channel recordings of three types of

calcium channels in chick sensory neurones. J Physiol. 1987, 394:173-200.

Fox AP, Nowycky MC, Tsien RW. Kinetic and pharmacological properties distinguishing three types of calcium currents in chick sensory neurones. J Physiol 1987; 394: 149−72.

Frew R. and Lundy PM., A role for Q-type $Ca^{2+}$ channels in neurotransmission in the rat urinary bladder. Br J Pharmacol 1995, 116: 1595−1598.

Gallagher JP., Higashi H., Nishi S., Characterization and ionic basis of GABA-induced depolarizations recorded in vitro from cat primary afferent neurones. J Physiol. 1978, 275:263-82.

Galvez A., Gimenez-Gallego G., Reuben J., Roy-Contancin L., Feigenbaum P., Kaczorowski G., and Garcia M., Purification and characterization of a unique, potent, peptidyl probe for the high conductance calcium-activated potassium channel from venom of the scorpion Buthus tamulus. J. Biol. Chem. 265 (1990), pp. 11083 −11090.

Galvez A., Gimenez-Gallego G., Reuben JP., Roy-Contancin L., Feigenbaum P., Kaczorowski GJ., Garcia ML., Purification and characterization of a unique, potent, peptidyl probe for the high conductance calcium-activated potassium channel from venom of the scorpion Buthus tamulus. J Biol Chem. 1990, 265(19):11083-90.

Giangiacomo KM, Garcia ML, McManus OB. Mechanism of iberiotoxin block of the large-conductance calcium-activated potassium channel from bovine aortic smooth muscle. Biochemistry. 1992, 31(29):6719-27.

Giuliano F., Rampin O., Schirar A., Jardin A., Rousseau J.P., Autonomic control of penile erection: modulation by testosterone in the rat. J Neuroendocrinol. 1993, 5(6):677-83.

Glossmann H, Striessnig J, Ferry DR, Goll A, Moosburger K, Schirmer M. Interaction between calcium channel ligands and calcium channels. Circ Res. 1987 (4 Pt 2):I30-6.

Greenwood D, Coggeshall RE, Hulsebosch CE. Sexual dimorphism in the numbers of neurons in the pelvic ganglia of adult rats. Brain Res. 1985, 340(1):160-2.

Greffrath W., Magerl W., Disque-Kaiser U., Martin E., Reuss S., Boehmer G., Contribution of $Ca^{2+}$-activated K+ channels to hyperpolarizing after-potentials and discharge pattern in rat supraoptic neurones. J Neuroendocrinol. 2004, (7):577-88.

Groat, WD., C., BoothA. M., and Yoshimura, N., Neurophysiology of micturation and its modification in animal models of human disease. In the autonomic Nervous System, vol. 2, Nervous Control of the Urogenital System, ed. MAGGI, C. A., 1992, pp. 227-290. Harwood Academic Publishers, London.

Groat, WD. C., and Booth, A. M., Neural control of penile erection. In The Autonomic Nervous System, vol. 2, Nervous Control of the Urogenital System, ed. MAGGI, C. A., 1992, pp. 467-524. Harwood Academic Publishers, London.

Hamill OP., Marty A., Neher E., Sakmann B., Sigworth FJ., Improved patch-clamp techniques for high-resolution current recording from cells and cell-free membrane patches. Pflugers Arch. 1981, 391(2):85-100

Hartzell C., Putzier I., Arreola J,. Calcium-activated chloride channels. Annu Rev Physiol. 2005, 67:719-58

Hirning LD., Fox AP., McCleskey EW., Olivera BM., Thayer SA., Miller RJ., Tsien RW., Dominant role of N-type $Ca^{2+}$ channels in evoked release of norepinephrine from sympathetic neurons. Science. 1988, 239(4835):57-61

Hussy N., Calcium-activated chloride channels in cultured embryonic Xenopus spinal neurons. J Neurophysiol. 1992, 68(6):2042-50.

Ikeda SR., Double-pulse calcium channel current facilitation in adult rat sympathetic neurones. J Physiol. 1991, 439:181-214

Ishii, TM., Silvia, C., Hirschberg, B., Bond, CT., Adelman, JP., Maylie, J., A human intermediate conductance calcium-activated potassium channel. Proceedings of the National Academy of Sciences of the USA. 1997, 94:11651−11656.

Jentsch TJ., Stein V., Weinreich F., Zdebik A.A., Molecular structure and physiological function of chloride channels. Physiol Rev. 2002, 82(2):503-68.

Jeong SM., Park HK., Yoon IS., Lee JH., Kim JH., Jang CG., Lee CJ., Nah SY., Cloning and expression of $Ca^{2+}$-activated chloride channel from rat brain. Biochem Biophys Res Commun. 2005, 334(2):569-76.

Jeong SW., and Wurster RD,. Calcium channel currents in acutely dissociated intracardiac neurons from adult rats. J Neurophysiol. 1997, 77(4):1769-78.

Jeong SW., and Wurster RD., Muscarinic receptor activation modulates $Ca^{2+}$ channels

in rat intracardiac neurons through a PTX- and voltage-sensitive pathway. J Neurophysiol. 1997, 78(3):1476-90.

Jeong SW., Ikeda SR., G protein alpha subunit G alpha z couples neurotransmitter receptors to ion channels in sympathetic neurons. Neuron. 1998, 21(5):1201-12.

Jobling P., Gibbins IL., Lewis RJ., and Morris JL., Differential expression of Calcium channels in sympathetic and parasympathetic preganglionic inputs to neurons in paracervical ganglia of guinea-pigs, Neuroscience 2004, 127: 455–466

Jongh KS., Warner C., Catterall WA., Subunits of purified calcium channels. Alpha 2 and delta are encoded by the same gene. J Biol Chem. 1990, 265(25):14738-41.

Johnson SW. and Seutin V., Bicuculline methiodide potentiates NMDA-dependent burst firing in rat dopamine neurons by blocking apamin-sensitive $Ca^{2+}$-activated $K^{+}$ currents. Neurosci. Lett. 1997, 231:13–16

Joiner, WJ., Wang, L.-Y., Tang, MD., Kaczmarek, LK.., The hSK4: a member of a novel subfamily of calcium-activated potassium channels. Proceedings of the National Academy of Sciences of the USA, 1997, 94: 11013–11018.

Jones K., Shmygol. A., Kupittayanant. S, and Wray. S., Electrophysiological characterization and functional importance of calcium-activated chloride channel in rat uterine myocytes. Pflugers Arch. 2004, 448: 36–-43

Joux N., Chevaleyre V., Alonso G., Boissin-Agasse L., Moos F.C., Desarmenien MG, Hussy N. High voltage-activated $Ca^{2+}$ currents in rat supraoptic neurones: biophysical properties and expression of the various channel alpha1 subunits. J

Neuroendocrinol. 2001, 13(7):638-49.

Hosseini R., Benton D.C.H., Dunn P.M., Jenkinson D.H. and Moss G.W.J., SK3 is an important component of K+ channels mediating the afterhyperpolarization in cultured rat SCG neurones. J. Physiol. 2001, 535: 323–334.

Kamal A., Artola A., Biessels GJ., Gispen WH., Ramakers GM.., Increased spike broadening and slow afterhyperpolarization in CA1 pyramidal cells of streptozotocin-induced diabetic rats. Neuroscience. 2003, 118(2):577-83.

Keast JR., Visualization and immunohistochemical characterization of sympathetic and parasympathetic neurons in the male rat major pelvic ganglion. Neuroscience. 1995 66(3):655-62.

Kenyon JL., The reversal potential of $Ca^{2+}$-activated $Cl^-$ currents indicates that chick sensory neurons accumulate intracellular $Cl^-$. Neurosci Lett. 2000, 296(1):9-12.

Kim HL., Kim H., Lee P., King RG., Chin H., Rat brain expresses an alternatively spliced form of the dihydropyridine-sensitive L-type calcium channel alpha 2 subunit. Proc Natl Acad Sci U S A. 1992, 89(8):3251-5

Klugbauer N., Lacinova L., Marais E., Hobom M., Hofmann F., Molecular diversity of the calcium channel alpha2delta subunit. J Neurosci. 1999, 19(2):684-91

Knaus HG, McManus OB, Lee SH, Schmalhofer WA, Garcia-Calvo M, Helms LM, Sanchez M, Giangiacomo K, Reuben JP, Smith AB 3rd, et al. Tremorgenic indole alkaloids potently inhibit smooth muscle high-conductance calcium-activated potassium channels. Biochemistry. 1994, 33(19):5819-28.

Kohler. M., Hischberg B., Bond CT., Kinzie JM., Marri NV, Maylie JA. and delman JP., Small-conductance, calcium-activated potassium channels from mammalian brain. Science. 1996, 273:1709−1714

Korn SJ., Bolden A., Horn R., Control of action potentials and $Ca^{2+}$ influx by the $Ca^{2+}$-dependent chloride current in mouse pituitary cells. J Physiol. 1991, 439:423-37

Koyama S., Kanemitsu Y., Weight FF., Spontaneous activity and properties of two types of principal neurons from the ventral tegmental area of rat. J Neurophysiol. 2005, 93(6):3282-93.

Kruger NJ., The Bradford method for protein quantitation. Methods Mol Biol. 1994;32:9-15.

Lancaster B., Nicoll RA., Properties of two calcium-activated hyperpolarizations in rat hippocampal neurones. J Physiol. 1987, 389:187-204.

Lancaster E., Oh EJ., Gover T., Weinreich D., Calcium and calcium-activated currents in vagotomized rat primary vagal afferent neurons. J Physiol. 2002, 540 (Pt 2):543-56.

Lang DG., and Ritchie AK., Large and small conductance calcium-activated potassium channels in the GH3 anterior pituitary cell line. Pflug. Arch. 1987, 410:614−622

Langworthy OR., Commissures of acutonomic fibers in the pelvic organs of rats. Anat Rec. 1965, 151:583-7.

Latour I., Hamid J., Beedle AM., Zamponi GW., Macvicar BA., Expression of voltage-gated $Ca^{2+}$ channel subtypes in cultured astrocytes. Glia. 2003, 41(4):347-53.

Lee JH., Kim EG., Park BG., Kim KH., Cha SK., Kong ID., Lee JW., Jeong SW., Identification of T-type alpha1H $Ca^{2+}$ channels ($Ca_v3.2$) in major pelvic ganglion neurons. J Neurophysiol. 2002, 87(6):2844-50.

Letts VA, Felix R., Biddlecome GH., Arikkath J., Mahaffey CL., Valenzuela A., Bartlett F.S. 2nd, Mori Y., Campbell K.P., Frankel W.N., The mouse stargazer gene encodes a neuronal $Ca^{2+}$-channel gamma subunit. Nat Genet. 1998, 19(4):340-7.

Lipscombe D., Pan JQ., Gray AC., Functional diversity in neuronal voltage-gated calcium channels by alternative splicing of a1. Mol Neurobiol. 2002, 26(1):21-44.

Liss B., Franz O., Sewing S., Bruns R., Neuhoff H., Roeper J., Tuning pacemaker frequency of individual dopaminergic neurons by Kv4.3L and KChip3.1 transcription. EMBO J. 2001, 20(20):5715-24.

Liu H, De Waard M, Scott VES, Gurnett CA, Lennon VA, Campbell KP. Identification of three subunits of the high-affinity -conotoxin MVIIC-sensitive $Ca^{2+}$ channel. J Biol Chem 1996; 271: 13804–10.

Llinás R, Sugimori M, Lin J-W, Cherksey B. Blocking and isolation of a calcium channel from neurons in mammals and cephalopods utilizing a toxin fraction (FTX) from funnel-web spider poison. Proc Natl Acad Sci USA 1989; 86: 1689–93.

Llinás R, Yarom Y. Properties and distribution of ionic conductances generating

electroresponsiveness of mammalian inferior olivary neurones in vitro. J Physiol 1981; 315: 569–84.

Marrion NV. and Tavalin SJ., Selective activation of $Ca^{2+}$-activated $K^{+}$ channels by co-localised $Ca^{2+}$ channels in hippocampal neurons. Nature 1998, 395: 900–905.

Martinez GM, Martinez-Zaguilan R, Gillies RJ. Effect of glucose on pHin and $[Ca^{2+}]_{in}$ in NIH-3T3 cells transfected with the yeast P-type H(+)-ATPase. J Cell Physiol. 1994, 161(1):129-41.

Martinez-Pinna J., McLachlan E.M., Gallego R., Distinct mechanisms for activation of $Cl^{-}$ and $K^{+}$ currents by $Ca^{2+}$ from different sources in mouse sympathetic neurones. J Physiol. 2000, 527 Pt 2:249-64.

Marrion NV., and Tavalin SJ., Selective activation of $Ca^{2+}$-activated $K^{+}$ channels by co-localized $Ca^{2+}$ channels in hippocampal neurons. Nature. 1998, 395(6705):900-5.

Mayer M.L., A calcium-activated chloride current generates the after-depolarization of rat sensory neurones in culture. J Physiol. 1985, 364:217-39

Meissner, G., Ryanodine receptor/$Ca^{2+}$ release channels and their regulation by endogenous effectors. Annual Review of Physiology 1994, 56:485-508

Mermelstein PG., Foehring RC., Tkatch T., Song WJ., Baranauskas G., and Surmeier D.J., Properties of Q-type calcium channels in neostriatal and cortical neurons are correlated with beta subunit expression. J Neurosci 1999, 19: 7268–7277.

Miller RJ. Voltage-sensitive $Ca^{2+}$ channels. J Biol Chem. 1992, 267(3):1403-6.

Moreno H., Rudy B., and Llinas R., Beta subunits influence the biophysical and pharmacological differences between P- and Q-type calcium currents expressed in a mammalian cell line. Proc Natl Acad Sci USA 1997, 94: 14042−14047.

McManus OB., Helms LM., Pallanck L., Ganetzky B., Swanson R and Leonard RJ., Functional role of the beta subunit of high conductance calcium-activated potassium channels, Neuron 1995,14; 645−650

Madison DV., and Nicoll RA., Noradrenaline blocks accommodation of pyramidal cell discharge in the hippocampus. Nature. 1982, 299(5884):636-8.

Madison DV., and Nicoll RA., Control of the repetitive discharge of rat CA 1 pyramidal neurones in vitro. J Physiol. 1984, 354:319-31.

Marty A., $Ca^{2+}$-dependent $K^{+}$ channels with large unitary conductance in chromaffin cell membranes. Nature. 1981, 291(5815):497-500.

Marubio LM., Roenfeld M., Dasgupta S., Miller RJ., Philipson LH., Isoform expression of the voltage-dependent calcium channel alpha1E. Receptors Channels. 1996, (4):243-51.

Maylie J., Bond CT., Herson PS., Lee WS., Adelman JP., Small conductance $Ca^{2+}$-activated $K^{+}$ channels and calmodulin. J Physiol. 2004, 554 (Pt 2):255-61.

Meera P., Wallner M, Toro L., A neuronal beta subunit (KCNMB4) makes the large conductance, voltage- and $Ca^{2+}$-activated $K^{+}$ channel resistant to charybdotoxin and iberiotoxin. Proc Natl Acad Sci U S A. 2000, 97(10):5562-7.

Mercuri NB., Bonci A., Calabresi P., Stefani A., Bernardi G., Properties of the hyperpolarization-activated cation current $I_h$ in rat midbrain dopaminergic neurons. Eur J Neurosci. 1995, 7(3):462-9.

Miller RJ. Multiple calcium channels and neuronal function. Science 1987; 235: 46–52.

Mills TM., Wiedmeier VT., Stopper VS., Androgen maintenance of erectile function in the rat penis. Biol Reprod. 1992, 46(3):342-8.

Moreno H., Rudy B., and Llinas R., Beta subunits influence the biophysical and pharmacological differences between P- and Q-type calcium currents expressed in a mammalian cell line. Proc Natl Acad Sci USA 1997, 94: 14042–14047.

Newcomb R., Szoke B., Palma A., Wang G., Chen X., Hopkins W., Cong R., Miller J., Urge L., Tarczy-Hornoch K., et al., Selective peptide antagonist of the class E calcium channel from the venom of the tarantula Hysterocrates gigas. Biochemistry 1998, 37: 15353–15362.

Nowycky MC, Fox AP, Tsien RW. Three types of neuronal calcium channel with different calcium agonist sensitivity. Nature 1985; 316: 440–3.

Olesen SP., Munch E., Moldt P. and Drejer J., Selective activation of $Ca^{2+}$-dependent $K^+$ channels by novel benzimidazolone. Eur. J. Pharmacol. 1994, 251:53–59.

Olivera BM., Miljanich GP., Ramachandran J., Adams M.E., Calcium channel diversity and neurotransmitter release: the omega-conotoxins and omega-agatoxins. Annu Rev Biochem. 1994, 63:823-67.

Owen, DG., Segal, M. and Barker, JL., A Ca-dependent $Cl^-$ conductance in cultured mouse spinal neurones. Nature 1984, 311, 567–570.

Owen DG., Segal M., Barker JL., Voltage clamp analysis of a $Ca^{2+}$-and voltage-dependent chloride conductance in cultured mouse spinal neurons. J Neurophysiol. 1986, 55(6):1115-35.

Pearson HA, Sutton KG, Scott RH, Dolphin AC. Characterization of $Ca^{2+}$ channel currents in cultured rat cerebellar granule neurones. J Physiol 1995; 482: 493–509.

Pedarzani P., Kulik A., Muller M., Ballanyi K. and Stocker M., Molecular determinants of $Ca^{2+}$-dependent $K^+$ channel function in rat dorsal vagal neurones. J. Physiol. 2000, 527: 283–290.

Perez-Reyes E., Castellano A., Kim HS., Bertrand P., Baggstrom E., Lacerda A.E., Wei X.Y., Birnbaumer L., Cloning and expression of a cardiac/brain beta subunit of the L-type calcium channel. J Biol Chem. 1992, 267(3):1792-7.

Pereverzev A., Leroy J., Krieger A., Malecot CO., Hescheler J., Pfitzer G., Klockner U., Schneider T., Alternate splicing in the cytosolic II-III loop and the carboxy terminus of human E-type voltage-gated $Ca^{2+}$ channels: electrophysiological characterization of isoforms. Mol Cell Neurosci. 2002, 21(2):352-65.

Pichler M., Cassidy TN., Reimer D., Haase H., Kraus R., Ostler D., Striessnig J., Beta subunit heterogeneity in neuronal L-type $Ca^{2+}$ channels. J Biol Chem. 1997, 272(21):13877-82.

Piedras-Renteria ES., and Tsien RW., Antisense oligonucleotides against alpha1E reduce R-type calcium currents in cerebellar granule cells. Proc Natl Acad Sci USA 1998, 95: 7760–7765.

Ramanathan K. Michael, TH. and Fuchs PA., beta subunits modulate alternatively spliced, large conductance, calcium-activated potassium channels of avian hair cells, J Neurosci 2000, 20, 1675–1684.

Randall A., and Tsien RW., Pharmacological dissection of multiple types of $Ca^{2+}$ channel currents in rat cerebellar granule neurons. J Neurosci. 1995, 15(4):2995-3012.

Reinhart PH., Chung S., Levitan IB., A family of calcium-dependent potassium channels from rat brain. Neuron. 1989, 2(1):1031-41.

Romey G., Hugues M.., Schmid-Antomarchi H..and Lazdunski. M., Apamin: a specific toxin to study a class of $Ca^{2+}$-dependent $K^{+}$ channels. J. Physiol. 1984, 79:259–264.

Saegusa H., Kurihara T., Zong S., Minowa O., Kazuno A., Han W., Matsuda Y., Yamanaka H., Osanai M., Noda T., Tanabe T., Altered pain responses in mice lacking alpha1E subunit of the voltage-dependent $Ca^{2+}$ channel. Proc Natl Acad Sci U S A. 2000, 97(11):6132-7

Sah, P., Different calcium channels are coupled to potassium channels with distinct physiological roles in vagal neurons. Proc. R. Soc. London, Ser. B 1995, 260: 105–111.

Sah P., $Ca^{2+}$-activated $K^{+}$ currents in neurones: types, physiological roles and

modulation. Trends Neurosci. 1996, 19(4):150-4.

Sah P, and Faber ES., Channels underlying neuronal calcium-activated potassium currents. Prog Neurobiol. 2002, 66(5):345-53.

Sah P, and McLachlan EM.,. $Ca^{2+}$-activated $K^{+}$ currents underlying the afterhyperpolarization in guinea pig vagal neurons: a role for $Ca^{2+}$-activated $Ca^{2+}$ release. J Neurophysiol. 2001, 85(2):714-23.

Sanchez-Vives MV., Cellular mechanisms of long-lasting adaptation in visual cortical neurons in vitro, J. Neurosci. 2000, 4286–4299.

Schneider T., Wei X., Olcese R., Costantin JL., Neely A., Palade P., Perez-Reyes E., Qin N, Zhou J., Crawford GD., Molecular analysis and functional expression of the human type E neuronal $Ca^{2+}$ channel alpha 1 subunit. Receptors Channels. 1994, 2(4):255-70.

Schramm, MR., Vajna, A., Pereverzev, A., Tottene, U., Klöckner, D., Pietrobon, J., Hescheler and Schneider. T, Isoforms of α1E voltage-gated calcium channels in rat cerebellar granule cells: Detection of major calcium channel α1-transcripts by reverse transcription–polymerase chain reaction. Neuroscience. 1999, 92(2):565-7

Scott RH., Sutton KG., Griffin A., Stapleton SR., Currie KP., Aspects of calcium-activated chloride currents: a neuronal perspective. Pharmacol Ther. 1995, 66(3):535-65.

Scott RH., Manikon MI., Andrews PL., Actions of cisplatin on the electrophysiological properties of cultured dorsal root ganglion neurones from neonatal rats. Naunyn

Schmiedebergs Arch Pharmacol. 1994, 349(3):287-94.

Shao LR., Halvorsrud R., Borg-Graham L., Storm JF., The role of BK-type $Ca^{2+}$-dependent $K^{+}$ channels in spike broadening during repetitive firing in rat hippocampal pyramidal cells. J Physiol. 1999, 521 Pt 1:135-46.

Singer D., Biel M., Lotan I., Flockerzi V., Hofmann F., Dascal N., The roles of the subunits in the function of the calcium channel. Science 1991, 253:1553-1557

Smith AB. and Cunnane TC., ω-Conotoxin GVIA-resistant neurotransmitter release in postganglionic sympathetic nerve terminals. Neuroscience 1996, 70: 817−824.

Sochivko D., Pereverzev A., Smyth N., Gissel C., Schneider T., Beck H., The $Ca_V2.3$ $Ca^{2+}$ channel subunit contributes to R-type $Ca^{2+}$ currents in murine hippocampal and neocortical neurones. J Physiol. 2002, 542(Pt 3):699-710.

Somlyo AP., and Somlyo AV., Signal transduction and regulation in smooth muscle. Nature. 1994, 372(6503):231-6.

Soong TW., Stea A., Hodson CD., Dubel SJ., Vincent SR., and Snutch TP., Structure and functional expression of a member of the low voltage-activated calcium channel family. Science (Wash DC) 1993, 260: 1133−1136.

Stanley EF, Atrakchi AH. Calcium currents recorded from a vertebrate presynaptic nerve terminal are resistant to the dihydropyridine nifedipine. Proc Natl Acad Sci USA 1990; 87: 9683−7.

Stocker M., Krause M, .and P. Pedarzani, An apamin-sensitive $Ca^{2+}$-activated $K^{+}$

current in hippocampal pyramidal neurons. Proc. Natl. Acad. Sci. U.S.A. 1999, 96: 4662–4667

Stocker M., and Pedarzani P., Differential distributions of three $Ca^{2+}$-activated $K^{+}$ channel subunits, SK1, Sk2 and SK3 in the adult rat central nervous system. Mol. Cell. Neurosci. 2000, 15: 476–493

Storm JF., Action potential repolarization and a fast after-hyperpolarization in rat hippocampal pyramidal cells. J Physiol. 1987, 385:733-59.

Storm JF., Potassium currents in hippocampal pyramidal cells. Prog Brain Res. 1990, 83:161-87.

Strobaek D., Jorgensen TD., Christophersen P., Ahring PK., Olesen SP., Pharmacological characterization of small-conductance $Ca^{2+}$-activated $K^{+}$ channels stably expressed in HEK 293 cells. Br J Pharmacol. 2000,129(5):991-9.

Swensen AM., and Bean BP., Ionic mechanisms of burst firing in dissociated Purkinje neurons. J Neurosci. 2003, 23(29):9650-63.

Takahashi T and Momiyama A., Different types of calcium channels mediate central synaptic transmission. Nature. 1993, 366(6451):156-8.

Tang ZZ., Liang MC., Lu S., Yu D., Yu C.Y., and Yue DT., Transcript scanning reveals novel and extensive splice variations in human L-type voltage-gated calcium channel, Cav1.2 alpha1 subunit, J Biol Chem 2004, 279: 44335–44343.

Toth PT., Bindokas VP., Bleakman D., Colmers WF., Miller RJ., Mechanism of

presynaptic inhibition by neuropeptide Y at sympathetic nerve terminals. Nature. 1993, 364(6438):635-9.

Tottene A., Moretti A., Pietrobon D.. Functional diversity of P-type and R-type calcium channels in rat cerebellar neurons. J Neurosci. 1996, 16(20):6353-63.

Tottene A., Volsen S., and Pietrobon D., Alpha(1E) subunits form the pore of three cerebellar R-type calcium channels with different pharmacological and permeation properties. J Neurosci 2000, 20: 171−178.

Tran S., and Boot JR., Differential effects of voltage-dependent $Ca^{2+}$ channels on low and high frequency mediated neurotransmission in guinea-pig ileum and rat vas deferens. Eur J Pharmacol 1997, 335: 31−36.

Usowicz MM., Sugimori M., Cherksey B., Llinas R., P-type calcium channels in the somata and dendrites of adult cerebellar Purkinje cells. Neuron. 1992, 9(6):1185-99.

Vajna R., Schramm M., Pereverzev A., Arnhold S., Grabsch H., Klockner U., Perez-Reyes E., Hescheler J., Schneider T., New isoform of the neuronal $Ca^{2+}$ channel alpha1E subunit in islets of Langerhans and kidney--distribution of voltage-gated $Ca^{2+}$ channel alpha1 subunits in cell lines and tissues. Eur J Biochem. 1998, 257(1):274-85

Wallner. M., Meera P., Ottolia M., Kaczorowski GJ., Latorre R., and Garcia M.L. Characterization of and modulation by a beta-subunit of a human maxi $K_{Ca}$ channel cloned from myometrium, Recept Channels 3 (1995), pp. 185−199.

Wang G., and Lemos JR., Tetrandrine blocks a slow, large-conductance, $Ca^{2+}$-activated

potassium channel besides inhibiting a non-inactivating $Ca^{2+}$ current in isolated nerve terminals of the rat neurohypophysis. Pflugers Arch. 1992, 421(6):558-65.

Waterman SA., Voltage-gated calcium channels in autonomic neuroeffector transmission. Prog Neurobiol 2000, 60: 181−210.

Welling A., Bosse E., Cavalié A., Bottlender G., Ludwig A., Nastainczyk W., Flockerzi V., Hofmann F., Stable co-expression of calcium channel, α1, β and α2δ subunits in a somatic cell line. J Physiol (Lond) 1993, 471:749-765

Wikstrom MA, El Manira A., Calcium influx through N- and P/Q-type channels activate apamin-sensitive calcium-dependent potassium channels generating the late afterhyperpolarization in lamprey spinal neurons. Eur J Neurosci. 1998, (4):1528-32.

Williams ME., Marubio .LM., Deal CR., Hans M., Brust PF., Philipson LH., Miller RJ., Johnson EC., Harpold MM., Ellis SB., Structure and functional characterization of neuronal alpha 1E calcium channel subtypes. J Biol Chem. 1994, 269(35):22347-57.

Wilson SM, Toth PT, Oh SB, Gillard SE, Volsen S, Ren D, Philipson LH, Lee EC, Fletcher CF, Tessarollo L, Copeland NG, Jenkins NA, Miller RJ. The status of voltage-dependent calcium channels in alpha 1E knock-out mice. J Neurosci. 2000, 20(23):8566-71.

Wolfart J., Neuhoff H., Franz O., Roeper J., Differential expression of the small-conductance, calcium-activated potassium channel SK3 is critical for pacemaker control in dopaminergic midbrain neurons. J Neurosci. 2001, 21(10):3443-56.

Wright CE., and Angus JA., Effects of N-, P- and Q-type neuronal calcium channel antagonists on mammalian peripheral neurotransmission. Br J Pharmacol 1996, 119: 49–56

Xia XM., Ding JP., and Lingle CJ., Molecular basis for the inactivation of $Ca^{2+}$-and voltage-dependent BK channels in adrenal chromaffin cells and rat insulinoma tumor cells. J Neurosci 19 (1999), pp. 5255–5264.

Xu ZJ., and Adams DJ., Voltage-dependent sodium and calcium currents in cultured parasympathetic neurones from rat intracardiac ganglia. J Physiol (London) 1992, 456: 425–441.

Xu Y., Dong PH., Zhang Z., Ahmmed G.U., Chiamvimonvat N. Presence of a calcium-activated chloride current in mouse ventricular myocytes. Am J Physiol Heart Circ Physiol. 2002, 283(1):H302-14.

Yamazaki J., Okamura K., Ishibashi K., Kitamura K., Characterization of CLCA protein expressed in ductal cells of rat salivary glands. Biochim Biophys Acta. 2005, 1715(2):132-44.

Yang J., Ellinor PT., Sather WA., Zhang JF., Tsien RW., Molecular determinants of $Ca^{2+}$ selectivity and ion permeation in L-type $Ca^{2+}$ channels. Nature. 1993, 366(6451):158-61

Yang Y., Chen X., Margulies K., Jeevanandam V., Pollack P. and Bailey BA., L-type $Ca^{2+}$ channel alpha a1c subunit isoform switching in failing human ventricular myocardium, J Mol Cell Cardiol 2000, 32 :973–984.

Zamponi GW., Bourinet E., and Snutch TP., Nickel block of a family of neuronal calcium channels: subtype- and subunit-dependent action at multiple sites. J Membr Biol 1996, 151: 77−90.

Zhang JF., Randall AD., Ellinor PT., Horne WA., Sather WA., Tanabe T., Schwarz TL., and Tsien RW., Distinctive pharmacology and kinetics of cloned neuronal $Ca^{2+}$ channels and their possible counterparts in mammalian CNS neurons. Neuropharmacology 1993, 32: 1075−1088.

Zhu Y., Zboran EL., and Ikeda SR., Phenotype-specific expression of T-type calcium channels in neurons of the major pelvic ganglion of the adult male rat. J Physiol (Lond) 1995, 489: 363−375.

Zhu Y., and Yakel JL., Modulation of $Ca^{2+}$ currents by various G protein-coupled receptors in sympathetic neurons of male rat pelvic ganglia. J Neurophysiol. 1997, 78(2):780-9.

## ABSTRACT IN KOREAN

# 비뇨 생식계를 지배하는 주골반 자율 신경절에서 칼슘 채널의 발현 및 기능


자율 신경절 중에서도 비뇨 생식계를 지배하고 있는 수컷 쥐의 주골반 신경절은 하나의 신경절 캡슐 안에 교감 신경과 부교감 신경이 동시에 존재하고 있는 독특한 특성을 지니고 있다. 주골반 신경절에서 교감 신경은 저전압에서 활성되어 low-threshold spike를 유발하는 α1H T-type 칼슘 채널의 발현 여부에 의해 부교감 신경과 구별된다. 주골반 신경절은 α1A를 제외한 모든 고전압 활성 칼슘 채널의 α1 subunit (α1B, α1C, α1D and α1E)을 발현하였다. 주골반 신경절의 고전압 활성 칼슘 채널 아형 발현 양상은 교감 및 부교감 신경에서 동일하였다. 흥미롭게도, 주골반 신경절에 발현되어 있는 R-type 칼슘 전류는 $NiCl_2$에 의해서는 억제되지만, 특이적 차단제로 알려진 SNX-482에 의해서는 효과를 나타내지 않았다. 그러나 SNX-482는 HEK 293 세포에 recombinant $\alpha 1E/\delta_2 a/\beta_2$를 이형 발현 시켰을 경우 발현되는 칼슘 전류에 대해서는 차단 효과를 나타내었다. RT-PCR 수행 결과, 기존에 알려진 α1E prototype (rbEII, accession number : L15453)과 비교해 본 결과 주골반 신경절에서는 상대적으로 짧은 II-III loop와 긴 N- 및 C-말단을 지닌 한 종류의 splice variant α1E가 검출되었다. 주골반 신경절에 존재하는 이러한 특성의 α1E splice variant는 소뇌에 발현되는 SNX-482에 저항성을 보이는 "G3" 또는 “Rc" 또는 "$\alpha 1_{Ee}$"와 유사할 것으로 추측된다.

역치점보다 높은 탈분극 전류 자극에 대하여 교감 신경은 tonic firing을 부교감

신경은 phasic firing 패턴을 보인다. 교감 및 부교감 신경의 이러한 firing 패턴의 차이는 칼슘 이온에 의해 활성화되는 또 다른 채널의 작용에 의해 결정된다. RT-PCR 분석 결과 골반 신경절에서 $Ca^{2+}$-activated $K^+$ channel, 즉 BK (α and β) 와 SK (SK2 and SK3) 채널 아형들의 mRNA가 확인되었다. 골반 신경절에서 SK channel은 mAHP를 유발하고 BK channel은 활동전압의 재분극과 fAHP을 유도함을 확인하였다. L- 과 N-type 칼슘 채널을 통해 세포내로 들어온 칼슘은 다른 방식으로 골반 신경절의 흥분성을 조절하였다. N-type 칼슘 채널은 $I_{AHP}$ 와 AHP를 증가시켜 교감 및 부교감 신경절의 spike firing을 감소시키는 반면 L-type 칼슘 채널은 교감 신경에서는 $I_{AHP}$ 와 AHP를 감소시켜 spike firing을 증가시키지만, 부교감 신경에서는 $I_{AHP}$ 와 AHP에 큰 변화를 주지 못했으며, 따라서 흥분성의 증가도 미약하였다. 비특이적 칼슘 채널 차단제인 $CdCl_2$를 처리했을 때 부교감 신경과는 달리 교감 신경에서 firing frequency에 큰 변화가 없었다. 이는 spike firing 조절에 있어서 N-type과 L-type 칼슘 채널 효과가 상쇄되었기 때문이라 추측된다. 교감 신경에서 또 하나의 firing 특성은 $Ca^{2+}$ activated $Cl^-$ channel에 의해 조절된다는 것이다. 교감 신경절에서 $Ca^{2+}$ activated $Cl^-$ channel에 의해 spike firing이 조절되는 패턴은 L-type에 의한 그것과 매우 유사하다. 결론적으로, 주골반 신경절은 기능적으로 L-, N- 그리고 R-type 고전압 활성 칼슘 채널을 발현하고 있고, 이들 중 L-type과 N-type 칼슘 채널은 골반 신경세포 타입에 따라 각기 다른 조합으로 $K^+$이나 $Cl^-$ 채널과 결합되어 있어서 서로 다른 메카니즘으로 신경 세포의 흥분성을 조절한다.

**핵심 되는 말** : 주골반 신경절, 칼슘, 전압비 의존 칼슘 채널, $Ca^{2+}$ activated $K^+$ channel, Afterhyperpolarization (AHP), 흥분성 조절